

# THE HIGH-REDSHIFT HE II GUNN-PETERSON EFFECT: IMPLICATIONS AND FUTURE PROSPECTS

Mark A. Fardal<sup>1</sup>, Mark L. Giroux<sup>1</sup>, and J. Michael Shull<sup>1</sup>  
 Center for Astrophysics and Space Astronomy,  
 Department of Astrophysical and Planetary Sciences  
 University of Colorado, Campus Box 389, Boulder, CO 80309

<sup>1</sup> also at JILA, University of Colorado  
 and National Institute of Standards and Technology.

## ABSTRACT

Absorption due to He II Ly $\alpha$  has now been detected at low resolution in the spectra of four quasars between redshifts  $z = 2.74 - 3.29$ . We assess these observations, giving particular attention to the radiative transfer of the ionizing background radiation, cloud diffuse emission and ionization physics, and statistical fluctuations. We use high-resolution observations of H I absorption towards quasars to derive an improved model for the opacity of the intergalactic medium (IGM) from the distribution of absorbing clouds in column density and redshift. We use these models to calculate the H I and He II photoionization history, the ratio  $\eta = \text{He II}/\text{H I}$  in both optically-thin and self-shielded clouds, and the average line-blanketing contribution of the clouds to He II absorption. The derived ionization rate,  $\Gamma_{HI} = (1 - 3) \times 10^{-12} \text{ s}^{-1}$  ( $z = 2 - 4$ ) is consistent with the ionizing background intensity inferred from the ‘‘proximity effect’’, but it remains larger than that inferred by N-body hydrodynamical simulations of the Ly $\alpha$  absorber distribution. The He II observations are consistent with line blanketing from clouds having  $N_{HI} \geq 10^{12} \text{ cm}^{-2}$ , although a contribution from a more diffuse IGM would help to explain the observed opacity. We compute the expected He II optical depth,  $\tau_{HeII}(z)$ , and examine the implications of the sizable fluctuations that arise from variations in the cloud numbers and ionizing radiation field. We assess how He II absorption constrains the intensity and spectrum of the ionizing radiation and the fractional contributions of the dominant sources (quasars and starburst galaxies). Finally, we demonstrate how high-resolution ultraviolet observations can distinguish between absorption from the diffuse IGM and the Ly $\alpha$  forest clouds and determine the source of the ionizing background.

*Subject headings:* galaxies: quasars: absorption lines– galaxies: intergalactic medium–galaxies: evolution

## 1. INTRODUCTION

Absorption in the He II  $\lambda 303.78$  Ly $\alpha$  line has long been considered a potentially important tool for studying the high-redshift universe (Miralda-Escudé & Ostriker 1990; Miralda-Escudé 1993; Shapiro, Giroux, & Babul 1994). As early estimates showed, He II is more abundant than H I in the highly ionized “Ly $\alpha$  forest clouds” that appear in quasar spectra, because He II has a lower photoionization cross section and a larger recombination rate. Comparison of the H I and He II absorption could tell us about the photoionizing background, the history of structure formation, and internal conditions in the Ly $\alpha$  clouds. Also, He II absorption from a smoothly distributed intergalactic medium (IGM) should be more easily detectable than the corresponding H I absorption, which has proven difficult to measure unambiguously (Giallongo et al. 1994; Williger et al. 1994; Fang & Crotts 1995).

These hopes have partially been realized by recent observations of He II toward four quasars. Q0302-003 was observed with two instruments on the Hubble Space Telescope (HST): at low resolution with the Faint Object Camera (FOC) (Jakobsen et al. 1994) and at higher resolution with the Goddard High Resolution Spectrograph (GHRS) (Hogan, Anderson, & Rutgers 1997). Q1935-69 was observed with HST using both the Faint Object Spectrograph (FOS; Tytler et al. 1995) and the FOC (Tytler 1997). HS1700+6416 was observed with the Hopkins Ultraviolet Spectrometer (HUT) during the Astro-2 mission (Davidsen et al. 1996, hereafter D96). Most recently, HE2347-4342 was observed with HST/GHRS (Reimers et al. 1997). The resolution of the HUT spectrum is  $\sim 3$  Å while that of the HST/FOS spectra is  $\sim 15$  Å in the FOC spectra. The HST/GHRS spectra potentially have higher resolution, although the data are usually binned to enhance the signal-to-noise ratio. Thus, individual absorption lines are not resolved. Instead, the results are reported (see also Figure 1) in terms of an average optical depth:  $1.3 \leq \tau_{HeII} \lesssim 4$  towards Q0302-003 ( $z_{em} = 3.29$ ),  $1.0 \leq \tau_{HeII} \leq 2.0$  ( $z_{em} = 3.18$ ) towards Q1935-69,  $\tau_{HeII} = 1.00 \pm 0.07$  towards HS1700+6416 ( $z_{em} = 2.74$ ), and  $\tau_{HeII}$  varying from  $\sim 1$  to  $\geq 4.8$  toward HE2347-4342. As shown by the error estimates, the HUT result is the most restrictive of the four, and we normalize our plot to that point. We anticipate our discussion in §3–4 by placing these data points in the context of two simple models for the evolving He II Ly $\alpha$  opacity. As we indicate in Fig. 1 and will discuss in detail below, a single high-precision measurement is inadequate to constrain models for the He II opacity since the intrinsic fluctuations in the opacity at a given epoch are significant.

Early interpretation of these results in the discovery papers, as well as by Madau & Meiksin (1994), Zheng & Davidsen (1994), Giroux, Fardal, & Shull (1995, hereafter Paper I), and Songaila, Hu, & Cowie (1995), has focused on the requirements for reproducing the observed He II absorption. As yet, it has been difficult to place strong constraints on the required assumptions. These include the distribution of absorption-line clouds in redshift, H I column, and H I line width, and the populations of ionizing sources and their intrinsic spectra. Assumptions about the physical properties of the clouds must also be made, both to derive the ionization correction necessary to convert  $N_{HI}$  to  $N_{HeII}$  and to estimate the distribution of He II line widths. In

addition, an unknown amount of He II absorption may arise in diffuse gas in the IGM, i.e. the true Gunn-Peterson effect (Gunn & Peterson 1965, hereafter GP). These uncertainties also affect the analysis of H I and He II absorption by numerical hydrodynamical simulations (cf. Zhang et al. 1997).

A further complication, discussed by Zheng & Davidsen (1995) and in Paper I, is that ionizing radiation from the observed quasar itself may alter the level of He II ionization in nearby clouds. This “He II proximity effect” is expected to be larger than the corresponding H I proximity effect if, as is believed, intervening clouds strongly depress the level of He II-ionizing radiation for the general metagalactic background. This effect is not obvious in the spectrum of HS1700+6416, but it has been claimed in the spectrum of Q0302-003 (Hogan et al. 1997; Heap 1997).

Fortunately, a substantial reduction in the volume of model parameter space is possible. A high-resolution *Keck* spectrum of Q0302-003 (Songaila, Hu, & Cowie 1995) has provided the actual set of H I absorption lines to which the observed He II line-blanketing absorption must correspond. It is likely that similar line lists will be generated for the other quasars used to measure He II absorption. In addition, high-quality spectra along the lines of sight to many quasars are providing increasingly good statistics on the average distribution in column density, Doppler  $b$ -values, and redshift of H I absorbing clouds. Additional He II absorption observations are planned with HST, and significant advances are expected to come from the Far Ultraviolet Spectroscopic Explorer (FUSE), scheduled for launch in late 1998, and the Cosmic Origins Spectrograph (COS) scheduled for the HST refurbishment mission in late 2002. The FUSE spectrograph may be able to resolve individual lines at wavelengths down to 915 Å ( $z_{\text{HeII}} \geq 2.01$ ), providing line widths and directly giving the ionization correction in the absorbing clouds. The COS instrument offers significantly greater throughput, to study faint QSOs at  $z_{\text{HeII}} > 2.9$ .

The purpose of this paper is to ask whether any simple model fits all of the current observations and to identify important questions that could be answered in the future. Our approach is phenomenological; we do not employ a fundamental theory of the Ly $\alpha$  forest, as has been attempted in Gnedin & Hui (1996) or Bi & Davidsen (1997), nor do we use a numerical hydrodynamical approach. Instead, we employ the standard, observationally oriented division between “clouds” and a diffuse IGM. In § 2, we outline our calculation of the cosmological radiative transfer of direct and diffuse photoionizing radiation through the absorbing clouds. We compile a new absorption-line sample and construct from it accurate models for the distribution of clouds in redshift and H I column density, constraining the opacity of the universe to H I- and He II-ionizing photons. We describe our assumptions about the physical properties of these absorbers and our models for the evolution and spectral shape of ionizing sources. In § 3, we describe the results of our radiative transfer calculations. These give the relation between the emitted spectrum of sources and the spectrum seen by the absorbing matter, as well as the implied opacity of the universe to He II-ionizing photons. Using these models, we discuss the ionization conditions necessary to reproduce the mean levels of H I and He II Ly $\alpha$  absorption seen in the current observations. In § 4, we discuss the fluctuations in the He II absorption expected from

variations in the number density of lines and the metagalactic radiation field. In § 5, we show how the effects discussed in this paper could be studied by future ultraviolet observations of He II absorption.

## 2. THE AVERAGE HE II ABSORPTION

### 2.1. The Observations at Present

To date, every quasar observation that has been made at appropriate wavelengths has detected an absorption trough due to redshifted He II Ly $\alpha$ . The observations of Q0302-003 by Hogan et al. (1997) and of HS1700+6416 by Davidsen et al. (1996) are of particular interest because they have sufficient resolution and signal-to-noise ratio to show some structure in the absorption. The new observations of HE2347-4342 (Reimers et al. 1997) may also prove valuable, because they appear to exhibit a wide variance in He II absorption. However, the average transmission and its corresponding “effective” optical depth shown in Figure 1 remain the most useful statistics derived from these observations.

Hogan et al. (1997) draw some interesting conclusions by comparing their spectrum with a *Keck* spectrum of the same quasar (Songaila et al. 1995). They claim to see two separate He III ionization bubbles around the quasar and suggest that the gas far from the quasar has a significant Gunn-Peterson opacity due to an IGM. They place a lower limit of  $\eta \equiv N_{\text{HeII}}/N_{\text{HI}} > 100$  far away from the quasar. However, these conclusions are based on a potentially optimistic error estimate for the flux calibration. While Hogan et al. quote a 95% confidence range of  $1.5 < \tau < 3.0$  in a region far from the quasar, a separate analysis of the GHRS data (Heap 1997) yields  $\tau = 1.5 \pm 0.2$  from the ACCUM mode of exposure and  $\tau \approx 4$  for the FLYLIM mode. We also note that the sudden drop in the spectrum at  $\lambda = 1283 \text{ \AA}$  could be due to a Lyman limit system at  $z = 0.41$ , although the probability of this is only  $\sim 3\%$ . This hypothesis could be checked by looking for the Mg II doublet at 3942 and 3952  $\text{\AA}$ .

Because of binning, the published spectrum of HS1700+6416 (Davidsen et al. 1996) does not show the full resolution of the observations on which it was based. Nevertheless, some interesting structural features are apparent. There is no sign of the He II proximity effect in this quasar, contrary to predictions (Miralda-Escudé & Ostriker 1992; Zheng & Davidsen 1995; Paper I). This allows one to set a limit on the ionizing flux at  $h\nu \geq 4 \text{ Ryd}$ . Also, there are two bumps in the spectrum which seem statistically significant. One matches the He II Ly $\beta$  emission wavelength, but by analogy with H I Ly $\beta$ , this line is expected to be weak. In § 4 we will consider whether these bumps might be caused by variations in the ionization level of the clouds.

## 2.2. Physical Considerations

The problem of modeling the He II Ly $\alpha$  absorption can be broken into two parts. First, one estimates the photoionizing background by making assumptions about the ionizing sources and estimating the population of quasar absorption line clouds from H I measurements. This is an iterative process, as the amounts of He I and He II in the absorbing clouds both depend on and alter the ionizing spectrum. This process gives an estimate of the He II/H I ratio  $\eta$ . Second, one derives the He II line opacity, using  $\eta$  and H I measurements of the IGM and absorption-line clouds. The basic principles and equations involved in this process have been discussed in many papers (Miralda-Escudé & Ostriker 1990, Miralda-Escudé 1993; Jakobsen et al. 1994; Madau & Meiksin 1994; Paper I; Davidsen et al. 1996). For reference, we state the main equations here.

A continuous IGM containing a species  $s$  with proper number density  $n_s(z)$  and resonant scattering cross section  $\sigma_s \equiv (\pi e^2/m_e c^2) f_s \lambda_s$  gives a line optical depth of

$$\tau_s^{\text{GP}}(z) = \left( \frac{c}{H_0} \right) n_s(z) \sigma_s (1+z)^{-1} (1 + \Omega_0 z)^{-1/2}, \quad (1)$$

(Gunn & Peterson 1965). We assume  $\Omega_0 = 1$  throughout; as shown below, many of our results turn out to be independent of  $\Omega_0$ . The large cross sections for resonant scattering imply that only a small density of the scattering particles is needed for sizable GP absorption. This density is sufficiently low that it makes a negligible contribution to the continuum (bound-free) opacity in H I and He II. The continuum opacity of a continuous IGM is related to the Gunn-Peterson optical depth by  $d\tau_s^{\text{cont}}/dz = (\sigma_s^{\text{cont}}/\sigma_s^{\text{line}}) \tau_s^{\text{GP}}/(1+z)$ . For both H I and He II,  $(\sigma_s^{\text{cont}}/\sigma_s^{\text{line}}) = 1.42$ . Limits on the smooth GP trough in the H I Ly $\alpha$  line [ $\tau_{\text{HI}}^{\text{GP}}(z=3-4) \lesssim 0.1$ ] (Giallongo et al. 1994; Williger et al. 1994; Fang & Crots 1995) imply a very low smoothly distributed density of H I in the IGM. Even if the corresponding He II Ly $\alpha$  depth were much larger—for example, if it provided almost all of the optical depth  $\tau_{\text{HeII}}(z \approx 2.4) = 1.0$  seen in HS1700+6416—the smoothly distributed He II density would contribute only a few percent of the total He II bound-free opacity, as we shall see in § 2.3. Indeed, one of the conclusions of numerical hydrodynamic models (Zhang et al. 1997) is that the He II Ly $\alpha$  absorption may be dominated by the contribution from low density regions (“voids” in the gas distribution), which are far too low in density to have significant bound-free opacity. The bound-free opacity arises almost entirely from the discrete absorbers (Ly $\alpha$  forest and Lyman limit systems).

For the Ly $\alpha$  absorption-line forest (LF), the effective line optical depth is

$$\tau_s^{\text{LF}}(z) = \frac{(1+z)}{\lambda_s} \int \frac{\partial^2 \mathcal{N}}{\partial N_{\text{HI}} \partial z} W_\lambda dN_{\text{HI}}, \quad (2)$$

with  $W_\lambda$  the equivalent width of the line in wavelength units. (Note: the term “effective” optical depth denotes the optical depth corresponding to the average transmission,  $\langle T \rangle \equiv \langle \exp(-\tau) \rangle = \exp(-\tau_{\text{eff}})$ . This is not the same as the average optical depth. We

will always refer to the former in this paper.) The effective continuum optical depth is

$$\frac{d\tau_{\text{eff}}(\nu)}{dz} = \int \frac{\partial^2 \mathcal{N}}{\partial N_{\text{HI}} \partial z} [1 - \exp(-N_{\text{HI}} \sigma_{\text{tot}}(\nu))] dN_{\text{HI}}, \quad (3)$$

where the continuum cross section is summed over species  $s$ ,

$$\sigma_{\text{tot}}(\nu) = \sum_s \left( \frac{N_s}{N_{\text{HI}}} \right) \sigma_s^{\text{cont}}(\nu). \quad (4)$$

Usually only one species will contribute appreciably at any frequency.

As the term  $N_s/N_{\text{HI}}$  implies, the relative column densities must be estimated based upon physical modeling of the clouds. The usual approach is to assume that the clouds are highly photoionized, and that helium is so highly ionized that He I may be neglected. Thus, both H and He within the clouds have only two stages to consider. In photoionization equilibrium,

$$n_{\text{HI}} = \frac{n_e n_{\text{HII}} \alpha_{\text{H}}^{(A)}}{\Gamma_{\text{HI}}}, \quad n_{\text{HeII}} = \frac{n_e n_{\text{HeIII}} \alpha_{\text{He}}^{(A)}}{\Gamma_{\text{HeII}}}. \quad (5)$$

Here,  $\alpha_{\text{H}}^{(A)} = (2.51 \times 10^{-13} \text{ cm}^3 \text{ s}^{-1}) T_{4.3}^{-0.76}$  and  $\alpha_{\text{He}}^{(A)} = (1.36 \times 10^{-12} \text{ cm}^3 \text{ s}^{-1}) T_{4.3}^{-0.70}$  are the case-A recombination rate coefficients, appropriate for the low column density gas in these absorbers at temperature  $T = (10^{4.3} \text{ K}) T_{4.3}$ . If we define  $\alpha_1$  and  $\alpha_4$  as the spectral indexes of the radiation field just above the thresholds for ionizing H I (1 Ryd) and He II (4 Ryd), we can write the specific intensities near these thresholds as  $J_\nu = J_{\text{HI}} (\nu/\nu_{\text{HI}})^{-\alpha_1}$  and  $J_\nu = J_{\text{HeII}} (\nu/\nu_{\text{HeII}})^{-\alpha_4}$ . In the approximation that the photoionization cross sections scale as  $\nu^{-3}$  above threshold, the photoionization rates of the two species are  $\Gamma_{\text{HI}} \approx 4\pi J_{\text{HI}} \sigma_{\text{HI}}/h(3 + \alpha_1)$  and  $\Gamma_{\text{HeII}} \approx 4\pi J_{\text{HeII}} \sigma_{\text{HeII}}/h(3 + \alpha_4)$ . The ratio of He II to H I is then

$$\eta \equiv \frac{N_{\text{HeII}}}{N_{\text{HI}}} = \left( \frac{n_{\text{HeIII}}}{n_{\text{HII}}} \right) \left( \frac{\alpha_{\text{HeII}}}{\alpha_{\text{HI}}} \right) \left( \frac{\Gamma_{\text{HI}}}{\Gamma_{\text{HeII}}} \right). \quad (6)$$

If the ionization level is high enough that  $n_{\text{HeIII}} \approx n_{\text{He}}$  and  $n_{\text{HII}} \approx n_{\text{H}}$ , the first ratio simplifies to the abundance ratio  $n_{\text{He}}/n_{\text{H}} = (Y/4)/(1 - Y)$ , where estimates of the primordial helium mass abundance range from  $Y = 0.22\text{--}0.25$  (Schramm & Turner 1997). Recent analyses of metal-poor extragalactic H II regions find  $Y = 0.232 \pm 0.003(\text{stat}) \pm 0.005(\text{sys})$  (Olive & Steigman 1995) and  $Y = 0.243 \pm 0.003(\text{stat})$  (Izotov et al. 1997). On the theoretical side, the recent provisional value for primordial D/H =  $(2.7 \pm 0.6) \times 10^{-5}$  (Tytler, Fan, & Burles 1995) corresponds to  $Y = 0.248 \pm 0.002$  (Schramm & Turner 1997). For our work, we adopt a value  $Y = 0.239$  corresponding to  $n_{\text{He}}/n_{\text{H}} = 0.0785$ . The electron density in fully ionized gas is then  $n_e \approx 1.16n_{\text{H}}$ , and the column ratio is

$$\eta \approx 1.70 \left( \frac{J_{\text{HI}}}{J_{\text{HeII}}} \right) \left( \frac{3 + \alpha_4}{3 + \alpha_1} \right) T_{4.3}^{0.06}. \quad (7)$$

In our radiative transfer calculations, we derive the photoionization rates by integrating over the ionizing spectrum, and take into account the ionization balance between H I, H II, He II, and

He III. The approximations above are usually quite good, except that  $J_{HI}$  and  $J_{HeII}$  should be qualified to be the portion of the background resulting from direct emission from ionizing sources. As shown in § 3, when the re-emission from absorbing clouds is included it would be inappropriate to simply picture the shape of the metagalactic ionizing background as a piecewise power law with the two exponents  $\alpha_1$  and  $\alpha_4$ .

The absence of a smooth Gunn-Peterson trough in the H I Ly $\alpha$  line suggests both that most of the baryons are clumped into distinct structures at  $z \lesssim 4$  and that the H II regions around emitting sources have overlapped by that time. The observations of HS1700+6416 give a similar conclusion for helium at redshifts  $z < 2.7$ . Combining the Gunn-Peterson limits of  $\tau_{HeI}(z = 2.7) < 0.05$  for He I  $\lambda 584$  (Reimers et al. 1992) with the condition  $\tau_{HeII} < 1.0$  for He II, we see that  $\lesssim 10^{-3}$  of the baryons can be in the form of smoothly distributed He I or He II. This implies either an implausibly efficient clearing-out of the spaces between clouds or the overlap of He III spheres by  $z = 2.7$ . The same argument could be extended to redshift  $z = 3.1$ , if there is indeed flux at all observed wavelengths below the He II edge in the spectrum of Q0302-003 (Hogan et al. 1997). However, the observed patchy He II absorption toward the  $z = 2.9$  quasar HE2347-4342 (Reimers et al. 1997) casts some doubt on this simple picture of reionization.

We adopt the standard parameterization for the absorption-line distribution in equations (2) and (3),

$$\frac{\partial^2 \mathcal{N}}{\partial N_{HI} \partial z} = (A/N_r)(N_{HI}/N_r)^{-\beta}(1+z)^\gamma, \quad (8)$$

with a reference column of  $N_r \equiv 10^{17} \text{ cm}^{-2}$ . New high-resolution spectra of Ly $\alpha$  clouds have enabled us to construct a new, more accurate opacity model for the IGM. A simple, but reasonably accurate single power-law fit to the data in § 2.3 has  $A = 0.054$ ,  $\beta = 1.51$ , and  $\gamma = 2.58$ . Better models with breaks and multiple power laws are discussed in § 2.3. The spectral filtering by the IGM produces an effective spectral index of the background ( $\alpha_b$ ) that is considerably larger (softer radiation field) than that of the intrinsic sources ( $\alpha_s$ ). (As we have stated, the background spectrum is not a power law, but since the ionization balance of H I and He II is controlled by the flux at the ionization edges, it is useful to define  $J_{HeII}/J_{HI} \equiv 4^{-\alpha_b}$ .) The value of  $\eta$  can be estimated in this simple model by using the source-function approximation, in which  $J_\nu \approx S_\nu = j_\nu/\kappa_\nu$ . Here  $j_\nu$  is the proper volume emissivity and  $\kappa_\nu \equiv (dz/dt)(d\tau_\nu/dz)/c$  is the opacity per unit length. It is easy to show that the threshold opacities of He II (at 4 Ryd) and H I (at 1 Ryd) are in the ratio  $\kappa_{HeII}/\kappa_{HI} = (\eta/4)^{\beta-1}$ . The sources of ionizing emissivity have a spectral index  $\alpha_s$ , so that  $j_{HeII}/j_{HI} = 4^{-\alpha_s}$ . Combining this with equation (7), in which we take  $\alpha_1 \approx \alpha_4$  to obtain  $\eta = 1.70 \times 4^{\alpha_b}$ , we derive the relation  $(2 - \beta)\alpha_b = \alpha_s - [1 - (\ln 1.7)/(\ln 4)](\beta - 1)$ . For  $\beta = 1.51$ , we then have  $\alpha_b \approx 2.0\alpha_s - 0.64$ . We shall see later that  $\alpha_s \approx 1.8$  (Zheng et al. 1997) is a plausible value for the 350–912 Å spectra of quasars, implying a background spectral index  $\alpha_b \approx 3.0$ , a continuum opacity ratio  $\kappa_{HeII}/\kappa_{HI} \approx 5.5$ , and a column ratio  $\eta \approx 110$ . In the remainder of this paper, we employ our new opacity models as well as more accurate numerical models of radiative transfer to derive the ionizing spectrum and the ratio  $\eta$ . However, this simple analytic model demonstrates both that the background should be softer than the emitted flux and

that its index  $\alpha_b$  is quite sensitive to the source index  $\alpha_s$ .

As the forms for equations (2), (3), and (8) suggest, the clouds that dominate either the line or the continuum opacity (if  $1 < \beta < 2$ , as is observed) are those that are marginally saturated, with optical depths  $\tau \sim 1$ . However, the column densities at which this occurs are quite different for line and continuum absorption and for H I versus He II. For example, the H I continuum opacity at 1 Ryd is dominated by clouds with  $N_{HI} \sim 1/\sigma_{HI} \sim 10^{17} \text{ cm}^{-2}$ , while the H I Ly $\alpha$  opacity is dominated by clouds with  $N_{HI} \sim 10^{13} \text{ cm}^{-2}$ . The clouds that dominate the He II continuum opacity at 4 Ryd have columns  $N_{HI} = N_{HeII}/\eta \sim (\sigma_{HeII}\eta)^{-1} \sim 10^{15} \text{ cm}^{-2}$ , while the absorption in the He II Ly $\alpha$  line is controlled by clouds with columns around  $N_{HI} \sim 10^{12} \text{ cm}^{-2}$ . The most important column ranges for our problem are thus  $N(\text{H I}) \approx 10^{12}\text{--}10^{13} \text{ cm}^{-2}$  and  $10^{15}\text{--}10^{17} \text{ cm}^{-2}$ . Because the absorption-line distribution is so crucial to understanding the He II absorption, we examine it in more detail in the next section and derive a new opacity model.

### 2.3. Absorption-Line Models

Although many authors have fitted the column density distribution over a limited range in  $N_{HI}$ , the last attempt to find a global fit was that of Petitjean et al. (1993). Since then, spectra of higher quality and greater redshift coverage have appeared, which should allow us to achieve greater accuracy and to fit the distribution at lower columns. In addition, by constructing a new sample, we can estimate the errors in the column density distribution and the resulting opacities. Because clouds of different column densities are found by different observational methods, fits to the column density distribution in the literature have generally contained artificial discontinuities at certain columns. For example, our Paper I relied on a combination of the Press & Rybicki (1993) distribution for low columns and the Sargent, Steidel, & Boksenberg (1989) distribution for Lyman-limit systems (LLS). This distribution had a mismatch of a factor of  $\sim 5$  at  $N_{HI} = 10^{17} \text{ cm}^{-2}$  and  $z \sim 3$ , which had drastic effects on the continuum opacities. The fits we obtain below should give much more reliable results.

To estimate the distribution of absorbers in  $N_{HI}$  and  $z$ , we have taken line lists from the following sources: Lu et al. (1996), Kulkarni et al. (1996), Hu et al. (1995), Giallongo et al. (1993), Cristiani et al. (1995), Rauch et al. (1992), and Carswell et al. (1991) for Ly $\alpha$  forest lines, and from Stengler-Larrea et al. (1995) and Storrie-Lombardi et al. (1994) for Lyman-limit absorbers. The objects in our sample overlap somewhat with those of Petitjean et al. (1993). However, about half the lines are from new *Keck* spectra, and thus many lines have much lower columns (down to  $2 \times 10^{12} \text{ cm}^{-2}$ ) than were detectable a few years ago.

By constructing several models for the absorption-line distribution, denoted A1 through A4, we hope to illustrate the range of uncertainty in  $\eta$  due to the cloud distribution. To arrive at our fits, we use a maximum-likelihood method, which avoids binning the data in H I column. To treat the Lyman limit systems with continuum  $\tau_{HI} > 3$ , for which  $N_{HI}$  is difficult to determine,

we include in the likelihood function the binomial probability of seeing the observed number of these systems in the sample. Completeness corrections have been included for the low-column clouds seen in the *Keck* spectra. Explicit formulae for this method are given in Appendix B. The column density distribution in our sample is shown in Figure 2. We have included the best single power-law fit, which was already mentioned in § 2.2, but it is clear from the graph that this fit is poor, with fit probability  $P_{\text{fit}} = 3 \times 10^{-5}$ . The poor fit is caused by a deficit of clouds with  $N_{\text{HI}} \sim 10^{15} \text{ cm}^{-2}$ , in agreement with Petitjean et al. (1993).

In deriving models A1 and A2, we have assumed that  $N_{\text{HI}}$  and  $z$  are statistically independent. As in equation (8), we assume an evolution in  $z$  proportional to  $(1+z)^\gamma$ . A three-power-law model is required to get a good fit to the observed column density distribution, which we require to be continuous. Our model A1 is designed to minimize, and A2 to maximize, the He II line and continuum opacity relative to that of hydrogen. These models are not reliable in the damped ( $N_{\text{HI}} > 10^{20} \text{ cm}^{-2}$ ) region, so there we have switched over to the distribution described in Storrie-Lombardi, Irwin, & McMahon (1997), although this does cause a small discontinuity in the column distribution. In any case, this region has little effect on our results.

In the past, it has been controversial whether the Ly $\alpha$  forest clouds and LLS evolve at different rates, and whether this indicates a difference in their origin. The redshift exponent  $\gamma$  derived in Stengler-Larrea et al. (1995) is  $\gamma = 1.55 \pm 0.39$ , more consistent with our estimate of  $\gamma = 2.58 \pm 0.27$  for the total sample than was the Sargent, Steidel, & Boksenberg (1989) estimate of  $\gamma = 0.68 \pm 0.54$  we used in Paper I. A value of  $\gamma = 2.58$  for the LLS is acceptable if one considers only the limited redshift range  $2 < z < 4$ , which contains most of the Ly $\alpha$  forest lines in our sample. However, this does not *rule out* a difference in the evolution rates, which would produce faster redshift evolution of  $\eta$ . To see the strength of this effect, we use our model A3, which is exactly the same as A2 up to  $N_{\text{HI}} = 10^{17} \text{ cm}^{-2}$  but switches over to the redshift evolution of Stengler-Larrea et al. (1995) above this column density. For purposes of comparison with Paper I, we have included that paper’s absorption-line model (based on Press & Rybicki 1993), here labeled A4. All of these models are summarized in Table 1 and displayed in Figure 2.

A conversion of models for the average column density distribution of intervening absorbers to estimates of the corresponding line optical depth  $\tau_s^{LF}(z)$  must also assume a distribution in line widths  $b$ . Our calculations assume the line width distribution inferred by Hu et al. (1995), which is a gaussian with  $\langle b \rangle = 28 \text{ km s}^{-1}$  and  $\sigma(b) = 10 \text{ km s}^{-1}$  but truncated below  $b = 20 \text{ km s}^{-1}$ . Strictly speaking, this distribution is not based on the full data sample we use to derive our column density models. We have performed calculations which assume different line width distributions, including simulations in which we assume all absorbers have  $b = 25 \text{ km s}^{-1}$  and  $b = 35 \text{ km s}^{-1}$ . The variation in line optical depth due to these differing line-width distributions is less than 5%. Our calculation of the He II line optical depth is dependent on the relation of the measured H I line widths to the corresponding He II line widths, since  $b_{\text{HeII}} = (0.5 - 1)b_{\text{HI}}$  (see §3).

Our models A1–A3 agree well with the observed number of Lyman limit systems. They are in

poor agreement with model A4 and with the observed H I Ly $\alpha$  decrements,  $D_A$ , found in various low-resolution surveys. Here,  $1 - D_A$  is the ratio of the fluxes below (1050 – 1170 Å in the QSO rest frame) and above ( $\lambda \geq 1216$  Å) the H I edge. Figure 3 shows this quantity, which is related to the effective optical depth by  $D_A = [1 - \exp(-\tau_{eff})]$ . We have included the  $D_A$  calculated from our quasar line lists, our models, and measurements from several low-resolution samples. Our models and line lists tend to show less absorption than is measured in the low-resolution observations, although there is a large scatter in the low-resolution measurements.

This discrepancy may indicate a shortcoming in the line-list sample, such as an insufficient completeness correction at low H I columns. There are other interpretations as well. The low-resolution observations are based on extrapolating a power-law continuum from longward of the Ly $\alpha$  emission line, while the high-resolution line lists involve local continuum fits on the shortward side. If the spectra have significant curvature, as indicated by the composite spectrum of Zheng et al. (1997), the low-resolution spectra will overestimate the continuum and  $D_A$  as well. The discrepancy could be also caused by a smooth Gunn-Peterson effect. It will be important to resolve this question. The apparent presence of breaks in the H I column-density distribution (Fig. 2) and the resulting deficit of observed lines around  $10^{15}$  cm $^{-2}$  have a large impact on the He II continuum opacity. In Paper I, we extrapolated the Press & Rybicki (1993) distribution up to  $10^{17}$  cm $^{-2}$ , giving an unphysical discontinuity in the column density distribution there. Since the Press & Rybicki distribution is based on Ly $\alpha$ -forest absorption, which is insensitive to the clouds with  $N_{HI} \sim 10^{17}$  cm $^{-2}$ , this extrapolation is doubtful, and the H I continuum opacities are almost certainly described better by our models A1–A3.

Although the spread among our models does serve to indicate the observational errors in our opacity estimates, we can get a better estimate of the errors involved by performing a “bootstrap resampling”, as discussed in Appendix B. This technique does not take into account errors in the observed columns, or systematic effects such as errors in the completeness functions or the results of clustering. As a result, this estimate is probably a minimal estimate of the errors involved. The H I and He II continuum opacities derived from the sample are shown in Fig. 4, together with the opacities derived from our models. The derived uncertainties are only about 15%, much smaller than the dispersion among estimates in the literature. Partly because our models A1 and A2 assume continuity of the H I column distribution, whereas our bootstrap error estimate does not, models A1 and A2 are not quite  $2\sigma$  apart from each other, despite our best efforts to maximize the difference. This difference should be sufficient to indicate the observational errors.

## 2.4. Diffuse IGM vs. Clouds

A framing question for the interpretation of the He II observations has been whether the absorption occurs in low-column Ly $\alpha$  clouds or in a smooth IGM. An implicit question is whether the distinction has any real meaning. A picture in which physically distinct clouds are embedded in a more uniform medium has been implied by models in which the clouds are pressure-confined

by surrounding hotter gas (Ostriker & Ikeuchi 1983) or represent self-gravitating bodies within a more tenuous medium (Rees 1986). Amplifying the latter hypothesis, Shapiro, Giroux, & Babul (1994) defined the IGM as gas whose thermal velocity exceeds the circular velocity of all of its encompassing structures, and is thus smeared out. Reisenegger & Miralda-Escudé (1995) used a modified Zel’dovich approximation to follow the evolution of structure, and suggested a division between clouds and IGM based on the local deformation tensor.

A more recent view, inspired by recent N-body/hydrodynamic simulations (e.g., Cen et al. 1994; Zhang et al. 1995, 1997; Miralda-Escudé et al. 1996; Hernquist et al. 1996), is that there is no physical motivation for a distinction. The distribution in velocity space and the physical state of the baryons determine the shape of the quasar absorption spectra, which may include features that have historically been associated with the “uniform IGM” and “clouds.” Rather than counting and tabulating the properties of discrete lines and measuring any remaining absorption trough, the new challenge is to directly compare the absorption profile of quasar spectra with that predicted by large-scale models for the evolution of density fluctuations combined with estimates of the metagalactic ionizing background. This has inspired promising new statistical methods (e.g., Croft et al. 1997; Miralda-Escudé et al. 1996).

A distinction between Ly $\alpha$  forest clouds and a “smooth” IGM remains useful even within this latest view. In this paper, we use the terms “cloud” or “absorber” to denote the structures that result in Ly $\alpha$  absorption lines (the “Ly $\alpha$  forest”) with H I column densities ranging from about  $10^{17}$  cm $^{-2}$  down to  $10^{12}$  cm $^{-2}$  and perhaps even lower. High-resolution spectra taken with the *Keck* Telescope (Hu et al. 1995) show that discrete absorption features exist whose equivalent widths correspond to column densities down to at least  $N_{HI} = 10^{12.3}$  cm $^{-2}$ . This may be taken to represent a cloud distribution whose number, line widths, and column densities are well characterized, and whose properties may be extrapolated to somewhat lower column densities.

As discussed above, models for the averaged mean intensity and shape of the metagalactic background depend in part on the averaged distribution in column density and redshift of the high column density end of the Ly $\alpha$  forest. It is likely that N-body/hydrodynamical simulations will continue to depend on these models, and hence on an empirical column density distribution, to translate their baryon distributions into absorption spectra. Recent *Keck* spectra at high S/N and high resolution (Fan & Tytler 1995; Cowie et al. 1995; Songaila & Cowie 1996) have shown that 50%–75% of the Ly $\alpha$  forest clouds with  $\log N_{HI} > 14.5$  have undergone some chemical enrichment, as evidenced by weak but measurable C IV and Si IV absorption lines. The typical inferred metallicities range from 0.003 to 0.01 of solar values (see Giroux & Shull 1997). Lyman limit systems have somewhat higher metal abundances (Reimers & Vogel 1993), with possible contributions from local sources of hot gas (Giroux, Sutherland, & Shull 1994; Gruenwald & Viegas 1993; Petitjean, Rauch, & Carswell 1994). The presence of these metals provides strong evidence for “feedback” from star formation. Evidently, many of the Ly $\alpha$  absorbers have been affected by physical processes besides gravitational clustering, perhaps outflows from star-forming regions or mergers of star-forming galaxies. These processes have not been reliably incorporated

into the current generation of large-scale simulations.

Although a fundamental theory of the IGM and Ly $\alpha$  forest is beyond the scope of the paper, we do require a physical model for the absorbers in order to infer, for example, the likely levels of He II present in an H I absorber. As a result, we summarize below the physical properties of our absorbers. We also show that they are compatible with the properties ascribed to the corresponding absorption lines by the results of large scale structure simulations.

One can show that absorbers down to  $N_{HI} \sim 10^{12} \text{ cm}^{-2}$  still have a density contrast with the mean diffuse IGM. By redshift  $z \approx 3\text{--}5$ , many of the baryons have already collapsed into galaxies and clouds. We take the baryon density to be  $\Omega_b h_{75}^2 = 0.038 \pm 0.007$ , corresponding to primordial  $D/H = (2.7 \pm 0.6) \times 10^{-5}$  (Schramm & Turner 1997). This density is an upper limit to baryons in the diffuse IGM. Suppose that a fraction  $f_{IGM}$  of the baryons resides in the diffuse IGM. The mean hydrogen density of the diffuse IGM at  $z \approx 3$  is then

$$\langle n_H \rangle = (1.16 \times 10^{-5} \text{ cm}^{-3}) \left( \frac{1+z}{4} \right)^3 f_{IGM}. \quad (9)$$

To produce an H I absorption cloud with column density  $N_{HI} = (10^{14} \text{ cm}^{-2})N_{14}$ , we first approximate the absorber as a slab of thickness  $L = (100 \text{ kpc})L_{100}$  with constant total hydrogen density  $n_H$ , H I density  $n_{HI}$ , and ionized hydrogen density  $n_{HII}$ . We assume that the cloud temperature is set by photoelectric heating at  $T = (10^{4.3} \text{ K})T_{4.3}$ .

If then we set the baryon density  $n_{HI} = N_{HI}/L$ , the mean hydrogen density in the cloud is (from § 2.2)

$$n_H = (5.9 \times 10^{-5} \text{ cm}^{-3}) J_{-21}^{1/2} T_{4.3}^{0.38} N_{14}^{1/2} L_{100}^{-1/2}, \quad (10)$$

assuming an ionizing background of  $J_{HI} = 10^{-21} J_{-21} \text{ ergs cm}^{-2} \text{ s}^{-1} \text{ Hz}^{-1} \text{ sr}^{-1}$  and a spectral index near 1 Ryd of  $\alpha_1 \approx 1.0$ , after filtering by the IGM. The cloud contrast factor is

$$\delta_c \equiv \frac{n_H}{\langle n_H \rangle} = (5.1) J_{-21}^{1/2} T_{4.3}^{0.38} N_{14}^{1/2} L_{100}^{-1/2} \left( \frac{1+z}{4} \right)^{-3} f_{IGM}^{-1}, \quad (11)$$

and approaches 1 at a column density

$$N_{HI} \approx (3.8 \times 10^{12} \text{ cm}^{-2}) f_{IGM}^2 J_{-21}^{-1} T_{4.3}^{-0.76} L_{100} \left( \frac{1+z}{4} \right)^6. \quad (12)$$

Therefore, for a diffuse fraction  $f_{IGM} \lesssim 0.5$  and standard values of the other scaling parameters, we see that clouds with  $N_{HI}$  at or below  $10^{12} \text{ cm}^{-2}$  retain some contrast with diffuse portions of the IGM. This is consistent with the results of numerical models (e.g., Zhang et al. 1997) which associate underdensities with these column densities but which also assume a low background of  $J_{-21} \sim 0.1\text{--}0.4$ .

In addition, many of the Ly $\alpha$  clouds probably have some flattening in order to avoid problems of having volume filling factors greater than 1 or exceeding the baryonic nucleosynthesis limit (Rauch & Haehnelt 1995; Madau & Shull 1996). We can address this question with the opacity

models of § 2.3. Let us suppose that almost all of the baryons are in clouds with  $10^{12}$ – $10^{17}$   $\text{cm}^{-2}$ . At  $z = 3$ , the clouds have  $L = (21, 17, 17, 6) J_{-21}^{-1}$  kpc for opacity models A1–A4, respectively. These thicknesses are much smaller than the observed  $\sim 200h_{75}^{-1}$  kpc transverse sizes of the Ly $\alpha$  clouds (Bechtold et al. 1994) consistent with the general flattening of such clouds in the numerical simulations. However, they are comparable to the estimated sizes of Lyman limit systems, consistent with evidence that suggests these systems are roughly spherical (Steidel et al. 1997). The volume filling factors are less than 1 in this model for columns down to  $N_{HI} = (2.1, 3.0, 3.0, 1.6) \times 10^{10}$   $\text{cm}^{-2}$ . If fewer baryons are in the Ly $\alpha$  forest, the thicknesses become even smaller.

The total hydrogen densities obtained in the above model are  $n_H = (4.1, 4.6, 4.6, 7.7 \times 10^{-3} \text{ cm}^{-3}) J_{-21} (N_{HI}/10^{17} \text{ cm}^{-2})^{1/2}$ . Based on QSO luminosity functions Q1 and Q2 with  $J_{-21} = 0.3$ – $1.0$ , we take the density in the clouds to be

$$n_H = (2 \times 10^{-3} \text{ cm}^{-3}) (N_{HI}/10^{17} \text{ cm}^{-2})^{1/2} \quad (13)$$

throughout our calculations. This assumption admittedly has large uncertainties, but the effect of density in our radiative transfer calculations will turn out to be small. This  $n_H$ – $N_{HI}$  relation is also favored by numerical simulations for  $N_{HI} < 10^{14.5}$   $\text{cm}^{-2}$  (e.g., Zhang et al. 1997).

## 2.5. Ionizing Emissivity

By now, it is clear that quasars produce an appreciable fraction of the H-ionizing radiation at high redshifts, and probably almost all of the He II-ionizing radiation. The observed quasars are probably sufficient to provide the flux deduced from the proximity effect at  $z \approx 2.5$ , within the uncertainties (Haardt & Madau 1996), as well as ionize the IGM (Miralda-Escudé & Ostriker 1992). The actual spectral index of quasars in the EUV has been determined only recently. Based on HST-FOC prism spectra of quasars with  $z_{em} \sim 3$ , Tytler et al. (1996) suggested an average spectral index of  $\alpha_Q = 1.5 \pm 0.2$  for 330–1300 Å in the quasar rest frame, a softer index than seen at higher wavelengths. Using FOC spectra of 41 radio-quiet quasars, most with  $z_{em} < 1.5$ , Zheng et al. (1997) find that the slope steepens below 1000 Å, producing a slightly softer index of  $\alpha_Q = 1.77 \pm 0.15$  for 350–1050 Å, with no clear redshift dependence. The results are completely consistent, given the different wavelength coverage. Zheng et al. find that they can explain the observed spectrum if photons are Compton-scattered above an H I Lyman continuum edge; this model implies that the frequency power-law continues up to the X-rays, where it does indeed match the observed spectrum (Laor et al. 1997).

To compute the ionizing photon emissivity, we use the empirical quasar luminosity function from Pei (1995). This fit uses a Gaussian dependence on redshift, implying a steep cutoff of the quasar emissivity at high  $z$ . The resulting comoving emissivity for ( $\nu > \nu_H$ ) can be expressed as

$$j_\nu = j_{H*} \left( \frac{\nu}{\nu_H} \right)^{-\alpha_s} \exp \left[ -\frac{(z - z_*)^2}{2\sigma_*^2} \right] (1 + z)^{\alpha_{BH}-1}. \quad (14)$$

We assume a spectral slope of  $\alpha_{BH} = 0.83$  from the B-band (4400 Å) to the H I Lyman edge (912 Å) to be consistent with the mean quasar spectra discussed above. Pei used values of  $\alpha_{BH} = 0.5$  and 1.0, but the value has little effect on the value of  $j_\nu$  because B-band observations of high- $z$  quasars fall fairly close to the Lyman edge. We refer to the emissivity model resulting directly from Pei’s luminosity function as model Q1. The parameters for this model are given in Table 2.

We also consider a variant, model Q2, that has more quasars at high redshifts. There are several reasons to consider such a model. It is possible that dust in intervening galaxies reduces the observed number of high- $z$  quasars. Model Q2 lies between the “medium” and “high” absorption cases of Fall & Pei (1993). In addition, there may be systematic biases against the detection of high- $z$  quasars. Finally, we shall see that the flux derived from model Q1 is insufficient to match that estimated from the proximity effect at high  $z$ , while model Q2 will be much more consistent. The Gaussian form assumed by Pei is well constrained at  $z < 3$ , but the falloff at  $z > 3$  is less certain and even a constant comoving density of quasars is not ruled out. On the other hand, a recent search (Shaver et al. 1996) for radio-loud quasars found none with  $z > 5$ , even though there should be no bias from dust in this case. This radio survey is consistent with model Q1 but not with model Q2, unless radio-loud quasars behave differently than the more numerous radio-quiet quasars.

An important question is at what epoch the universe became ionized in H I and He II (Shapiro & Giroux 1987; Donahue & Shull 1987). The average recombination rate in the universe is probably small enough that one can estimate this epoch simply by integrating the number of photons until it matches the number of atoms, assuming standard nucleosynthesis and neglecting the fraction of atoms that are not in the IGM or Ly $\alpha$  forest. We have done this for our quasar emission models. The universe reionizes in H I at  $z = 4.7$  in model Q2, but only at  $z = 3.7$  in model Q1. Thus, model Q1 may need to be supplemented by Lyman continuum emission from massive stars to produce the smooth evolution of H I opacity seen to redshifts as high as  $z = 4.7$  (Schneider, Schmidt & Gunn 1991b). For He II, the results depend slightly on the spectrum, but the ionized redshifts are not necessarily lower than for H I. In fact, even for model Q1 the spectrum must be as steep as  $\alpha_s = 2.3$  for He II reionization to be delayed to a redshift of  $z = 3.2$ , the highest redshift probed by current He II observations. The critical slope for He II ionization fronts to lie inside of H I fronts is  $\alpha_{cr} = 1.84$  for  $Y = 0.239$  (Giroux & Shull 1997), close to our standard value of  $\alpha_s = 1.8$ . This slope gives reionization epochs both H I and He II of  $z = 3.7$  and  $z = 4.7$  for models Q1 and Q2 respectively. Since the Pei luminosity function extends only to  $z = 4.5$ , our calculation thus involves a mild extrapolation. However, these luminosity functions are declining rapidly at high  $z$ , and may underestimate the population of quasars at  $z > 4$ . It thus seems likely that most of the universe has become ionized in He II by the observed redshifts.

As noted above, hot stars are another possible source of hydrogen-ionizing photons. In our radiative transfer models, we use a fit to the composite spectrum of an OB association undergoing a starburst (Madau & Shull 1996; Sutherland & Shull 1998). This spectrum is fairly hard

( $j_{st} \propto \nu^{-1.5}$ ) just above the H I edge, but it falls off rapidly past 45 eV with negligible radiation beyond 4 Ryd. Thus, the effect of starlight is like that of the decaying neutrinos in Sciama’s (1994) model, in that it can ionize H I effectively but not He II. Suppose the stellar and AGN emissivities at the H I edge are in the ratio  $\phi_{st} \equiv \dot{j}_{st}/\dot{j}_q$ . Then the spectral index from 1 to 4 Rydbergs is given by  $\alpha_s = \alpha_q + \ln(1 + \phi_{st})/\ln(4)$ . We would like to calculate an upper limit to  $\phi_{st}$  based on observations of  $\tau_{HeII}$ . However, as we shall see below, it is at present difficult to obtain an upper limit on  $\alpha_s$  from  $\tau_{HeII}$ , so this constraint is actually much weaker than the constraint relating H I Lyman continuum radiation to metal production in stars (Madau & Shull 1996). Future observations should change this situation (see § 5).

One could also consider the possibility that the Ly $\alpha$  clouds are photoionized by “local” sources—a class of sources (e.g., local starbursts) that dominate the ionizing flux at the observed clouds but contribute little to the background  $J_\nu^{bg}$  at an average point in space. We can actually rule out this scenario by the following argument. If clouds have a typical size  $R_{cl}$ , their space density  $n_{cl}$  is related to their redshift frequency by  $(dN/dz) = \pi R_{cl}^2 n_{cl} (dl/dz)$ , where  $dl$  is the proper length increment. Suppose that each cloud contains its own ionizing source, which dominates the ionizing flux out to the edge of the cloud. This requires its luminosity  $L_\nu^{loc}$  to satisfy  $L_\nu^{loc}/4\pi R_{cl}^2 \gtrsim 4\pi J_\nu^{bg}$ . These sources collectively produce an ionizing emissivity of  $\dot{j}_\nu^{loc} = n_{cl} L_\nu^{loc}/4\pi \gtrsim 4J_\nu^{bg} (dz/dl)(dN/dz)$ . In the source-function approximation discussed above, the additional background due to these “local” sources is  $J_\nu^{loc} \approx \dot{j}_\nu^{loc}/\kappa_\nu \gtrsim 4J_\nu^{bg} (dN/dz)/(d\tau_\nu/dz)$ . Considering the case of the H I Ly $\alpha$  forest clouds, which are easily visible for  $N_{HI} > 10^{13.5} \text{ cm}^{-2}$ , we find  $(dN/dz) \sim 220$  and  $d\tau_{HI}/dz \sim 3$  at  $z \sim 3$ . One can see that  $J_\nu^{loc} \gg J_\nu^{bg}$ , violating our original assumption that  $J_\nu^{loc}$  is a minor part of the background. This *reductio ad absurdum* shows that the abundant Ly $\alpha$  clouds really are a probe of the metagalactic background.

The above reasoning therefore provides strong justification for assuming a general metagalactic background of ionizing radiation that controls the ionization state of Ly $\alpha$  forest clouds. The argument is not quite as strong for Lyman-limit systems, which at  $z \approx 3$  have  $(dN/dz) \approx 2$ . Neither does it rule out the presence of a population of absorbers with  $N(\text{H I}) \geq 10^{15} \text{ cm}^{-2}$  that are dominated by their “local” radiation field. Giroux & Shull (1997) have argued that the high Si IV/C IV and low C II/C IV ratios found in a sub-sample of Ly $\alpha$  clouds with  $N(\text{H I}) \geq 10^{15} \text{ cm}^{-2}$  (Songaila & Cowie 1996) may be compatible with photoionization by a locally dominated radiation field.

## 2.6. Radiative Transfer Calculations

In Paper I, we used the source function approximation to relate the emitted ionizing spectrum to the He II/H I ratio. As a rule of thumb, the source function approximation is good only when emitted photons are absorbed within a Hubble length. The universe becomes less opaque as cosmic time increases, however, so this approximation is not as good for the case of HS1700+6416 ( $z_{em} = 2.74$ ) as for Q0302-003 ( $z_{em} = 3.29$ ). In addition, Haardt & Madau (1996, hereafter HM96;

see also Fardal & Shull 1993) have shown that several new processes alter  $\eta$  slightly, including emission from Ly $\alpha$  clouds in He II and H I lines and continua as well as self-shielding effects in high-column clouds. We have thus carried out radiative transfer calculations to derive  $\eta(z)$ .

The spatially-averaged specific intensity at a given redshift and frequency (in  $\text{erg s}^{-1} \text{cm}^{-2} \text{Hz}^{-1} \text{sr}^{-1}$ ) is given by

$$J_\nu(z_{obs}) = \int_{z_{obs}}^{\infty} \left( \frac{1+z_{obs}}{1+z} \right)^3 j_\nu(\nu_{em}, z) \frac{dl}{dz} \exp(-\tau_{eff}) dz \quad (15)$$

(Bechtold 1993), where  $j_\nu$  is the proper volume emissivity ( $\text{erg s}^{-1} \text{cm}^{-3} \text{Hz}^{-1} \text{sr}^{-1}$ ) equal to  $\epsilon(\nu, z)/4\pi$  in the notation of HM96,  $dl/dz = (c/H_0)(1+z)^{-2}(1+\Omega_0 z)^{-1/2}$  is the proper length increment, and  $\tau_{eff}$  is the effective continuum optical depth from  $z$  to  $z_{obs}$ , as given by equation (3). We note here that, although the flux depends on many parameters, it is at least independent of the cosmological parameters  $H_0$ ,  $\Omega_0$ , and the cosmological constant,  $\Lambda$ , as long as the emissivity is actually determined observationally, as in a quasar survey, and not assumed *a priori*. First of all, the optical depth  $\tau$  is independent of these parameters. The emissivity  $j_\nu$  depends on the quasar luminosities and densities as  $j_\nu \propto n_Q L_{Q,\nu}$ , where an integration over the luminosity function is implied. In turn,  $L_{Q,\nu} \propto r_A^2$  where  $r_A$  is the angular size distance. The quasar density is  $n_Q \equiv dN_Q/dV$  with  $N_Q$  the number of quasars seen in a survey, and  $V$  the proper volume sampled, or  $n_Q = (dN/dz)/(dl/dz)/r_A^2$ . The ionizing flux is proportional to  $j_\nu(dl/dz) \propto n_Q L_{Q,\nu}(dl/dz) \propto dN/dz$ , an observed quantity, and thus is independent of  $H_0$ ,  $\Omega_0$ , and  $\Lambda$ .

If we use the two luminosity functions from Pei (1995), with  $\Omega_0 = 1$  and  $\Omega_0 = 0.2$ , and correct for the quasar spectral slope that differs as well, we find that the low- $\Omega_0$  model gives a higher photoionization rate by about 40%. This difference cannot be rooted in the original observations. Instead, the difference arises from the method by which the QSO luminosity function is propagated from low- $z$  to high- $z$  assuming pure luminosity evolution. This parameterization depends only on  $z$  and not on appropriate cosmological distances and luminosity evolution parameters. Thus, this introduces a dependence on  $H_0$  and  $\Omega_0$ .

In our computer code, we compute the ionizing flux by setting up a grid in  $(z, \nu)$  space and propagating the flux according to equation (15) along photon trajectories,  $\nu \propto (1+z)$ . The column ratio  $\eta$  is adjusted to match the photoionization rates at each epoch. The radiative transfer models incorporate emission from the H I Lyman continuum and the He II Lyman, Balmer, and 2-photon continua, as well as He II Ly $\alpha$  emission from the clouds. In order to find the opacity of He II, we compute  $N_{HeII}$  in an approximate manner as a function of  $N_{HI}$ , the photoionization rates  $\Gamma_{HI}$  and  $\Gamma_{HeII}$ , and the cloud density (see § 2.4). Details of this treatment are explained in Appendix A. We neglect the opacity of He I. Miralda-Escudé & Ostriker (1992) and Haardt & Madau (1996) have considered the effects of He I theoretically and conclude that if the sources of ionization are quasars or stars, the net effect is small, but not completely negligible. For our new models for the distribution and physical properties of absorbers, our conclusions are similar, and we discuss the

small effects of He I opacity in Appendix C. In the few absorbers at  $z > 2$  for which measurements of He I absorption exist (Reimers et al. 1992; Reimers & Vogel 1993), our assumed density and photoionization models are consistent with observations (see Appendix C).

### 3. RESULTS

A typical spectrum resulting from our radiative transfer code is shown in Figure 5. Parameters commonly used to describe the spectrum are:  $J_{HI}$  and  $J_{HeII}$ , the fluxes at the ionization thresholds of H I (1 Ryd) and He II (4 Ryd);  $S_L \equiv J_{HI}/J_{HeII}$ ; and  $B$ , the strength of the break at 4 Ryd. The effect of the line and continuum emission can clearly be seen in the He II 304 Å line and the recombination continua, although the contribution from He II 2-photon emission is spread over a large frequency range and is thus difficult to discern. The ionization edges are not sharp, but blurred by redshifting below the threshold and by recombination radiation above it. The spectrum is poorly approximated by a power law above the ionization thresholds, unless the cloud re-emission is omitted. We *define* the effective threshold power-law indices  $\alpha_1$  and  $\alpha_4$  by the relations  $\Gamma_{HI} = (2.53 \times 10^9 \text{ sr cm}^2 \text{ erg}^{-1} \text{ s}^{-1}) J_{HI} [5/(3 + \alpha_1)]$  and  $\Gamma_{HeII} = (6.33 \times 10^8) J_{HeII} [5/(3 + \alpha_4)]$ , which hold true for pure power-law spectra. For  $z = 3$ , absorption model A2, and quasar model Q2 with spectral index  $\alpha_s = 2.1$ , these effective indices are  $\alpha_1 = 1.4$  and  $\alpha_4 = 1.0$  omitting cloud re-emission and  $\alpha_1 = 2.6$  and  $\alpha_4 = 6.6$  including re-emission. Using the metagalactic background from our simulations, we have calculated the equilibrium temperatures in photoionized clouds with and without re-emission. In general, temperatures are 10% lower if re-emission is included.

The qualitative appearance of the spectrum is similar to that in HM96. However, as discussed in Appendix A, the differences in our treatment of self-shielding and cloud re-emission lead to values of  $\eta$  that are  $\sim 70\%$  higher than theirs. This difference is small compared to the differences induced by uncertainties in the observational parameters.

The effect of stellar emission is shown in Figure 6, and the evolution of the spectrum with redshift in Figure 7. The intensity of the spectrum peaks at  $z \sim 3$ . The features in the spectrum gradually disappear with cosmic time as the universe becomes less opaque. The break parameter in Figure 7 evolves approximately as  $B \approx 3.2z$  over the plotted redshift range ( $0.5 < z < 5$ ), although  $B$  at a given redshift depends strongly on the assumed  $\eta$  and opacity model.

The intensity of the ionizing background in these models spans a large range, depending on the assumed quasar luminosity function, the stellar contribution, and the opacity model. The H I proximity effect gives an independent estimate of the intensity, although many systematic uncertainties could be involved. Recently, Giallongo et al. (1996) found a value of  $J_{HI} \approx (5 \pm 1) \times 10^{-22} \text{ erg s}^{-1} \text{ cm}^{-2} \text{ Hz}^{-1} \text{ sr}^{-1}$ , while Cooke, Espey, & Carswell (1997) found  $J_{HI} \approx 10^{-21 \pm 0.4} \text{ erg s}^{-1} \text{ cm}^{-2} \text{ Hz}^{-1} \text{ sr}^{-1}$ , with very little evolution over the redshift range of  $2.0 < z < 4.5$ . These estimates assume that the quasar has the same spectrum as the ionizing background; in view of the bumps and wiggles in the background shown in Figure 6, this is unlikely.

The photoionization rate  $\Gamma_{HI}$  is a better measure of the integrated background. Assuming that the clouds see the “bare” spectrum of the quasar observed in the proximity effect, and that this bare spectrum typically has a spectral index  $\alpha_s = 1.8$  as argued above, the conversion from the estimated fluxes to the photoionization rate is  $\Gamma_{HI} = (2.64 \times 10^9 \text{ sr cm}^2 \text{ erg}^{-1} \text{ s}^{-1}) J_{HI}$ , based on the photoionization rate equation above.

An additional constraint on the photoionizing background radiation comes from N-body hydrodynamical simulations of the Ly $\alpha$  forest (e.g., Cen et al. 1994; Hernquist et al. 1996). For these optically thin clouds, the column density distribution determines, via recombination theory, the ratio of  $n_H^2/\Gamma_{HI}$  times  $dl/dz$ , or equivalently  $\Omega_b^2 h^3/J_{HI}$ . One recent simulation (Zhang et al. 1997) finds that, in order to reproduce the Ly $\alpha$  column density distribution, the ionization rate must lie in the range  $0.3 < \Gamma_{-12} < 1.0$ , somewhat lower than estimates  $\Gamma_{-12} \approx 2 - 3$  ( $J_{-21} \approx 1$ ) from the proximity effect. For  $\alpha_s \approx 1.8$ , the range  $\Gamma_{-12} = 0.3 - 1.0$  corresponds to  $0.1 < J_{-21} < 0.4$  (see Fig. 6). Similar conclusions are found from other simulations (Miralda-Escudé et al. 1996; Hernquist et al. 1996). Thus, one must conclude that an inconsistency still exists for the ionizing radiation field inferred from the proximity effect, from Ly $\alpha$  simulations, and from cosmological radiation transfer of QSO sources. In the most extreme case,  $\Gamma_{-12} = 0.3$  from simulations and  $\Gamma_{-12} = 2.6$  from the proximity effect, the discrepancy could be almost a factor of 10. Moreover, the discrepancy is larger when one adopts the “standard” value  $\Omega_b h_{75}^2 = 0.022 \pm 0.018$  from Big Bang Nucleosynthesis (Copi, Schramm, & Turner 1995) instead of the somewhat higher value  $\Omega_b h_{75}^2 = 0.038 \pm 0.007$  implied by deuterium measurements in two high- $z$  QSO absorption systems (Tytler, Fan, & Burles 1995). Thus, many details of these estimates remain to be pinned down.

Estimates of the photoionization rates are shown in Figure 8, along with the results of our models. These rates are well described by the analytic form of HM96,

$$\Gamma_{HI} = A_\Gamma (1+z)^{B_\Gamma} \exp[-(z-z_c)^2/S]. \quad (16)$$

This is not surprising, since we are both using versions of the Pei (1995) luminosity function. With spectral slope  $\alpha_s = 2.1$ , we find  $A_\Gamma = 0.56 \times 10^{-12} \text{ s}^{-1}$ ,  $B_\Gamma = 0.60$ ,  $z_c = 2.22$ , and  $S = 1.90$  for model Q1, and  $A_\Gamma = 1.26 \times 10^{-12} \text{ s}^{-1}$ ,  $B_\Gamma = 0.58$ ,  $z_c = 2.77$ , and  $S = 2.38$  for model Q2. If the proximity effect really gives an accurate estimate of  $J_{HI}$ , the unmodified Pei (1995) luminosity function (model Q1) fails to produce enough photons at high redshifts ( $z > 3.5$ ). The dramatic fall-off in quasar flux past this point also might tend to produce a sharp increase in the opacity of the Ly $\alpha$  forest, which clashes with the observed smooth behavior seen in quasars with redshifts up to  $z_{em} = 4.9$  (Schneider, Schmidt, & Gunn 1991b). Our model Q2 is in agreement with the proximity effect estimates, as is model Q1 if it is supplemented by a large contribution from star-forming galaxies. In view of the objections to model Q2 raised by the radio observations of Shaver et al. (1996), this constitutes circumstantial evidence for a significant stellar contribution to the ionizing background at high  $z$ .

In Figure 9 we show the column ratio  $\eta(z) = N_{HeII}/N_{HI}$  that results from our photoionization models. This value is only valid for the optically thin clouds, as self-shielding affects  $\eta$  in the

thicker clouds. For comparison with Paper I, we have shown the results of the source-function approximation. Since the universe is less opaque in H I than in He II, more of the H I-ionizing flux is redshifted away, and  $\eta$  is smaller than in the source-function approximation.

Figure 9 also shows the effects of our main parameters upon  $\eta$ . It can be seen that the most important variables are the intrinsic spectral index  $\alpha_s$  of the ionizing sources and the continuum opacity model. The quasar luminosity function, the cloud density, and the cloud emissivity are less important. The large difference between A4 and the other absorption models is explained simply by Figure 4, where the continuum opacities of both species but especially that of He II are much higher than in the other models. The parameter  $\eta$  depends on the ionizing emissivity in two distinct ways. The smaller the He II-ionizing intensity, the easier it is to make almost all the He into He II in the clouds that dominate the He II continuum opacity, saturating  $d\tau_{HeII}/dz$  and lowering  $\eta$ . This effect is generally confined to large redshifts ( $z \gtrsim 3.5$ ), where the ionizing flux is low, with our assumption for the density within the clouds. For  $z \sim 3$ , the ionizing intensity is large; while it drops again at low redshifts, the continuum opacity is not as important as cosmological redshifting there. The change with redshift of the ionizing emissivity also affects  $\eta$ . The ionizing photons seen at a given point in space come from a range of redshifts; because the universe is less opaque in H I than in He II, this range is larger for H I. Consequently, an increase in ionizing emissivity with redshift tends to increase the H I-ionizing flux relative to the He II-ionizing flux and thus increase  $\eta$ . Both of these effects make  $\eta$  higher in model Q2 than in model Q1.

With our QSO emission models, which peak at  $z \sim 3$ ,  $\eta$  increases slightly with redshift up to  $z \sim 4$ . Beyond this redshift He II becomes a majority species and equation (7) is no longer valid. The increase before this point is slight over the observable range of redshifts, because we have assumed the shapes of the column density distribution and ionizing spectrum to be constant with redshift. Between  $z = 2.4$  (HS1700+6416) and  $z = 3.15$  (Q0302-003),  $\eta$  increases by only 5–10%.

We find that the cloud re-emission contributes a fair fraction,  $\sim 20\%$ , of the total ionizations of both H I and He II at  $z \approx 3$ . However, the fractional increase is roughly the same for both species, so the net effect on  $\eta$  is not large. For the purpose of calculating  $\eta$  to within  $\sim 5\%$ , we could leave out all cloud emission except for the Lyman recombination continuum. However, these diffuse emission processes may have a larger effect on photoionization of metal ions.

In Figure 10 we have plotted the intrinsic (emitted) index  $\alpha_s$  versus  $\eta$  and the spectral index  $\alpha_b$  of the background at a redshift of  $z = 3$ . This plot clearly displays the strong dependence of  $\alpha_b$  on  $\alpha_s$  discussed in § 2.2. If quasars are the principal source of ionizing photons, our models predict a plausible range for the column ratio of  $25 < \eta < 400$ . We would like to use the He II Ly $\alpha$  absorption measurements to constrain the models further.

The dependence of the  $\tau_{HeII}$  on the various parameters is shown in Figures 11 and 12. For the parameters chosen,  $\tau_{HeII}$  has mostly converged by a lower limit of  $N_{HI}^{\min} \sim 10^{11}\text{--}10^{12} \text{ cm}^{-2}$ . Mildly damped He II lines, with  $N_{HeII} \gtrsim 10^{18} \text{ cm}^{-2}$ , make a minor contribution to  $\tau_{HeII}$ , as can

be seen by the turn-down around  $N_{HI} \sim 10^{17} \text{ cm}^{-2}$  in Figure 11. The He II Ly $\alpha$  optical depth depends not only upon  $\eta$  and the absorption-line model, but also on the line velocity widths, parameterized by Doppler width  $b_{HeII} = \xi_{HeII} b_{HI}$ , and on the IGM density. If we simply try the combinations of absorption models, spectra, and luminosity function shown in Figure 9, choose  $N_{min} = 10^{11}$  or  $10^{12} \text{ cm}^{-2}$ , and consider the extremes of either pure thermal ( $\xi_{HeII} = 0.5$ ) or pure bulk-velocity line broadening ( $\xi_{HeII} = 1$ ), we find that *none* of the individual parameters are constrained by the He II measurements. A value of one parameter that minimizes  $\tau_{HeII}$  can be traded off against other parameters that maximize it. (Our criterion for a successful value is that it lie within the  $2\sigma$  boundaries of the observed quasars; in practice, the models are constrained mainly by HS1700+6416. It is worth keeping in mind, though, that fluctuations in the observed optical depth are likely to be substantial, as explored in the next section, and the D96 limits may be an underestimate of the true uncertainty.) For the successful models,  $\eta$  falls in the range 70–400. However, most of these successes come with the deprecated absorption model A4, which gives a higher  $\eta$  by a factor 2–3 than other models.

For example, one can satisfy the optical depth constraint with bulk motions,  $N_{min} = 10^{11} \text{ cm}^{-2}$ , a spectral index of  $\alpha_s = 2.1$ , and the quasar model Q2, giving  $\eta = 125$  and  $\tau_{HeII} = 1.12$  at  $z = 2.4$ ; we will refer to this as our “standard” model below. If we define the Lyman forest to consist only of clouds with  $N_{HI} > 10^{12} \text{ cm}^{-2}$ , it is still possible to satisfy the observed limits without invoking a smooth Gunn-Peterson effect. Absorption model A4 and quasar model Q2 with  $\alpha_s = 1.8$  give  $\eta = 120$ , and, with bulk motions, produce  $\tau_{HeII} = 1.07$  at  $z = 2.4$ . Thus, pure line-blanketing can explain at least the mean level of absorption. As shown in Figure 12, however, this requires some combination of high  $\alpha_s$ , low  $N_{min}$ , maximal Doppler widths, and a favorable opacity model, particularly if we restrict our attention to the favored opacity models A1–A3. There is thus some weak evidence for a diffuse Gunn-Peterson effect and/or a stellar contribution to the ionizing background.

The above results are even less restrictive if a diffuse Gunn-Peterson effect is allowed, since we now have an additional free parameter. Nevertheless, we can look for a lower limit on the column ratio  $\eta$  by considering the maximal contribution to  $\tau_{HeII}$  from the Ly $\alpha$  forest and diffuse IGM at a given  $\eta$ . Fang & Crofts (1995) found evidence for a small Gunn-Peterson effect in H I ( $\tau_{GP} = 0.115 \pm 0.025$ ), although as we have argued above this could also be induced by a turnover in the quasar spectrum. We take  $\tau_{HI}^{(GP)} < 0.19$  as an upper limit, which corresponds to  $\tau_{HeII}^{(GP)} < 0.0475\eta$ . The argument of Fang & Crofts includes an extrapolation of the Ly $\alpha$  forest down to  $N_{min} = 10^{12} \text{ cm}^{-2}$ . By considering model A2 with this lower limit and  $\xi_{HeII} = 1$ , we get a Ly $\alpha$  forest contribution of  $\tau_{HeII}^{(LF)} = 0.30$  at  $\eta = 10$ . Combined with the Gunn-Peterson opacity, this is enough to account for the observations of D96 within  $2\sigma$ . We thus find a lower limit of  $\eta > 10$ .

A corresponding upper limit on  $\eta$  *cannot* be set this way. Assuming that He II has not yet reionized, so that all the He in the clouds is in the form of He II, and using the density model of equation (13), we obtain  $\eta_{max} = 144 \Gamma_{-12} (N_{HI}/10^{17} \text{ cm}^{-2})^{-1/2}$  up to  $N_{max} = 10^{17} \text{ cm}^{-2}$ , where the H I becomes self-shielded and  $\eta_{max}$  decreases sharply. If we now adopt unfavorable

assumptions of thermal linewidths,  $N_{min} = 10^{12} \text{ cm}^{-2}$ , and absorption model A1, we obtain  $\tau_{HeII} = 1.0$  at  $z = 2.4$ , in perfect agreement with the observations of D96. This is because the high  $\eta$  simply pushes the lines further up the saturated portion of the curve of growth. In this case  $\tau_{IGM}^{LF} \lesssim 0.2$ , showing that a fraction  $f_{IGM} < 3 \times 10^{-4}$  of the baryons are in structures with column density less than  $10^{12} \text{ cm}^{-2}$ . This seems physically implausible, but we would not venture to calculate an upper limit to  $\eta$  based on this argument.

It has in fact been suggested that the high He II optical depths towards Q0302-003 (Jakobsen et al. 1993) and the redshift dependence of the Si IV/C IV ratio (Songaila & Cowie 1996) both constitute evidence that ionization bubbles around individual quasars may have not yet overlapped at a redshift of  $z \approx 3.2$ . Reimers et al. (1997) suggests a similar explanation for the patchy He II absorption observed at  $z \approx 2.9$  towards HE2347-4342. We consider this explanation unlikely for two reasons mentioned above: the total number of 4 Ryd continuum photons emitted by this redshift is likely to be sufficient to fully ionize helium, while the space between the Ly $\alpha$  lines must be extraordinarily clear of gas at  $z \lesssim 3.2$  according to the flux measurements of Hogan et al. (1997). Although these statements depend on the poorly known QSO luminosity function at  $z > 4$  and uncertain ionizing spectra above 4 Ryd, we have nevertheless considered what would happen to  $\eta$  if the non-overlapping I-front explanation was correct. If we mimic the overlap of He III spheres by fixing  $\eta$  to an arbitrary high value for  $z \geq 3.2$  and then releasing it, we find that  $\eta$  recovers by  $z = 2.7$  to the value it has in our standard models. Observations of HS1700+6416 thus cannot help us to decide this question; future observations should preferably include some quasars at  $2.7 < z < 3.2$ .

Our results show that the mean He II Ly $\alpha$  opacity  $\tau_{HeII}$  and the He II/H I ratio  $\eta$  are not strongly constrained by theory at this point, as they are too sensitive to the observational parameters. In addition,  $\tau_{HeII}$  is not uniquely determined by  $\eta$ , as the Doppler widths and the distribution of low-column gas are also involved. However, if it were possible to determine  $\eta$  accurately from observations that resolve the He II lines, its sensitivity to the background spectrum would tightly constrain the spectrum, as discussed in § 2.5.

#### 4. HE II ABSORPTION FLUCTUATIONS

We have argued for a picture in which the He II absorption occurs in density structures where helium is mostly photoionized to He III by quasars. To explain the mean level of the absorption, it appears that  $N_{HeII}/N_{HI} \equiv \eta \sim 100$ . As a result, the universe is optically thick to He II-ionizing radiation at high redshifts. A consequence of this picture, however, is that there should be fluctuations in the He II absorption, from both intrinsic structure in the gas and fluctuations in the level of the ionizing background. Some questions then arise: how large should these fluctuations be? If we wish to find the mean level of absorption, must we observe many different quasars at a given redshift? How can one distinguish between fluctuations in the gas density and in the ionization level? What can these fluctuations tell us about the properties of

quasars and the process of structure formation? In this section we address these questions.

#### 4.1. Intrinsic fluctuations

The very existence of discrete absorbers (“clouds”) implies fluctuations in the gas density at high redshifts. Since the clustering of Ly $\alpha$  clouds with  $N_{HI} \sim 10^{13} \text{ cm}^{-2}$  is small (Cristiani et al. 1997), it is probably sufficient to regard the random fluctuations from these clouds as a Poisson process. However, the clustering of clouds with lower columns, which produce a large portion of the He II Ly $\alpha$  absorption, is not known observationally. We will assume that Poisson statistics apply to these clouds as well. We also assume that the smooth IGM component, if present, does not fluctuate. In our Poisson idealization, the absorption loses correlation over velocity scales of  $\sim 30\xi_{HeII}^{-1} \text{ km s}^{-1}$ , since each absorption line is independent. Observations (Cristiani et al. 1997) and hydrodynamical simulations (Miralda-Escudé et al. 1996) support the notion that the clouds are very weakly clustered beyond  $\sim 150 \text{ km s}^{-1}$ .

This point of view is, of course, naive. In hydrodynamical simulations of the IGM, as in the real universe, no distinction is made between the clouds and the IGM. Local density maxima in the simulations are generally fairly sharp, which gives rise to the appearance of “clouds”, while local density minima are generally less sharp. If one chooses to define an IGM as the matter outside detectable clouds, it will have large fluctuations in optical depth. Since the density structure reflects the large-scale structure of the universe, there is no *a priori* reason to expect the clouds to obey Poisson statistics. In our defense, we can offer two reasons for proceeding: first, our method at least gives an estimate for the fluctuations that can be improved upon in future work. Also, an estimate based on the observed almost-Poisson nature of the H I Ly $\alpha$  is in the same spirit as semi-analytic treatments (Bi & Davidsen 1996), which assume a simplified global model for density fluctuations and reproduce many of the qualitative properties of the IGM and absorbers seen in the output of hydrodynamical simulations.

The level of fluctuations expected from variation in cloud numbers is easy to estimate. We have found that half of the He II absorption is due to clouds with  $N_{HI} \gtrsim 5 \times 10^{12} \eta_{100}^{-1} \text{ cm}^{-2}$ , which (in model A2) have a line density  $d\mathcal{N}/dz \sim 590[(1+z)/4]^{2.6} \eta_{100}^{0.5}$ . Using our Poisson idealization, we can guess that, over an observed redshift interval  $\Delta z_{obs}$ , the fluctuations in optical depth would satisfy  $(\Delta\tau/\tau)_{HeII} \sim [\Delta z_{obs}(d\mathcal{N}/dz)]^{-1/2} \approx 0.041 \eta_{100}^{-0.25} \Delta z_{obs}^{-0.5} [(1+z)/4]^{-1.3}$ . From Monte Carlo simulations with our model column density distributions, we have found a slightly lower result,

$$\left(\frac{\Delta\tau}{\tau}\right)_{HeII} \approx 0.03(\xi_{HeII}\eta_{100})^{-0.1} \Delta z_{obs}^{-0.5} \left[\frac{1+z}{4}\right]^{-1.0}. \quad (17)$$

Here we have defined  $\tau \equiv -\log(\bar{T})$  where  $\bar{T}$  is the mean transmission within the redshift interval. The exponents differ slightly from their expected values because the absorption is beginning to be nonlinear ( $\tau_{HeII} \gtrsim 1$ ). For the observations of D96, which measured He II absorption with  $\tau_{HeII} = 1.00 \pm 0.07$  in the redshift range  $2.23 < z < 2.60$ , we expect intrinsic fluctuations in optical

depth of about  $\delta\tau_{\text{HeII}} = 0.06(\xi_{\text{HeII}}\eta_{100})^{-0.1}$ , of the same order as the observational error from photon statistics.

#### 4.2. Ionization fluctuations

Thus far, our computations have assumed the ionizing flux to be uniform in space. However, as pointed out by Zuo (1992), much of the ionizing flux comes from bright but rare quasars, and there should actually be substantial variation in the flux level from point to point in space. Fardal & Shull (1993, henceforth FS93) calculated the consequent statistical effect on the H I Ly $\alpha$  forest, predicting a weak, large-scale correlation. It is intriguing that such a correlation was found in the data analysis of Press & Rybicki (1993), although the authors caution that the correlation is at the expected level of systematic errors.

In the case of He II, the ionizing flux is even more likely to come from a few discrete sources. Star-forming galaxies may produce a large fraction of the H I-ionizing photons but are unlikely to emit appreciable He II-ionizing photons (Sutherland & Shull 1998). Even if quasars are the main sources of both types of photons, the universe is more opaque in the He II continuum than in H I (see Fig. 4). Thus, far fewer quasars contribute to the flux at a given point, and the resulting variations in the He II ionization level are much larger than those in H I. Effects on the He II absorption can show up in three ways: as the proximity effect, where the quasar providing the background source also provides the enhanced ionization; as the influence of known quasars on neighboring lines of sight; and as a statistical effect, independent of knowledge of the positions of any observed quasars. We discuss the latter here.

How large are these statistical fluctuations in the He II line absorption expected to be? To answer this, we adapt the methods and notation that FS93 used to discuss the analogous case of ionization fluctuations in the H I forest. We assume for now that quasars emit ionizing radiation isotropically and are not variable except on cosmological time scales. As in FS93, we conduct simple Monte Carlo experiments, placing a sample of randomly distributed quasars in a three-dimensional box and seeing what effect this has on the optical depth along a line of sight. Here, we consider only the *mean* optical depth at a given wavelength. For now, we ignore the intrinsic fluctuations in the line absorption, just as we ignored the ionization fluctuations in § 4. Later we will give examples that combine the two effects.

We draw our sample of quasars from the Pei luminosity function with  $\Omega_0 = 1$  (our model Q1), with a cutoff imposed three magnitudes fainter than the characteristic luminosity  $L_z$ . The comoving density of the quasars above this threshold is  $\phi = 2.4 \times 10^{-5} h_{75}^3 \text{Mpc}^{-3}$ , independent of redshift, since pure luminosity evolution is assumed. Emission from fainter quasars could smooth out the flux but is not well-constrained observationally. However, we do account for the re-emitted radiation, representing it as a perfectly smooth background radiation field. We found above that it typically contributes  $\sim 20\%$  of the He II ionizations, so we take the quasar flux fraction to be

$f_Q = 0.8$ .

In FS93, the quantity calculated was the correlation function of the number density of H I clouds. In the He II case, we would instead like to know the statistical properties of the optical depth  $\tau_{HeII}$ . There are two cases to consider, depending on whether the absorption is dominated by discrete lines or by a diffuse IGM. In both cases the density of He II ions at a given point  $\vec{x}$  goes like  $[J_{HeII}(\vec{x})]^{-1}$ , barring any *dynamical* effect of the ionizing flux on the absorbing gas. However, equation (1) shows that the optical depth of a diffuse IGM scales as  $\tau_{HeII}^{GP} \propto [J_{HeII}(\vec{x})]^{-1}$ . The optical depth of discrete lines is less sensitive to the flux,  $\tau_{HeII}^{LF} \propto [J_{HeII}(\vec{x})]^{1-\beta}$  (equation 2). We found that  $\beta \approx 1.5$  for the column densities that contribute the most to the He II line opacity (§ 2.3). In reality, the behavior may be intermediate between these two cases. These cases are equivalent to the formalism of FS93 for the number density of H I Ly $\alpha$  clouds, with  $\beta = 2.0$  and  $\beta = 1.5$  respectively.

The most important difference from the H I fluctuations is a shorter attenuation length, defined as the inverse of the continuum opacity. For example, if we evaluate opacity model A2 with  $\alpha_s = 2.1$  and  $\eta \approx 100$  at the mean energy,  $h\nu = [(\alpha_s + 3)/(\alpha_s + 2)]h\nu_{HeII} = 5.0$  Ryd, of a He II-ionizing photon, we find a comoving attenuation length of

$$r_0 \equiv \frac{dl/dz}{d\tau_{HeII}/dz} = \frac{(500h_{75}^{-1}\text{Mpc}) \left(\frac{1+z}{4}\right)^{-1.5}}{13.9 \left(\frac{1+z}{4}\right)^{2.6}} \approx (36 \text{ Mpc})h_{75}^{-1} \left(\frac{1+z}{4}\right)^{-4.1}. \quad (18)$$

This gives only  $\bar{N} = 1.1[(1+z)/4]^{-12.3}$  quasars brighter than our luminosity threshold within a “flux sphere”, or one attenuation length. The rapid diminution of this number with redshift suggests that the spatially-averaged models used in § 3 may break down as  $z$  increases beyond 3.

In our Monte Carlo simulations, we assume that the flux drops off as  $r^{-2}e^{-r/r_0}$  where  $r$  is the distance from the quasar (a more sophisticated treatment would treat the opacity in a Monte Carlo fashion as well, and integrate the flux over frequency to get the ionization rate). We then adjust the ionization level and resulting optical depth at each point for the flux observed at that point, as discussed above. As expected, we see substantial variation in the mean absorption, which we can describe statistically in several ways.

The main statistic used in FS93 was the correlation function of the normalized absorption. The correlation function at zero separation is the variance, denoted by  $\xi_0$  in FS93. The  $1\sigma$  level of the fluctuations in the local mean optical depth, which we call  $(\delta\tau/\tau)_{HeII}$ , is the square root of the variance. In our Monte Carlo simulations, we find that the local fluctuations in the He II Ly $\alpha$  optical depth occur at a level

$$(\delta\tau/\tau)_{HeII} = \begin{cases} 0.19[(1+z)/4]^{2.1} & \text{(cloud-dominated);} \\ 0.33[(1+z)/4]^{2.2} & \text{(IGM-dominated).} \end{cases}$$

We have depicted this level of fluctuations by the shaded bands in Figure 1. However, this is a somewhat theoretical quantity, since the small-scale variations are dominated by the intrinsic

fluctuations in the gas properties. We also calculate the fluctuations within a fixed redshift interval, as in § 4:

$$(\Delta\tau/\tau)_{HeII} = \begin{cases} 0.078 \Delta z_{obs}^{-0.4} [(1+z)/4]^{2.9} & \text{(cloud-dominated);} \\ 0.15 \Delta z_{obs}^{-0.4} [(1+z)/4]^{3.2} & \text{(IGM-dominated).} \end{cases}$$

In both cases, the fluctuations with IGM-dominated absorption are nearly twice as strong as in the line-dominated case, because a smooth IGM is more sensitive to flux variations than discrete clouds. The ionization fluctuations within large redshift intervals dominate the expected intrinsic fluctuations, especially at higher ( $z \gtrsim 3$ ) redshifts.

The correlation length for H I fluctuations—the separation at which the correlation function falls off appreciably, say by 1/2—was found in FS93 to be a substantial fraction of the attenuation length  $r_0$ . For He II, we estimate a correlation length in redshift space of  $\Delta z \approx 0.06[(1+z)/4]^{1.1}$ , corresponding to a comoving length of  $\Delta r \approx 30h_{75}^{-1}[(1+z)/4]^{-0.4}$  Mpc or a velocity difference of 4000 km s<sup>-1</sup>. The fluctuations due to quasar ionization thus occur on larger scales than fluctuations induced by gravitational clustering. Indeed, the scale is so large that it may interfere with attempts to measure the average He II line opacity. A large redshift path is necessary to make sure the derived average is accurate. It is interesting to note that in the published spectrum of HS1700+6416 (D96), there are two apparent emission peaks (at  $\lambda_{obs} \approx 960$  Å and 1070 Å) extending over at least 10 Å. The former peak may correspond to He II Ly $\beta$  emission (256 Å rest frame), but we know of no line corresponding to the latter feature. One possibility is that this is a region of enhanced transmission induced by photoionization from a quasar about 7' away from the line of sight, with  $z \approx 2.5$ . We estimate that an isotropically emitting quasar capable of ionizing this region would need to have a blue magnitude of only  $B \approx 20$ .

Of course, our model of isotropically, steadily emitting quasars may be too simple. If quasars emit light in two oppositely oriented cones (Dobrzycki & Bechtold 1991) with total solid angle  $4\pi f_\Omega$ , there would need to be  $f_\Omega^{-1}$  more quasars than in the luminosity functions used here, but each quasar affects a volume smaller by  $f_\Omega$ . The regions strongly influenced by the quasars thus have the same filling factor as before, and the local fluctuation level  $(\delta\tau/\tau)_{HeII}$  is unchanged. The correlation length, however, goes down by  $\sim f_\Omega^{1/2}$ . If the cone opening angle is large, there is a quantitative but not qualitative change in the fluctuations. However, the best way to test this idea would be to look for the influence of quasars near the line of sight. If the cone emission idea is correct, the ionization zone should always be either completely absent or offset from the quasar redshift.

Quasar variability could also affect these results. The He II ions will reach equilibrium with the local ionization rate on a timescale given by the inverse of the photoionization rate,  $\Gamma_{HeII}^{-1} \sim 10^5$  yrs. Structure would be induced in the He II absorption if individual quasars vary more slowly than this timescale, but more quickly than the timescale  $\sim 3 \times 10^7$  yrs for photons to cross the quasar ionization zones we have discussed. Quasar lifetimes are not well known; one might invoke the Eddington accretion time ( $4 \times 10^8$  yrs) or the dynamical time for bright galaxies

( $\sim 10^8$  yrs). If nearly every galaxy once hosted a bright quasar, then quasar lifetimes may be as short as  $10^7$  yrs. On the other hand, the existence of the H I proximity effect argues that typical quasar lifetimes are at least  $10^7$  yrs. As in the case of anisotropic emission, the variance in the ionization level is unchanged by the fluctuations, since any reduction in the duty cycle or lifetime of quasars is compensated by an increase in the number of quasars deduced from observations. Again, however, the correlation length is potentially shortened. If a quasar emits a burst of radiation, it causes a shell of enhanced ionization to travel outwards. Because of the time needed for light to travel to the observer, this shell would appear not as a sphere but as a parabola cupped towards Earth, although we can think of no practical way to observe this curious pattern.

### 4.3. Influence on Observations

Because fluctuations in He II absorption could be quite large, how does this affect our interpretation of the observations? The most obvious effect is that it makes the true optical depth at a given redshift more uncertain and weakens any conclusions about  $\eta$ . Consider a thought experiment in which one measures the absorption along a line of sight many times, each time with a different realization of absorption lines and ionizing quasars. In Figure 13 we show the results of such an experiment for a line of sight with He II absorption observed in the quasar rest wavelength range  $262 \text{ \AA} < \lambda < 293 \text{ \AA}$ , similar to that of HS1700+6416 (D96). Even if ionization fluctuations are suppressed, as would be the case if quasars are short-lived, we find significant variation ( $\pm 20\%$ ) in the observed opacity. Ionization fluctuations due to isotropically emitting, constant-luminosity quasars contribute additional variation to the results, with the amount increasing rapidly with redshift. The uncertainty in the average optical depth could therefore be reduced by obtaining a larger redshift coverage.

In summary, fluctuations in He II absorption can come about on  $\sim 30 \text{ km s}^{-1}$  scales because of random variations in the number of clouds (and also clustering of these clouds, on scales corresponding to large-scale structure of galaxies), and on  $\sim 3000 \text{ km s}^{-1}$  scales because of variations in the He II-ionizing flux. The amount of ionization fluctuations depends on the quasar luminosity function and He II continuum opacity, as well as the quasar lifetime and beaming angle. Observations of the absorption fluctuations thus have the potential to constrain these parameters, which are difficult to measure by other means. To do this, it will be necessary to measure the absorption in the spectra of numerous quasars and to look for ionized zones from quasars close to the line of sight.

## 5. FUTURE ULTRAVIOLET OBSERVATIONS

Considerable scientific interest was generated by the first measurements of He II absorption, even those at low spectral resolution. Future UV instruments with greater throughput offer the

possibility of increasing the scientific information. First, from a single sightline, one can glean information about the He II opacity over a range of absorption redshifts. With  $\sim 5$  sightlines, one can look for the expected variations arising from Poisson fluctuations in ionizing sources and absorbers. Toward the brightest targets, one can hope to resolve individual absorption lines, patches of absorption, and voids in the absorption that may correspond to large-scale structure and voids in the gas distribution. Extending the wavelength coverage down to 912 Å opens up the IGM down to  $z = 2$ , allowing the study of evolution in the He II absorption and increasing the odds of finding a suitable target.

To date, there have been detections of He II absorption toward four QSOs, at emission redshifts  $z_{\text{em}} = 2.74, 2.90, 3.18,$  and  $3.29$ . These spectroscopic experiments are exceedingly difficult, even at low resolution, for two reasons. First, viable background targets with clear lines of sight for He II Gunn-Peterson studies are rare (Møller & Jakobsen 1990; Jakobsen et al. 1994), owing to the strong absorption by the IGM at the redshifts ( $z \geq 2.9$ ) needed to bring the He II  $\lambda 304$  absorption into the HST band. Observation at lower redshifts ( $z = 2-3$ ) is potentially more fruitful if one can observe down to the 912 Å limit, as was done with HUT (Davidsen et al. 1996). Second, most high-redshift QSOs are faint; the four observed targets have fluxes at the He II edge ranging from around  $0.3$  to  $3 \times 10^{-15}$  ergs  $\text{cm}^{-2} \text{s}^{-1} \text{Å}^{-1}$ . Thus, faint-object UV spectroscopy at moderate resolution ( $30 \text{ km s}^{-1}$ ) has been nearly impossible, even with the powerful spectrographs (FOS, GHRS, STIS) aboard the *Hubble* Space Telescope.

However, the future prospects for UV spectroscopy are somewhat brighter. In addition to the He II absorption studies planned with the Space Telescope Imaging Spectrograph (STIS), two future instruments will contribute to this subject. The first is the Far Ultraviolet Spectroscopic Explorer (FUSE), scheduled for launch in October 1998. The second is the Cosmic Origins Spectrograph (COS), planned for the HST 2002 refurbishment mission. We discuss the potential of FUSE in detail here as an example of what can be learned in future He II observations.

Because the FUSE satellite operates in the wavelength range 915–1196 Å, it will be able to detect He II Ly $\alpha$  absorption in the range  $2.01 < z < 2.94$ . Its effective area of 20–100  $\text{cm}^2$  is sufficient to perform moderate-resolution spectroscopic studies of QSOs to fluxes  $F_\lambda > 10^{-14}$  ergs  $\text{cm}^{-2} \text{s}^{-1} \text{Å}^{-1}$ . Although the limiting fluxes accessible to FUSE are comparable to those with HST/STIS, the access to shorter wavelengths opens up He II studies at redshifts ( $2.1 < z < 2.9$ ) with considerably less H I and He II absorption from the IGM. Its resolution of 0.03 Å is much better than that of the He II absorption spectra taken so far, although STIS and COS have similar resolution. However, FUSE has an estimated dark count of  $\sim 0.02$  counts  $\text{s}^{-1} \text{Å}^{-1}$ . This dark count, together with uncertainties in the calibration and scattered light, may be difficult to characterize. Separating continuous He II absorption from that arising in the Ly $\alpha$  forest would require binning of order 0.3–0.5 Å, and exposure times  $\sim 10^6$  s. Even if one takes shorter observations and bins the data to 3–10 Å resolution, the variable dark count may prevent measurements of  $\tau_{\text{HeII}}$  to the 10–20% accuracy needed to detect the predicted fluctuations (Fig. 1, Fig. 13). FUSE will clearly require long integration times to observe faint, high-redshift objects such as quasars. Thus, it pays

to think creatively about the sorts of physical inferences possible with such observations.

A basic question is whether FUSE is capable of determining the evolution and fluctuations of  $\tau_{HeII}$  in the range  $2.1 \lesssim z \lesssim 2.9$ . Such measurements would help to determine the evolution of low-column gas and the ionizing spectrum over this redshift range. As suggested by Figure 1, the evolution of  $\tau_{HeII}$  is probably quite rapid. The number of potential targets probably depends most on the efforts of observers on the ground; Picard & Jakobsen (1993) estimate that there may be several hundred quasars with He II threshold fluxes  $F_{-15} > 1$  in the range  $2 < z < 3$ , where  $F_{-15} \equiv F_\lambda / (10^{-15} \text{ erg s}^{-1} \text{ cm}^{-2} \text{ \AA}^{-1})$ . However, only six such quasars are known at present. The dark counts dominate the FUSE signal unless the quasar is bright,  $F_{-15} > 10$ ; hence the necessary exposure time is very sensitive to the quasar flux. For a quasar with redshift  $z \approx 2.5$ , we expect an optical depth  $\tau_{HeII} \sim 0.8$ . To determine the transmission in a  $10 \text{ \AA}$  interval to an accuracy of 10% would require  $\sim (5 \times 10^4 \text{ s}) (1 + 0.15F_{-15}) / (1.1F_{-15}^2)$ . This is feasible for  $F_{-15} \gtrsim 1$ , but it rapidly becomes impractical for fainter targets.

FUSE will also be able to make a contribution to understanding the large-scale fluctuations in the He II absorption. The top panel of Figure 14 shows a plausible spectrum in a model where quasars radiate isotropically and statically, as assumed in § 4. The regions of increased ionization due to quasars along the lines of sight are visible as broad bumps in the spectrum. We estimate that  $\sim 10$  such exposures would constrain the optical-depth correlation function well enough to be able to test the assumptions of isotropy and constant emission, although much depends on the contribution of unsaturated gas (because of its sensitivity to the ionization level) and on the brightness of the available targets.

FUSE will be able to distinguish between absorption from Ly $\alpha$  forest clouds and the diffuse IGM, even in highly binned spectra, by determining the amount of absorption at the rest 256.31  $\text{\AA}$  He II Ly $\beta$  edge. For discrete clouds, this absorption has an optical depth  $\tau_\beta \approx 0.47\tau_\alpha$ , whereas for a diffuse IGM the optical depth is  $\tau_\beta \approx 0.16\tau_\alpha$ ; the difference arises from saturation effects in the discrete lines. Thus, a measurement of the Ly $\beta$  decrement could strongly constrain the relative contributions of these two sources of absorption. FUSE is capable of measuring this decrement for quasars with  $z_{em} > 2.7$ , with exposure times  $\lesssim 10^4 \text{ s}$  for a quasar with  $F_{-15} \sim 3$  in the unabsorbed continuum.

Besides measuring the evolution of gross absorption properties for a large sample of quasars, FUSE will be capable of providing more spectral detail in a few lines of sight. Even for bright targets such as HS1700+6416 ( $z = 2.74$ ) and HE2347-4342 ( $z = 2.90$ ), which have fluxes  $F_\lambda = 1.2 \times 10^{-15}$  and  $3.6 \times 10^{-15} \text{ erg s}^{-1} \text{ cm}^{-2} \text{ \AA}^{-1}$ , respectively, above the He II break, these observations will require very long exposures. Consider He II lines with central optical depth  $\tau_0 \approx 4$ , which make the median contribution to the line absorption in most of our models. Just to ensure an average significance level of  $3\sigma$  in these lines will require an exposure of  $2 \times 10^5 \text{ s}$ . Binning the spectra at the full resolution will result in extremely noisy plots, with no apparent features. However, statistical methods may be able to pull out a great detail of information from

these spectra.

We have carried out simulations of a “mock” HS1700+6416 spectrum. We have chosen not to use the actual lines in the quasar spectrum, because of the lack of a published *Keck* spectrum (though a portion of such a spectrum is reproduced in Bi & Davidsen 1997); however, the redshift, flux level, and optical depth match that of the real HS1700+6416. Figure 14 shows a segment of a simulated spectrum with  $0.15 \text{ \AA}$  pixels, in the case of thermally broadened lines and a substantial IGM. Although the spectrum looks quite noisy, due to the small pixel size, it is possible to identify most of the saturated He II lines in this spectrum. Binning to the HUT resolution of  $3 \text{ \AA}$  would throw away most of this small-scale information but would retain important information about large-scale fluctuations such as those resulting from peaks in the photoionizing radiation, some of which are visible in the figure.

Such a high-resolution spectrum is probably most useful in combination with a high-resolution H I spectrum, such as those returned from *Keck*. Starting with a simulated H I spectrum of similar quality to those of Hu et al. (1995), we have computed the He II absorption spectrum attained in a FUSE exposure of  $3 \times 10^5 \text{ s}$ . We then find a global fit to the H I and He II spectra using the three parameters  $\eta$ ,  $\xi$ , and  $\Omega_{IGM}$ . In this idealized case,  $\eta$  is determined to an accuracy of 30% and  $\xi$  to within 10%. Thus, the high resolution of FUSE should enable observers to break the parameter degeneracy that plagues the low-resolution  $\tau_{HeII}$  measurements. The method of comparing H I and He II spectra should determine  $\eta$  to high accuracy even if the spectrum is produced by a fluctuating IGM rather than discrete lines (Bi & Davidsen 1997).

Two instruments aboard HST are also expected to make advances in the study of He II absorption. Many of the issues discussed in relation to FUSE apply to these instruments as well. The recently installed STIS will be able to perform better background subtraction in the far-UV with its 2-D detector than previous HST spectrographs. Whereas FUSE can observe He II absorption in the redshift range  $2.1 < z < 2.9$ , the HST optics are limited to  $z > 2.8$ , so the two instruments complement each other. The effective area, dark count, and energy resolution of STIS are all superior to the corresponding parameters for FUSE. On the other hand, at higher  $z$  it is more difficult to find suitable targets. The quasars are obviously farther away, and the larger He II opacity at higher  $z$  will make detection of flux below the He II Ly $\alpha$  edge more difficult. In addition, in most quasars the rest-frame flux at  $304 \text{ \AA}$  is obscured by Lyman limit systems, eliminating many of the intrinsically brightest targets from consideration. These problems will be partially alleviated by the Cosmic Origins Spectrograph (COS), which is scheduled for the 2002 HST refurbishment mission. The COS instrument will be much more powerful than any of the other instruments discussed here; it is designed to deliver  $\sim 1500 \text{ cm}^2$  effective area in the range 1150–1400  $\text{\AA}$ . This capability, some 10–20 times greater than that of STIS, will allow  $30 \text{ km s}^{-1}$  spectroscopy of sources down to  $10^{-15} \text{ ergs cm}^{-2} \text{ s}^{-1} \text{ \AA}^{-1}$ , and lower-resolution studies of even fainter sources. Astronomers may then be able to measure He II optical-depth fluctuations toward a sufficiently large number of sources to characterize the expected fluctuations.

We have argued above that He II absorption measurements have several important uses, but constraints on Big Bang nucleosynthesis are unfortunately not among them. To be useful, the  $^4\text{He}/^1\text{H}$  ratio must be obtained to high accuracy. As seen in this paper, however, the ionization corrections are large and uncertain. Ionization corrections would not affect the  $^3\text{He}/^4\text{He}$  ratio, if it could be derived from the  $\lambda 304$  line. However, this measurement will be nearly impossible, owing to saturation in the  $^4\text{He}$  line. The detection of deuterium in the blueward wing of H I Ly $\alpha$  is already difficult, because the isotopic shift is only  $82 \text{ km s}^{-1}$  and because there is a large risk of contamination by other H I Ly $\alpha$  lines. In He II, both of these problems are exacerbated. The isotopic shift of  $^3\text{He}^+$  Ly $\alpha$  is only  $14 \text{ km s}^{-1}$ . In order to detect a  $^3\text{He}$  line with central optical depth  $\tau_c \sim 1$ , the corresponding  $^4\text{He}$  line must have  $\tau_c \gtrsim 1000$  ( $^3\text{He}/^4\text{He} < 10^{-3}$  for  $\text{D}/\text{H} < 10^{-4}$ ) and will completely cover the  $^3\text{He}$  line for any Doppler width  $b > 5 \text{ km s}^{-1}$ . Also, the problem of contamination by ordinary Ly $\alpha$  lines is far worse for the  $^3\text{He}$  forest. We reluctantly conclude that this experiment is impractical.

However, there are several practical observations that could help to maximize the significance of future He II observations. Any quasar that is observed in He II with FUSE should also be observed in H I with *Keck* or another telescope capable of high-resolution, high-S/N spectra. In addition, concentrated surveys for neighboring quasars in a  $\sim 30'$  radius around primary targets would help to interpret ionization fluctuations in the He II absorption. A survey for low-optical-depth ( $\tau_{LL} < 1$ ) Lyman limit systems would help to determine the column density distribution for  $N_{\text{HI}} < 10^{17} \text{ cm}^{-2}$  and thus estimate the continuum opacity of H I and He II. Finally, the study of weak metal lines (C IV, Si IV, O VI) in Ly $\alpha$  clouds will continue to be relevant to the He II problem (Songaila & Cowie 1996; Giroux & Shull 1997) as they constrain the spectrum of ionizing radiation. However, the metal-line ratios often depend more strongly on the temperature and density than the He II/H I ratio.

## 6. SUMMARY

We have used a radiative transfer code and a new absorption-line sample to relate the spectrum of ionizing sources in the early universe to the ionization conditions in the Ly $\alpha$  forest and diffuse IGM. We find that a model with only line-blanketing and ionization by quasars is sufficient to explain the observed level of absorption, although contributions from stars or the presence of a diffuse IGM would help to explain the data. We show that the H I and He II absorption really does probe the metagalactic background radiation, and that the observed quasars are probably sufficient to ionize both H I and He II by redshift  $z \sim 3.5$ .

By considering fluctuations both in the density of clouds and the ionizing background, we find that a long redshift path is required to obtain the mean level of absorption. This is not entirely a drawback, however, as these fluctuations carry interesting information in themselves. Observations by FUSE, STIS, and future high-throughput spectrographs should allow us to determine the spectral shape and sources of the ionizing background with high accuracy and to

disentangle the properties of the ionizing sources from those of the absorbers, leading to a much better understanding of the latter.

We thank Arthur Davidsen, Sally Heap, Craig Hogan, Susanne Koehler, Jerry Kriss, Limin Lu, Piero Madau, and Michael Rauch for useful conversations, and Lisa Storrie-Lombardi for communicating the APM survey data on  $D_A$  in advance of publication. We also thank Ed Murphy for the use of the FUSE (FSIM) simulator. This work was supported by the Astrophysical Theory Program at the University of Colorado (NASA grant NAGW-766 and NSF grant AST-96-17073).

### A. Treatment of Cloud Re-emission and Self-Shielding

In this Appendix, we discuss two effects on the ionizing background. The first effect is the emission of diffuse radiation from the absorbing clouds, referred to as “cloud re-emission”. As was noted in Fardal & Shull (1993) and explored in detail in HM96, this diffuse radiation has a significant effect on the high- $z$  ionizing flux, because the universe as a whole is optically thick in the continuum for a wide range of redshifts.

The second effect is the self-shielding of the absorbing clouds. In the gas that produces most of the He II and H I Ly $\alpha$  absorption, the relationship between the ionizing background and  $\eta$  is probably quite simple (see equation 7). As the column density of an absorber increases, the gas becomes optically thick in the continuum, first in He II (as long as  $\eta > 4$ ) and then in H I, meaning that  $\eta$  becomes a function of column density. This effect, also studied by HM96, increases the He II continuum opacity slightly at 4 Ryd and more at higher energies. The He II Ly $\alpha$  opacity can also be affected, because of the damping wings that set in at  $N_{HeII} \sim 10^{19} \text{ cm}^{-2}$ .

Both of these problems can be treated by considering an ensemble of slabs of different column densities. As discussed in § 2.2, the clouds that dominate the continuum opacity are moderately optically thick. The same is true for the cloud re-emission, since the number of photoionizations saturates as the slab becomes optically thick. The absorbing clouds become optically thick in H I at H I column densities  $\eta/4$  times larger than those in clouds that are optically thick in He II, and the ionizing photons above 4 Ryd contribute little to the ionization of H I. The radiative transfer in the relevant H I and He II clouds are thus nearly separate problems, and we have treated them as such.

The ionization structure of these clouds depends on the transfer of LyC radiation within them. We choose to model clouds as slabs since this is specific, tractable, and the sheet or pancake is a generic feature of numerical simulations. We have treated the radiative transfer by solving an integral equation (the Milne solution for a grey atmosphere) for the number of photoionizations at any optical depth in a given slab. If  $\Gamma(\tau')$  is the total photoionization rate at an optical depth  $\tau'$  within a slab of total optical depth  $\tau$ , and  $\Gamma_{\text{dir}}(\tau')$  is the photoionization rate resulting from external photons only, then

$$\Gamma(\tau') = \Gamma_{\text{dir}}(\tau') + \frac{p_{HLY}}{2} \int_{-\tau_{HI}/2}^{\tau_{HI}/2} E_1(|\tau'' - \tau'|) \Gamma(\tau'') d\tau''. \quad (\text{A1})$$

In this equation, the recombination radiation is assumed to be emitted isotropically; the dependence of  $\sigma_{HI}$  on  $\nu$  is ignored, since the recombination photons have energies close to 1 Ryd for the temperatures under consideration. Our calculation of  $\Gamma_{\text{dir}}$  assumes an isotropic distribution of the incident flux and a power-law incident spectrum, although we could improve on this slightly by using the example spectra derived in this paper. We solve this equation for slabs of varying optical depth. Assuming constant density within the slabs, we can solve for the ionization fractions at every point. Integrating over the slab, we find  $N_{HeII}$  as a function of  $N_{HI}$ . In general,  $\eta(N_{HI})$

increases smoothly but rapidly once  $N_{\text{HeII}} \gtrsim 3 \times 10^{17} \text{ cm}^{-2}$ , only to turn over and fall nearly as  $N_{\text{HI}}^{-1}$  when  $N_{\text{HI}} \gtrsim 3 \times 10^{17} \text{ cm}^{-2}$  (HM96).

These columns are perpendicular columns, where the slab is viewed face-on. For consistency, we must consider inclined clouds, where the projected area goes down by a factor  $\mu \equiv \cos \theta$  while the column density goes up by the same factor. The cloud distribution that would be seen if the clouds were all face-on is related to the observed distribution by

$$\frac{\partial^2 \mathcal{N}}{\partial N_{\text{obs}} \partial z}(N_{\text{obs}}) = \int_0^1 \left( \frac{\partial^2 \mathcal{N}}{\partial N_{\perp} \partial z} \right)_{\text{face-on}} (N_{\perp}) \mu^2 d\mu, \quad (\text{A2})$$

with  $N_{\perp} = \mu N_{\text{obs}}$ . There are two approximate methods we consider to relate these two distributions. If the observed distribution is a pure power law in  $N_{\text{obs}}$ , as in equation (8), the face-on distribution is simply a factor of  $(3 - \beta) \approx 1.5$  higher. It is also useful to consider the clouds as being at a characteristic angle of  $\theta_1$  where  $\cos \theta_1 = \mu_1 = 1/\sqrt{3}$  according to the model of 2-beam ( $n = 1$ ) Gaussian quadrature. We actually use both approximations, as discussed below.

The above model is too complicated to compute within our radiative transfer code, especially for the sake of effects that will not change  $\eta$  radically. As did HM96, we need to find approximations that can be computed quickly. We begin with the cloud emissivity. The processes we consider are those that can contribute to the ionization of H I or He II, namely H I and He II LyC recombination radiation, He II BaC recombination radiation, and He II 2-photon and Lyman line emission.

Consider the H I Lyman recombination radiation from Ly $\alpha$  forest and Lyman limit clouds in ionization equilibrium. For clouds that are optically thin at the Lyman limit ( $\tau_{\text{HI}} \ll 1$ ), a fixed fraction of recombinations  $p_{\text{HLY}}$  go directly to the ground state and emit a Lyman continuum photon that escapes from the cloud ( $p_{\text{HLY}} = 0.43$  at a temperature of  $2 \times 10^4$  K). Thus, the H I atoms in the cloud emit recombination photons at an average rate  $\equiv f_{\text{HLY}} \Gamma_{\text{HI}}^{\text{thin}}$ , where  $\Gamma_{\text{HI}}^{\text{thin}}$  (written simply as  $\Gamma_{\text{HI}}$  in the rest of the paper) is the ionization rate of hydrogen atoms in optically thin clouds and  $f_{\text{HLY}}$  is the normalized emission probability; clearly  $f_{\text{HLY}} \approx p_{\text{HLY}}$  in this case. In optically thick clouds ( $\tau_{\text{HI}} \gg 1$ ), almost all of the incident photons are absorbed, and most of the ionizations and recombinations take place within a few optical depths of the cloud edge, no matter how large  $\tau_{\text{HI}}$  becomes. The average emission probability of atoms in these clouds is  $f_{\text{HLY}} \rightarrow \text{const}/\tau_{\text{HI}}$ . Note that the escape probability formalism would erroneously predict that the emission rate scales as  $f_{\text{HLY}} \propto \tau_{\text{HI}}^{-2}$ , a product of the average ionization rate ( $\propto \tau_{\text{HI}}^{-1}$ ) and the escape probability ( $\propto \tau_{\text{HI}}^{-1}$ ).

The dependence of  $f_{\text{HLY}} \tau_{\text{HI}}$  on  $\tau_{\text{HI}}$  is thus similar to the factor  $(1 - e^{-\tau_{\text{HI}}})$  contained in the integral for the H I continuum opacity. The space-averaged volume density of H I atoms in clouds with columns in the range  $[N_{\text{HI}}, N_{\text{HI}} + dN_{\text{HI}}]$  at a redshift  $z$  is  $N_{\text{HI}} (\partial^2 \mathcal{N} / \partial N_{\text{HI}} \partial z) (dz/dl) dN_{\text{HI}}$ . Multiplying this density by the emission rate,  $\equiv f_{\text{HLY}}(N_{\text{HI}}) \Gamma_{\text{HI}}^{\text{thin}}$ , we find that the total re-emission

of Lyman continuum photons from the clouds is

$$j_{\text{HLY}}(\nu, z) = \frac{h\nu}{4\pi} \frac{\phi_{em}(\nu)}{\sigma_{\text{HI}}} \frac{dz}{dl} \Gamma_{\text{HI}}^{\text{thin}} \int \frac{\partial^2 \mathcal{N}}{\partial N_{\text{HI}} \partial z} [f_{\text{HLY}}(\tau_{\text{HI}}) \tau_{\text{HI}}] dN_{\text{HI}}, \quad (\text{A3})$$

where  $\tau_{\text{HI}} = \sigma_{\text{HI}} N_{\text{HI}}$  and where  $\phi_{em}(\nu)$  is the frequency distribution of the recombination radiation. Compare the form of the integral here to that in equation (3) for the continuum opacity. As long as the column density distribution has a fixed shape, these two integrals are proportional and close in magnitude. Our strategy is to exploit this similarity to express the cloud emissivity as

$$j_{\text{HLY}}(\nu, z) = q_{\text{HLY}} \frac{h\nu}{4\pi} \frac{\phi_{em}}{\sigma_{\text{HI}}} \frac{dz}{dl} \Gamma_{\text{HI}}^{\text{thin}} \frac{d\tau_{\text{HI}}}{dz}, \quad (\text{A4})$$

where the ensemble-averaged emission probability is

$$q_{\text{HLY}} \equiv \left( \frac{d\tau_{\text{HI}}}{dz} \right)^{-1} \int \frac{\partial^2 \mathcal{N}}{\partial N_{\text{HI}} \partial z} [f_{\text{HLY}}(\tau_{\text{HI}}) \tau_{\text{HI}}] dN_{\text{HI}}. \quad (\text{A5})$$

We make use of the radiative transfer models discussed above to calculate  $q_{\text{HLY}}$ . The emission rate is given by the difference between emitted and destroyed recombination photons, integrated over the slab, and is equal to

$$f_{\text{HLY}}(\tau_{\text{HI}}) \Gamma_{\text{HI}}^{\text{thin}} = \frac{1}{\tau_{\text{HI}}} \left( p_{\text{HLY}} \int_{-\tau_{\text{HI}}/2}^{\tau_{\text{HI}}/2} \Gamma_{\text{dir}}(\tau') d\tau' - \int_{-\tau_{\text{HI}}/2}^{\tau_{\text{HI}}/2} [\Gamma(\tau') - \Gamma_{\text{dir}}(\tau')] d\tau' \right). \quad (\text{A6})$$

The results do not depend on the assumed density. We can then integrate over a power-law distribution of slabs of different  $N_{\text{HI}}$  to find  $q_{\text{HLY}}$ . The value of  $q_{\text{HLY}}$  turns out to be insensitive to the exact input spectrum, cloud temperature (which determines  $p_{\text{HLY}}$ ), or column density distribution. Because many of the Lyman continuum photons are unable to escape from moderately thick clouds,  $q_{\text{HLY}} < p_{\text{HLY}}$ . Our method is similar for the He II Lyman recombination radiation. The H I continuum opacity is generally negligible for the clouds with  $\tau_{\text{HeII}} \sim 1$  that dominate the emission, so the radiative transfer models can be reused, with the minor difference of a slightly different  $p_{\text{LY}}$ .

Photons in the He II Balmer continuum, Lyman 2-photon continuum, and Ly $\alpha$  line escape from clouds with  $\tau_{\text{HeII}} \sim 1$  (although the Ly $\alpha$  photons resonantly scatter off He II atoms many times first). We use Case B recombination coefficients, since if a cloud has any significant optical depth in the continuum the Lyman lines will be optically thick, and the only Lyman line photons that escape are Ly $\alpha$ . The emission from these processes is simply proportional to the total number of ionizations in the cloud. The He II Balmer emission rate is given by

$$f_{\text{HeBa}}(\tau_{\text{HeII}}) \Gamma_{\text{HeII}}^{\text{thin}} = \frac{p_{\text{HeBa}}}{\tau_{\text{HeII}}} \int_{-\tau_{\text{HeII}}/2}^{\tau_{\text{HeII}}/2} \Gamma(\tau') d\tau', \quad (\text{A7})$$

with similar expressions for the other processes. Since  $\Gamma_{\text{HeII}} > \Gamma_{\text{HeII}}^{\text{thin}}$  for moderately thick clouds, due to the He II LyC radiation, we find that  $q > p$  for these processes. The coefficients for all of these processes are listed in Table 3.

Our treatment of the re-emission differs substantially from HM96. Their method is based on an approximate integration over column density and energy, performed at each redshift step. In contrast, we perform the integration exactly but only for one model, and then parameterize the re-emission rates in terms of the continuum opacities. In addition, HM96 use an escape probability formalism, and they ignore the distinction between  $N_{obs}$  and  $N_{\perp}$  and the distribution of incident and re-emitted radiation in angle. Despite these differences, in the end our results agree fairly well. Our He II Ly $\alpha$  line intensity, for example, agrees with theirs to better than 20%.

The fraction of photoionizations due to photons emitted from the clouds depends on the number of photons that are absorbed before they can be redshifted below the ionization threshold. This fraction naturally drops at lower redshifts as the opacity decreases. At  $z = 3$ , we find that  $\sim 20\%$  of H I and He II ionizations are due to cloud re-emission. Usually the contribution of LyC emission to the ionization of each species is nearly equal, but the other processes give a slight extra ionization of H I, which is then amplified non-linearly by the dependence of the opacity on  $\eta$ . As shown in Figure 9, the effect of the re-emission is to increase  $\eta$  by 5–15% at  $z \sim 3$ . Our results differ in this respect from HM96, who found a 15% *decrease* in  $\eta$  from re-emission for  $z \approx 3$ , changing to an increase in  $\eta$  of about the same magnitude for  $z < 1.5$ .

We now turn to the self-shielding problem. In our model, self-shielding occurs only in He II; any effect of self-shielding on the H I column distribution is assumed to be reflected in the distribution we are using. (For discussion of whether its effect can actually be seen in the H I distribution, see Fardal & Maloney 1995). Its effect on a slab is not as simple a function of column density as the re-emission rate, so we choose to model it in a higher level of detail. Our radiative transfer models above give us the run of  $N_{HeII}$  with  $N_{HI}$ . We can obtain an approximation to this function by considering the equations of ionization balance for H I and He II. Neglecting He I and assuming  $n_{HI} \ll n_H$ ,

$$\Gamma_{HeII} n_{HeII} = \alpha_{HeII} n_e (n_{He} - n_{HeII}), \quad (A8)$$

$$\Gamma_{HI} n_{HI} = \alpha_{HI} n_e n_H. \quad (A9)$$

Solving for  $n_{HI}$  and  $n_{HeII}$ , integrating over the slab length, and equating the slab lengths in the two equations gives

$$\frac{\sigma_{HeII}}{\sigma_{HI}} \frac{n_{He}}{n_H} \int_{-\tau_{HeII}/2}^{+\tau_{HI}/2} \tilde{\Gamma}(\tau'_{HI}) d\tau'_{HI} I_{HI} = \tau_{HeII} + I_{HeII} \int_{-\tau_{HeII}/2}^{+\tau_{HeII}/2} \tilde{\Gamma}(\tau'_{HeII}) d\tau'_{HeII}, \quad (A10)$$

where the normalized photoionization rate is  $\tilde{\Gamma} \equiv \Gamma(\tau')/\Gamma^{\text{thin}}$  and where  $I_{HI} \equiv \Gamma_{HI}^{\text{thin}}/n_e \alpha_{HI}$  and  $I_{HeII} \equiv \Gamma_{HeII}^{\text{thin}}/n_e \alpha_{HeII}$  as in HM96. The point of this exercise is that the integrals depend only on the shape of the incident spectrum, and fairly weakly on that. We have found that, for realistic conditions,  $N_{HeII}$  can be calculated from the quadratic equation,

$$\frac{1}{4} \frac{n_{He}}{n_H} \left( \frac{\tau_{HI}}{1 + 0.5\tau_{HI}} \right) I_{HI} = \tau_{HeII} + I_{HeII} \left( \frac{\tau_{HeII}}{1 + 0.7\tau_{HeII}} \right). \quad (A11)$$

This approximation follows the numerical results closely, as shown in Figure 15. When the opacity is integrated over  $N_{HeII}$ , the approximation is usually accurate to within a few percent. Again, this equation applies to  $N_{\perp}$  not  $N_{obs}$ . In this case it is convenient to take  $N_{\perp} = \mu_1 N_{obs}$ , as discussed above. We find that for the opacity models discussed in this paper, this is accurate to within 3% over all frequencies, compared with an exact angular convolution. To get further computational speed, we break up the integral in equation (3) in § 2.2 into segments where  $N_{HI}$  increases by a factor of 3 or so. We interpolate  $N_{HeII}(N_{HI})$  in each segment with a power law. The integral can then be done semi-analytically.

The effect of self-shielding on  $\eta$  is also shown in Figure 9c. The threshold opacity is increased only slightly ( $\sim 5\%$ ) by the self-shielding at a fixed  $\eta$ , but because the strength of the effect increases with energy, and because the He II ionization fraction calculation is nonlinear,  $\eta$  typically increases by  $\sim 15\%$  at  $z = 3$ . This increase is nearly model-independent, since the onset of self-shielding is determined by the radiative transfer. The onset of the turnover in  $\eta(N_{HI})$  is, in contrast, dependent on the density in the clouds, which is in turn dependent on the poorly known cloud thicknesses. The spectrum at energies much higher than 4 Ryd, which probes the high columns where this turnover occurs, is thus more model-dependent, but it has a negligible effect on  $\Gamma_{HeII}$ .

In contrast to the case of cloud emission, our results for the self-shielding on the He II continuum opacity differ somewhat from those of HM96. Their use of face-on columns, the perpendicular (1-beam) approximation, and the escape probability formalism gives results that nearly match ours, but only if we leave out their final step of doubling  $N_{HI}$ . For optically thick slabs, this step effectively doubles the flux incident on a slab and thus reduces the strength of self-shielding. In addition, in our treatment  $\eta(N_{HI})$  rises smoothly, whereas in theirs it remains constant until it jumps at  $\tau_{HeII} = 4$ . The optical depth of this jump is too high to make any difference in the He II threshold opacity. We thus find a higher  $\eta$  if all other assumptions are held constant. Combined with the difference in our results for the re-emission, we find that  $\eta$  is nearly 70% higher in our models compared to the results of HM96.

We use the same approximations for  $N_{HeII}(N_{HI})$  to calculate the He II line opacity. The form of the curve of growth, as shown in Figure 15, means that the self-shielding is almost irrelevant until  $N_{HeII} \sim 10^{19} \text{ cm}^{-2}$ , where the damping wings set in (at a lower column than in H I). In future observations these damping wings may be seen at wavelengths corresponding to lines with  $N_{HI} \sim 10^{16} \text{ cm}^{-2}$ , depending on the typical density in Lyman limit systems. We find that these mildly damped systems contribute  $\Delta\tau_{HeII} \sim 0.1$  to the Ly $\alpha$  optical depth  $\tau_{HeII}$  at  $z = 3$ .

## B. Statistical Methods for Cloud Samples

Many current opacity models for the high- $z$  IGM are based on low-resolution spectra and uncertain column density distributions. One of the primary checks of the opacity models is the flux deficit shortward of the Ly $\alpha$  emission line (the  $D_A$  parameter discussed in § 2.3) which assumes a constant power-law extrapolation of the continuum longward of Ly $\alpha$ . However, new data from high-resolution spectrographs on large telescopes allows one to construct more accurate line lists with better column density distributions. One clear result of these studies is the turnover in Ly $\alpha$  clouds with  $N(\text{H I}) \geq 10^{14.5} \text{ cm}^{-2}$ . It is also possible to quantify the spectral curvature of the QSO continuum, which falls off in flux relative to a power-law extrapolation at wavelengths below 1216 Å (Zheng et al. 1997). For these reasons, we have developed a new statistical model for the column density distribution and the resulting IGM opacity.

Wherever possible, we have avoided binning the data in column density. To derive our fits to the absorption-line distribution, we use the maximum-likelihood method. By first fitting the number of clouds per unit redshift, we derive a redshift exponent  $\gamma$ , although we have chosen to use a different value for some parts of the models (see Table 1). The probability of finding a cloud with column  $N_i$  in the sample is, according to equation (8) integrated over redshift,

$$p_{obs}(N) = \sum_q \frac{1}{\gamma_i + 1} (1+z)^{\gamma_i+1} \Big]_{z_{min}^{(q)}}^{z_{max}^{(q)}} \frac{A_i}{N_r} \left( \frac{N}{N_r} \right)^{-\beta_i}, \quad (\text{B1})$$

where  $N$  lies in column range  $j$  and  $(q)$  denotes the quasars in the sample. We maximize the likelihood function by summing over the columns in the sample,

$$L = \prod_i p_{obs}(N_i), \quad (\text{B2})$$

subject to the constraint that the expected number of lines in the sample equal the number actually observed.

We would also like to have a means of estimating the errors in the quantities drawn from the column density distribution. The bootstrap procedure (Lupton 1993) is a means of calculating statistical quantities about a variable  $x$  without making assumptions about the form of its probability distribution  $p(x)$ . The central idea is to turn the observed dataset  $\{x_i, i = 1 \dots N\}$  into an “observed probability distribution”  $p_*(x) = (1/N) \sum_i \delta(x - x_i)$ . By drawing from this observed distribution, one may calculate statistical quantities in a Monte Carlo fashion. This process is usually carried out until the errors from the Monte Carlo process become small enough. The bootstrap is no guarantee of success. Some quantities, such as the sample mean and other linear functionals of  $p(x)$ , are well estimated by this procedure, while others, such as the two-point correlation function of  $x$ , are not.

The bootstrap procedure seems useful in the case of quasar absorption line samples, where one wants to know quantities such as the line and continuum opacities in H I and He II and their

associated errors. These errors have often been estimated by having several people make fits to different datasets and then comparing the dispersion among the fits. This procedure is suspect for several reasons, notably that the datasets usually overlap significantly!

However, to use the bootstrap here one must make some slight modifications to the standard procedure (discussed in Lupton 1993, for example). In our case, we have not a probability distribution but a *frequency* distribution, where the total number of data points is a Poisson variable. We can represent this as follows. Suppose the frequency distribution of our parameter  $x$  (counts per unit  $x$  per unit time) is  $f(x)$  and we observe for a “time”  $T$ . Then our bootstrap frequency distribution is  $f_*(x) = (1/T) \sum_i \delta(x - x_i)$ . In other words, the  $m^{\text{th}}$  Monte Carlo realization will be specified by  $f_m(x) = (1/T) \sum_i w_i^{(m)} \delta(x - x_i)$  where the  $w_i^{(m)}$  are Poisson variables with mean 1.

This procedure is especially useful in the case of linear functionals of the underlying distribution, i.e. a quantity  $G = \int g(x)f(x)dx$  where  $g(x)$  is some function. For example,  $G$  might represent the H I continuum opacity and  $g(x) = 1 - e^{-\tau}$ . These functionals are so simple that there is actually no need to run any Monte Carlo program. The bootstrap estimate of  $G$  is

$$\langle G \rangle_* = \langle \int g(x)f_m(x)dx \rangle_* = \langle \frac{1}{T} \sum_i w_i g(x_i) \rangle_* = \frac{1}{T} \sum_i g(x_i), \quad (\text{B3})$$

where the star denotes an average over the bootstrap ensemble. Of course, one might have naturally made this estimate of  $G$  without ever regarding it as a bootstrap procedure.

To estimate the uncertainty in this bootstrap estimate, we can calculate the bootstrap variance:

$$\begin{aligned} \langle \sigma_G^2 \rangle_* &= \langle G^2 \rangle_* - \langle G \rangle_*^2 = \frac{1}{T^2} \sum_{ij} g(x_i)g(x_j) [\langle w_i w_j \rangle_* - \langle w_i \rangle_* \langle w_j \rangle_*] \\ &= \frac{1}{T^2} \sum_i [g(x_i)]^2. \end{aligned} \quad (\text{B4})$$

It is not hard to show that this has an expectation value exactly the same as the variance in  $\langle G \rangle_*$  resulting from estimates drawn from different datasets. In other words, the error bar calculated by the above equation is, on average, the correct error bar. It is also simple to calculate and requires no arbitrary binning.

The observational problem at hand is rarely so simple, and one must extend these results in several ways. An important application is the case where one does not know the  $\{x_i\}$  exactly, but instead each has an error bar of its own. If we can suppose the true value of each  $x_i$  to have a distribution  $p_i(x_i)$ , then the bootstrap procedure is to draw a value from this distribution  $w_i^{(m)}$  times. If  $\langle g(x_i) \rangle_{p_i}$  represents the value of  $g(x)$  averaged over the distribution of  $x_i$ , the resulting bootstrap mean and variance are

$$\langle G \rangle_* = \frac{1}{T} \sum_i \langle g(x_i) \rangle_{p_i}, \quad (\text{B5})$$

$$\langle \sigma_G^2 \rangle_* = \frac{1}{T^2} \sum_i (\langle g(x_i) \rangle_{p_i})^2. \quad (\text{B6})$$

Another complication is that frequently the detection rate of the events  $\{x_i\}$  is not perfect, and instead one has some detection rate  $F_{\text{det}}(x)$ . To correct for this, we divide the “observed” bootstrap distribution by  $F_{\text{det}}(x)$ . The result is that  $g(x_i)$  gets replaced by  $g(x_i)/F_{\text{det}}(x_i)$  in the equations above.

In addition, the observed frequency of events is often not constant with time  $t$ , as was assumed above, and different ranges of  $x$  will often be observed for different amounts of time. If one *knows* that the  $t$  and  $x$  dependence are separate factors, it is not difficult to adjust the equations for the  $t$  dependence to derive a smooth function  $G(t)$ . If this is not known, but is consistent with the data set, one can assume a separable dependence (at the cost of an unquantified uncertainty). Suppose that  $f(x, t) = U(t)\tilde{f}(x)$ . Changing to the variable  $\tau \equiv \int U(t)dt$ , the distribution  $f(x, \tau)$  is constant in  $\tau$ , so we can just apply the theory above. If each value  $x_i$  was observable for a “time”  $\tau_i$ , and had a detection rate  $F_{\text{det}}(x_i)$ , we can write the bootstrap distribution as  $f_*(x, \tau) = \sum_i (w_i \delta(x - x_i)) / (\tau_i F_{\text{det}}(x_i))$ . Upon performing the bootstrap average and converting back to  $t$ , we get

$$\langle G \rangle_* = U(t) \sum_i \frac{g(x_i)}{\int_i U(t)dt \cdot F_{\text{det}}(x_i)} \quad (\text{B7})$$

$$\langle \sigma_G^2 \rangle_* = (U(t))^2 \sum_i \left( \frac{g(x_i)}{\int U(t)dt \cdot F_{\text{det}}(x_i)} \right)^2. \quad (\text{B8})$$

In the case of quasar absorption line distributions, the variable  $x$  becomes column density  $N_{\text{HI}}$ , the time  $t$  becomes redshift  $z$ , and the function  $G$  may be the continuum opacity  $d\tau_{\text{HI}}/dz$  or the line opacity  $\tau_{\text{HI}}$ . If the frequency of detecting absorption-line clouds is proportional to  $(1+z)^\gamma$ , and there are several quasars in the sample, the continuum opacity estimates become

$$\langle \frac{d\tau_{\text{HI}}}{dz} \rangle_* = (1+z)^\gamma \sum_i \frac{1 - \exp(-\tau(N_i))}{\sum_{(q)} \int^{(q)} (1+z)^\gamma dz F_{\text{det}}^{(q)}(N_i)}, \quad (\text{B9})$$

$$\langle \sigma_{d\tau_{\text{HI}}/dz}^2 \rangle_* = (1+z)^{2\gamma} \sum_i \left( \frac{1 - \exp(-\tau(N_i))}{\sum_{(q)} \int^{(q)} (1+z)^\gamma dz F_{\text{det}}^{(q)}(N_i)} \right)^2. \quad (\text{B10})$$

If  $\overline{W}_\lambda^{\text{rest}}(N)$  is the average equivalent width at a given column, the line opacity and its error estimate are calculated from the formulae

$$\langle \tau_{\text{HI}} \rangle_* = (1+z)^{\gamma+1} \sum_i \frac{\overline{W}_\lambda^{\text{rest}}(N)/\lambda^{\text{rest}}}{\sum_{(q)} \int^{(q)} (1+z)^\gamma dz F_{\text{det}}^{(q)}(N_i)}, \quad (\text{B11})$$

$$\langle \sigma_{\tau_{\text{HI}}}^2 \rangle_* = (1+z)^{2(\gamma+1)} \sum_i \left( \frac{\overline{W}_\lambda^{\text{rest}}(N)/\lambda^{\text{rest}}}{\sum_{(q)} \int^{(q)} (1+z)^\gamma dz F_{\text{det}}^{(q)}(N_i)} \right)^2. \quad (\text{B12})$$

### C. Small Effects on $N_{\text{HeII}}/N_{\text{HI}}$

In § 3 we examined the major effects on  $\eta$  resulting from uncertainties in parameter space. We list here some of the less significant effects, some of which we have ignored entirely in our calculations. We have tried varying the Pei (1995) luminosity function within the uncertainties given in the paper. The result was a variation in  $\eta$  of  $\sim 5\%$ , much less than the differences between our quasar models 1 and 2. Clearly, the uncertainty in the quasar luminosity function is mostly due to systematic effects such as dust obscuration.

The ionizing spectrum could also be affected by the line opacity of He II. A photon with energy slightly below 4 Ryd must run a gauntlet of He II absorption lines, many with significant opacity, before being redshifted below the Ly $\alpha$  energy of 3 Ryd. However, the mean spectrum is only affected by line splitting—e.g., the absorption of a Ly $\beta$  photon and subsequent re-emission of Ly $\alpha$  and Balmer- $\alpha$  photons. This splitting takes place only rarely, about 1 time in 8 for the process just described. We have modeled this process as repeated tosses of a photon against a screen that represents the Ly $\beta$  barrier. Each time the photon hits the screen, it can either bounce back, pass through, or undergo line-splitting. By solving the equation for the fraction of photons that eventually undergo line-splitting, we find that this process becomes significant for  $z \gtrsim 4.0$ . The splitting of higher Lyman-series lines will become significant at even higher redshifts. Since the energy region 3–4 Ryd has little effect on the H I or He II photoionization rates, we have ignored line-splitting processes in this paper. They may be of more significance for metal-line ratios like Si IV/C IV.

We also ignore the He I continuum opacity in this paper. Miralda-Escudé & Ostriker (1992) showed that the optical depth is quite small unless the ionizing background is dominated by decaying neutrinos. In the standard picture of highly photoionized clouds, the He I/He II ratio is  $\sim 0.2n_e J_{-21}^{-1}$  for  $\alpha_b \approx 1.8$  between 1.0 and 1.8 Ryd. Since the electron densities,  $n_e$ , in standard QSO absorption systems are expected to be quite small, the continuum opacity of He I is substantially less than that of He II and H I. Observational indications of the presence of He I in the IGM at  $z \gtrsim 2$  are limited. Reimers et al. (1992) and Reimers & Vogel (1993) find He I/H I = 0.026–0.05 in partial Lyman Limit systems with  $N_{\text{HI}} = 10^{16.6} - 10^{16.9} \text{ cm}^{-2}$ . Since He I/H I =  $\eta(\text{He I/He II}) = 0.2J_{-21}^{-1}n_e\eta$ , if  $n_e \approx n_H = (2 \times 10^{-3} \text{ cm}^{-3})(N_{\text{HI}}/10^{17} \text{ cm}^{-2})^{1/2}$ , He I/H I =  $0.04J_{-21}^{-1}\eta_{100}(N_{\text{HI}}/10^{17} \text{ cm}^{-2})^{1/2}$ , where  $\eta_{100} = \eta/100$ . Thus, the few known measurements are consistent with this density model, but our knowledge of the appropriate run of He I/H I with  $N_{\text{HI}}$  is still very tentative. If He I/H I  $\approx 0.03$  in all absorbers at  $z \gtrsim 3$ , the radiation at 2–3 Ryd is reduced by less than 10% over the case when He I opacity is neglected, and less at later times. For the more generous He I/H I ratio implied by our  $N_{\text{HI}}$  dependent density model, the reduction may approach 20–30% at high redshift. We have also ignored the continuum opacity of metals in absorption-line clouds, an approximation which has negligible effect on our results.

The column ratio  $\eta$  is proportional to the primordial abundance of He, which is probably uncertain by about 5% (Schramm & Turner 1997). It also depends on the temperature of the

Ly $\alpha$  clouds, but even for temperature uncertainties of a factor  $\sim 2$ , equation (7) shows that this introduces an uncertainty  $\lesssim 5\%$ . It is clear that these small uncertainties do not present obstacles to progress on this problem.

Table 1. Absorption Line Distributions<sup>a</sup>

Model	$N_{min}$ (cm <sup>-2</sup> ) <sup>b</sup>	$N_{max}$ (cm <sup>-2</sup> ) <sup>b</sup>	$A$ <sup>c</sup>	$\beta$ <sup>c</sup>	$\gamma$ <sup>c</sup>	$P_{fit}$ <sup>d</sup>
A1	...	$1 \times 10^{14}$	$1.45 \times 10^{-1}$	1.40	2.58	0.15
	$1 \times 10^{14}$	$1 \times 10^{16}$	$6.04 \times 10^{-3}$	1.86	2.58	
	$1 \times 10^{16}$	$1 \times 10^{19}$	$2.58 \times 10^{-2}$	1.23	2.58	
	$1 \times 10^{19}$	$1 \times 10^{22}$	$8.42 \times 10^{-2}$	1.16	1.30	
A2	...	$2 \times 10^{14}$	$6.69 \times 10^{-2}$	1.49	2.58	0.04
	$2 \times 10^{14}$	$2 \times 10^{15}$	$5.93 \times 10^{-3}$	1.88	2.58	
	$2 \times 10^{15}$	$1 \times 10^{19}$	$2.95 \times 10^{-2}$	1.47	2.58	
	$1 \times 10^{19}$	$1 \times 10^{22}$	$8.42 \times 10^{-2}$	1.16	1.30	
A3	...	$2 \times 10^{14}$	$6.69 \times 10^{-2}$	1.49	2.58	0.04
	$2 \times 10^{14}$	$2 \times 10^{15}$	$5.93 \times 10^{-3}$	1.88	2.58	
	$2 \times 10^{15}$	$1 \times 10^{17}$	$2.95 \times 10^{-2}$	1.47	2.58	
	$1 \times 10^{17}$	$1 \times 10^{22}$	$1.58 \times 10^{-1}$	1.50	1.50	
A4	...	$1 \times 10^{17}$	$1.32 \times 10^{-1}$	1.43	2.46	$< 10^{-24}$
	$1 \times 10^{17}$	$1 \times 10^{22}$	$4.22 \times 10^{-1}$	1.39	0.68	

<sup>a</sup> Models of opacities from different H I column density distributions (see § 2.3).

<sup>b</sup> Limits on H I column density for subrange. The minimum column for the lowest subrange is left blank, since we treat it as a free parameter.

<sup>c</sup> Parameters used in equation 8.

<sup>d</sup> Formal fit probability from combined K-S/binomial test.

Table 2. Quasar emission models <sup>a</sup>

Model	$j_{H*}$	$z_*$	$\sigma_*$
Q1	$2.7 \times 10^{24}$	2.75	0.93
Q2	$6.2 \times 10^{24}$	3.37	1.03

<sup>a</sup> The parameters are used in § 2.5 [eq. (14)] of the text. The comoving emissivity,  $j_{H*}$ , is given in units of ( $h_{75}$  erg s<sup>-1</sup> Mpc<sup>-3</sup> Hz<sup>-1</sup> sr<sup>-1</sup>). Corrections have been applied for the different Hubble constant and spectral slope  $\alpha_{BH}$  assumed by Pei (1995).

Table 3. Coefficients of continuous emission.

Process	$p_{process}$ <sup>a</sup>	$q_{process}$ <sup>b</sup>
H I Lyman continuum	0.43	0.22
He II Lyman continuum	0.33	0.16
He II Balmer continuum	0.17	0.22
He II 2- $\gamma$	0.20	0.26
He II Ly $\alpha$	0.45	0.58

<sup>a</sup>  $p_{process}$  denotes the probability of this process occurring in a single recombination.

<sup>b</sup>  $q_{process}$  denotes a dimensionless factor that accounts for its likelihood integrated over clouds of all columns. (Since the integral converges at both its upper and lower limits, we have neglected the finite cutoffs used in our paper.)

Note. — A temperature of  $T = 2 \times 10^4$  K is assumed.

## REFERENCES

- Bajtlik, S., Duncan, R. C., & Ostriker, J. P. 1988, *ApJ*, 327, 570
- Bechtold, J. 1993, in *The Environment and Evolution of Galaxies*, ed. J. M. Shull & H. A. Thronson, (Dordrecht: Kluwer), p. 559
- Bechtold, J. 1994, *ApJS*, 91, 1
- Bechtold, J., Crotts, A. P., Duncan, R. C., & Fang, Y. 1994, 437, L83
- Bi, H.-G., & Davidsen, A. F. 1997, *ApJ*, 479, 523
- Carswell, R. F., Lanzetta, K. M., Parnell, H. C., & Webb, J. K. 1991, *ApJ*, 371, 36
- Cen, R., Miralda-Escudé, J., Ostriker, J. P., Rauch, M. 1994, *ApJ*, 437, L9
- Copi, C. J., Schramm, D. N., & Turner, M. S. 1995, *Science*, 267, 192
- Cooke, A. J., Espey, B., & Carswell, B. 1997, *MNRAS*, 284, 552
- Cristiani, S., Giallongo, E., Buson, L. M., Gouiffes, C., & La Franca, F. 1993, *A&A*, 268, 86
- Cristiani, S., D’Odorico, S., Fontana, A., Giallongo, E., & Savaglio, S. 1995, *MNRAS*, 273, 1016
- Cristiani, S., D’Odorico, S., D’Odorico, V., Fontana, A., Giallongo, E., Savaglio, S. 1997, *MNRAS*, 285, 209
- Davidsen, A. F., Kriss, G. A., & Zheng, W. 1996, *Nature*, 380, 47
- Dobrzycki, A., & Bechtold, J. 1991, *ApJ*, 377, L69
- Donahue, M., & Shull, J. M. 1987, *ApJ*, 323, L13
- Donahue, M., & Shull, J. M. 1991, *ApJ*, 383, 511
- Fang, Y. & Crotts, A. P. S. 1995, *ApJ*, 440, 69
- Fardal, M. A., & Maloney, P. R. 1995, in *QSO Absorption Lines*, ed. G. Meylan (Berlin: Springer), 437
- Fardal, M. A., & Shull, J. M. 1993, *ApJ*, 415, 524
- Giallongo, E., & Cristiani, S. 1990, 247, 696
- Giallongo, E., Cristiani, S., Fontana, A., & Trèvese, D. 1993, *ApJ*, 416, 137
- Giallongo, E., D’Odorico, S., Fontana, A., McMahon, R. G., Savaglio, S., Cristiani, S., Molaro, P., & Trèvese, D. 1994, *ApJ*, 425, L1
- Giallongo, E., Cristiani, S., D’Odorico, S., Fontana, A., & Savaglio, S. 1996, *ApJ*, 466, 46
- Giroux, M. L., Fardal, M. A., & Shull, J. M. 1995, *ApJ*, 451, 477 (Paper I)
- Giroux, M. L., & Shapiro, P. R. 1996, *ApJS*, 102, 191
- Giroux, M. L., Sutherland, R. S., & Shull, J. M. 1994, *ApJ*, 435, 97
- Giroux, M. L., & Shull, J. M. 1997, *AJ*, 113, 1505

- Gnedin, N. Y., & Hui, L. 1996, *ApJ*, 472, L73
- Green, J., et al. 1997, proposal for “Cosmic Origins Spectrograph”, selected by NASA for *Hubble Space Telescope* 2002 Refurbishment Mission.
- Gruenwald, R., & Viegas, S. M. 1993, *ApJ*, 415, 534
- Gunn, J. E., & Peterson, B. A. 1965, *ApJ*, 142, 1633 (GP)
- Haardt, F., & Madau, P. 1996, *ApJ*, 461, 20
- Heap, S. R. 1997, in *Young Galaxies and QSO Absorption-line Systems*, ASP Conference Series vol. 114 (San Francisco: Astr. Society of Pacific)
- Hernquist, L., Katz, N., Weinberg, D. H., & Miralda-Escudé, J. 1996, *ApJ*, 457, L51
- Hogan, C. J., Anderson, S. F., & Rugers, M. H. 1997, *AJ*, 113, 1495
- Hu, E. M., Kim, T.-S., Cowie, L. L., Songaila, A., & Rauch, M. 1995, *AJ*, 110, 1526
- Izotov, Y., Thuan, T. X., & Lipovetsky, V. A. 1997, *ApJS*, 108, 1
- Jakobsen, P., Boksenberg, A., Deharveng, J. M., Greenfield, P., Jedrzejewski, R., & Paresce, F. 1994, *Nature*, 370, 35
- Kulkarni, V. P., Huang, K., Green, R. F., Bechtold, J., Welty, D. E., & York, D. G. 1996, *MNRAS*, 279, 197
- Laor, A., Fiore, F., Elvis, M., Wilkes, B., McDowell, J. 1997, *ApJ*, 477, 93
- Lu, L., Sargent, W. L. W., Womble, D. S., & Takada-Hidai, M. 1996, *ApJ*, 472, 509
- Lupton, R. 1993, *Statistics in Theory and Practice*, (Princeton: Princeton University Press)
- Madau, P., & Meiksin, A. 1994, *ApJ*, 433, L53
- Madau, P., & Shull, J. M. 1996, *ApJ*, 457, 551
- Miralda-Escudé, J. 1993, *MNRAS*, 262, 273
- Miralda-Escudé, J., & Ostriker 1990, *ApJ*, 350, 1
- Miralda-Escudé, J., & Ostriker 1992, *ApJ*, 392, 15
- Miralda-Escudé, J., Cen, R., Ostriker, J. P., & Rauch, M. 1996, *ApJ*, 471, 582
- Møller, P., & Jakobsen, P. 1990, *A&A*, 228, 299
- Olive, K. A., & Steigman, G. 1995, *ApJS*, 97, 49
- Ostriker, J. P., & Ikeuchi, S. 1983, *ApJ*, 268, L63
- Pei, Y.-C. 1995, *ApJ*, 438, 623
- Petitjean, P., Rauch, M., & Carswell, R. F. 1994, *A&A*, 291, 29
- Petitjean, P., Webb, J. K., Rauch, M., Carswell, R. F., & Lanzetta, K. 1993, *MNRAS*, 262, 499
- Petitjean, P., Riediger, R., & Rauch, M. 1996, *A&A*, 307, 417

- Picard, A. & Jakobsen, P. 1993, *A&A*, 276, 331
- Press, W. H., & Rybicki, G. B. 1993, *ApJ*, 418, 585
- Rauch, M., & Haehnelt, M. G. 1995, *MNRAS*, 275, L76
- Rauch, M., Carswell, R. F., Chaffee, F. H., Foltz, C. B., Webb, J. K., Weymann, R. J., Bechtold, J., & Green, R. F. 1992, *ApJ*, 390, 387
- Rauch, M., Carswell, R. F., Webb, J. K., & Weymann, R. J. 1993, *MNRAS*, 260, 589
- Rees, M. J. 1986, *MNRAS*, 218, 25
- Reimers, D., & Vogel, S. 1993, *A&A*, 276, L13
- Reimers, D., Vogel, S., Hagen, H.-J., Engels, D., Groote, D., Wamsteker, W., Clavel, J., & Rosa, M. R. 1992, *Nature*, 360, 561
- Reimers, D., Koehler, S., Wisotzki, L., Groote, D., Rodriguez-Pascual, P., & Wamsteker, W. 1997, *A&A*, 327, 890
- Reisenegger, A., & Miralda-Escudé, J. 1995, *ApJ*, 449, 476
- Sargent, W. L. W., Steidel, C. C., & Boksenberg, A. 1989, *ApJS*, 69, 703
- Schneider, D., Schmidt, M., & Gunn, J. 1991a, *AJ*, 101, 2004
- Schneider, D., Schmidt, M., & Gunn, J. 1991b, *AJ*, 102, 837
- Schramm, D. N., & Turner, M. S. 1997, *subm. to Rev. Mod. Phys. Colloquia*, (astro-ph/9706069)
- Sciama, D. W. 1994, *ApJ* 422, L49
- Shaver, P. A., Wall, J. V., Kellermann, K. I., Jackson, C. A., & Hawkins, M. R. S. 1996, *Nature*, 384, 439
- Shapiro, P. R., & Giroux, M. L. 1987, *ApJ*, 321, L107
- Shapiro, P. R., Giroux, M. L., & Babul, A. 1994, *ApJ*, 427, 25
- Songaila, A., Hu, E. M., & Cowie, L. L. 1995, *Nature*, 375, 124
- Songaila, A., & Cowie, L. L. 1996, *AJ*, 112, 335
- Steidel, C. C., & Sargent, W. L. W. 1987, *ApJ*, 318, L11
- Steidel, C. C., Dickinson, M., Meyer, D. M., Adelberger, K. L., & Sembach, K. R. 1997, *ApJ*, 480, 568
- Stengler-Larrea, E. A. et al. 1995, *ApJ*, 444, 64
- Storrie-Lombardi, L. J., McMahon, R. G., Irwin, M. J., & Hazard, C. 1994, *ApJ*, 427, L13
- Storrie-Lombardi, L. J., Irwin, M. J., & McMahon, R. G. 1997, in preparation
- Sutherland, R. S., & Shull, J. M. 1998, in preparation
- Tytler, D. 1997, private communication
- Tytler, D., & Fan, X.-M. 1992, *ApJS*, 79, 1

Tytler, D. 1997, private communication

Tytler, D., Fan, X.-M., & Burles, S. 1995, *Nature*, 381, 207

Tytler, D., Fan, X.-M., Burles, S., Cottrell, L., Davis, C., Kirkman, D., & Zuo, L. 1995, in *QSO Absorption Lines*, ed. G. Meylan (Berlin: Springer), 289

Williger, G. M., Baldwin, J. A., Carswell, R. F., Cooke, A. J., Hazard, C., Irwin, M. J., McMahon, R. G., & Storrie-Lombardi, L. J. 1994, *ApJ*, 428, 574

Zhang, Y., Anninos, P., & Norman, M. L. 1995, *ApJ*, 453, L57

Zhang, Y., Meiksin, A., Anninos, P., & Norman, M. L. 1997, *ApJ*, 485, 496

Zheng, W., & Davidsen, A. 1995, *ApJ*, 440, L53

Zheng, W., Kriss, G. A., Telfer, R. C., Grimes, J. P., & Davidsen, A. F. 1997, *ApJ*, 475, 469

Zuo, L. 1992, *MNRAS*, 258, 36

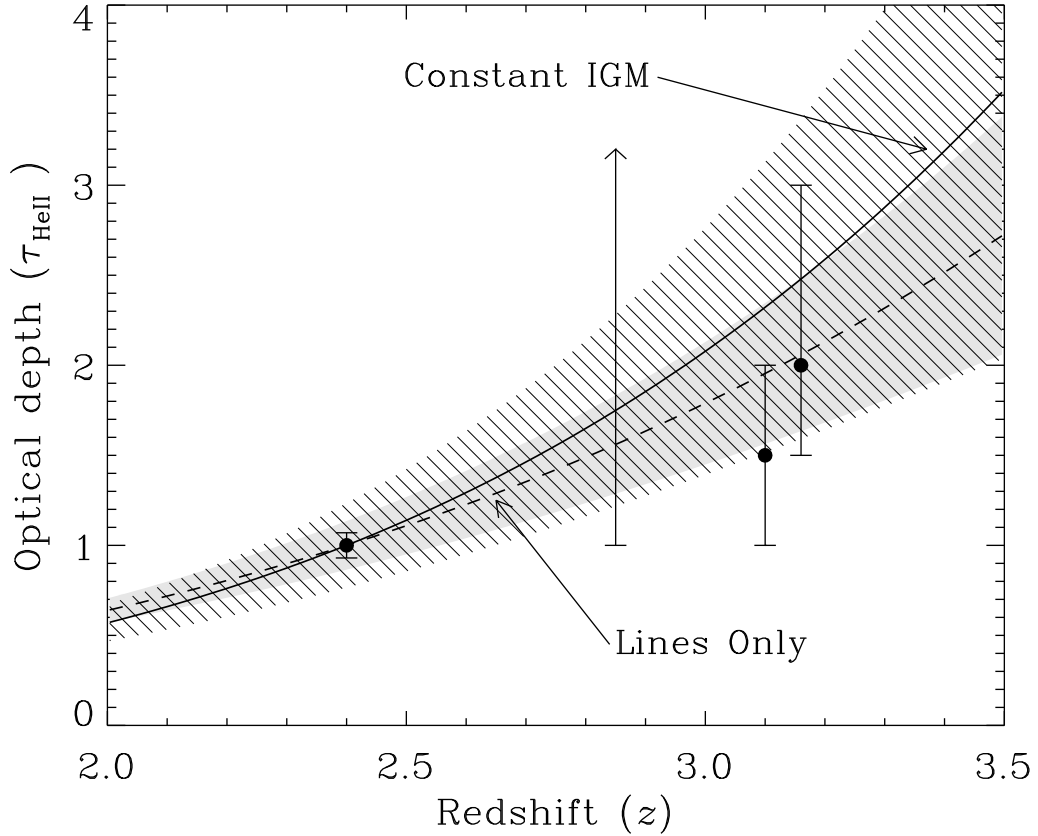


Fig. 1.— Mean He II line opacity  $\tau_{HeII}(z)$ . Points show the four current measurements: HS1700+6416 (Davidsen et al. 1996) at  $z_{em} = 2.74$ ; HE2347-4342 (Reimers et al. 1997) at  $z_{em} = 2.90$ ; Q1935-69 (Tytler et al. 1995) at  $z_{em} = 3.18$ ; and Q0302-003 (Jakobsen et al. 1994) at  $z_{em} = 3.29$ . The points are plotted at the mean redshifts of the He II absorption. The curves show the expected evolution for an IGM of constant comoving density (*solid*) and for pure line-blanketing (*dashed*), with constant  $\eta$ . We have also indicated the expected range of fluctuations in optical depth due to ionization fluctuations discussed in § 4, for the IGM-dominated (hatched region) and line-dominated (shaded region) cases respectively. However, since the four observed redshift windows are larger than the expected correlation length of the fluctuations, the expected fluctuations of the observed optical depth  $\tau_{HeII}$  are smaller than the regions shown.

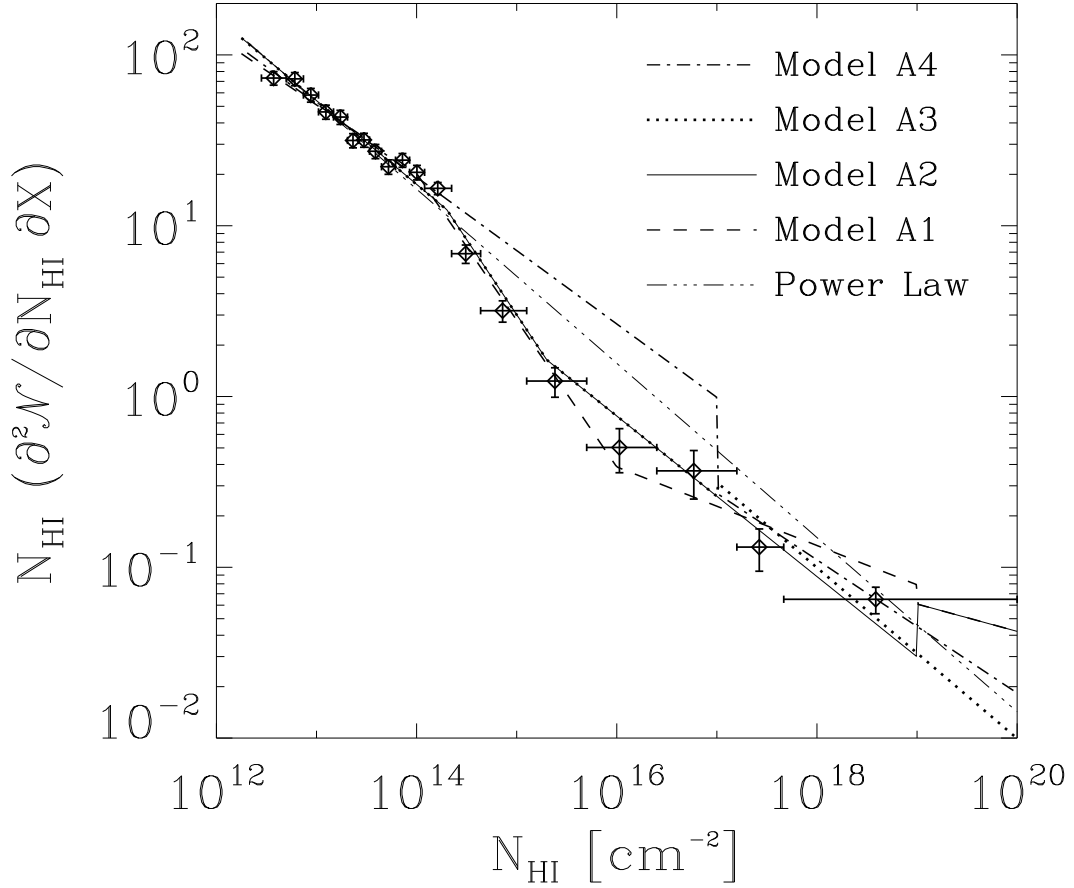


Fig. 2.— Data and models for the H I column density distribution. The sources for the data are discussed in the text; error bars are based on  $N^{1/2}$  statistics. The variable  $X$  refers to the “absorption path length”, defined as in Petitjean et al. (1993) by  $dX = (1+z)dz$ . This makes the distribution less sensitive to redshift, while the choice of  $y$ -axis makes the structure in the spectrum easier to see and reduces the effect of binning on the plotted points. Our four absorption-line models are plotted for the mean redshift of the sample,  $\bar{z} = 3.0$ .

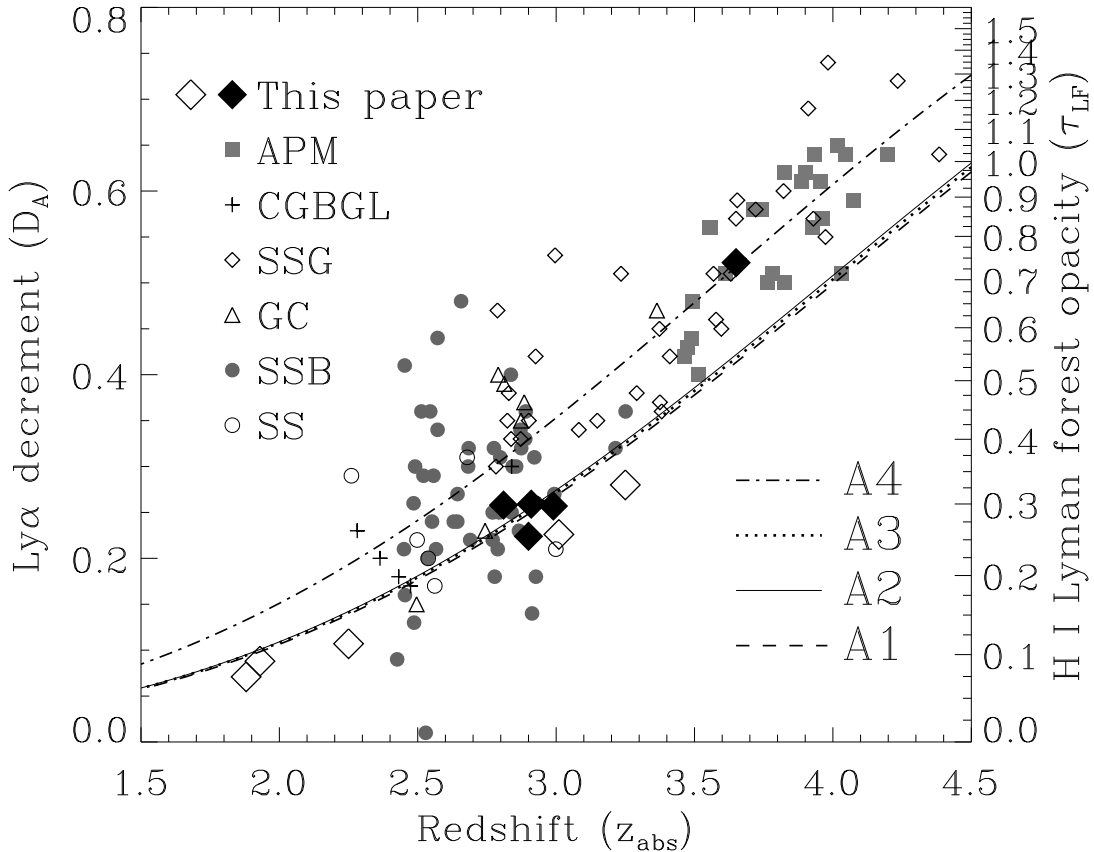


Fig. 3.— The H I Ly $\alpha$  effective optical depth and Ly $\alpha$  decrement,  $D_A$ , as a function of mean absorption redshift. The quasar emission redshift is somewhat higher, as the observations are taken typically from 1050–1170 Å rest frame. Data points marked “this paper” are computed from reconstructed spectra, given the sample of lines discussed in § 2.3. Large filled diamonds are based on *Keck* spectra; large empty diamonds are based on other, lower S/N spectra. Small data points are from samples of low-resolution observation. The different samples are labeled in the legend: (APM) Automated Plate Measurement QSO Survey of Storrie-Lombardi, Irwin, & McMahon (1997); (CGBGL) Cristiani et al. (1993); (SSG) Schneider, Schmidt, & Gunn (1991a,b); (GC) Giallongo & Cristiani (1990); (SSB) Sample of Sargent, Steidel, & Boksenberg (1989) as analyzed by Storrie-Lombardi et al. (1997); and (SS) Steidel & Sargent (1987). The results of our opacity models are also shown. Model A4, which is based on the Press & Rybicki (1993) distribution and is a reasonable fit to the low-resolution measurements, lies far above the others. Models A1, A2, and A3 are based on the absorption-line sample in § 2.3 and are a good fit to the data points measured by the high-resolution technique.

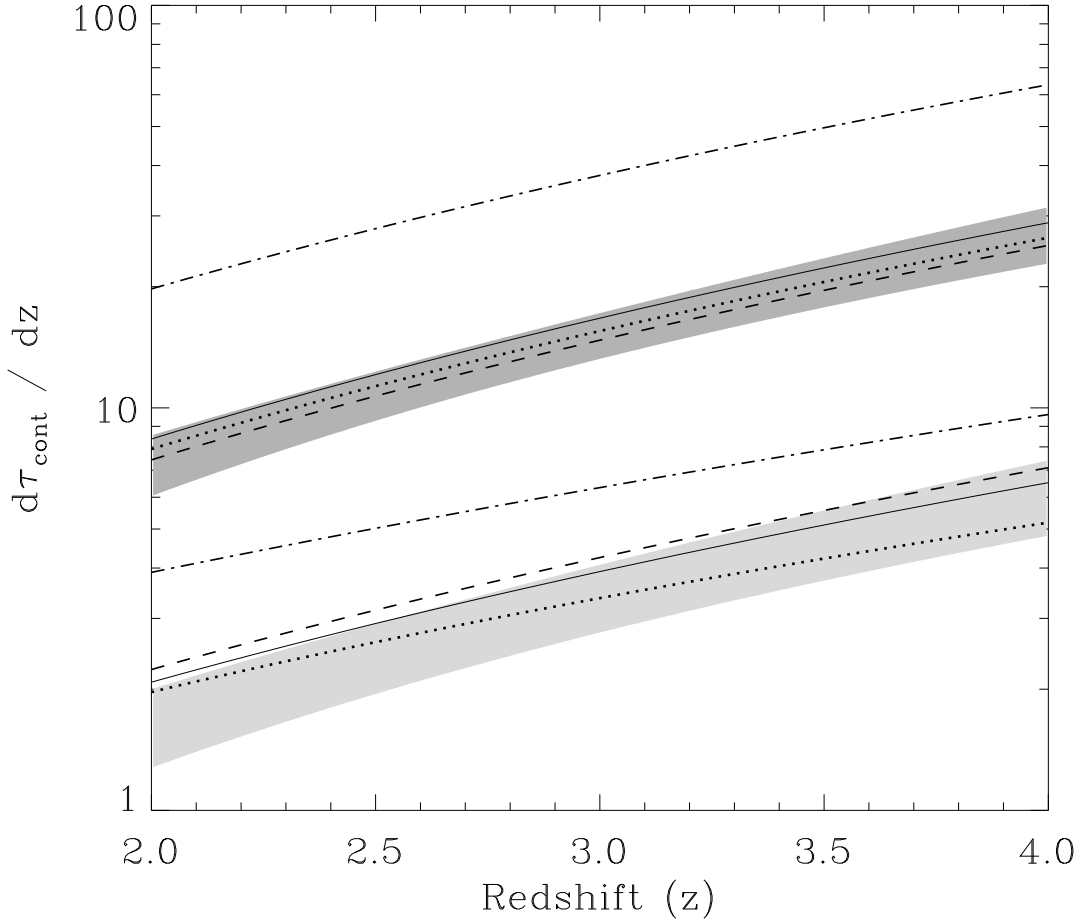


Fig. 4.— The H I (*lower*) and He II (*upper*) threshold continuum opacities as a function of redshift, as derived from the absorption-line sample directly (*shaded region*) and from the model fits. Line codes for opacity models (A1–A4) are same as in Figure 3. To make comparing the models easier, the He II opacities assume  $\eta = 70$ , instead of deriving  $\eta$  from the simulations. The shaded regions represent  $1\sigma$  errors derived from the bootstrap technique discussed in the text. While models A1–A3 are reasonable fits, model A4 (from Paper I) gives much more opacity.

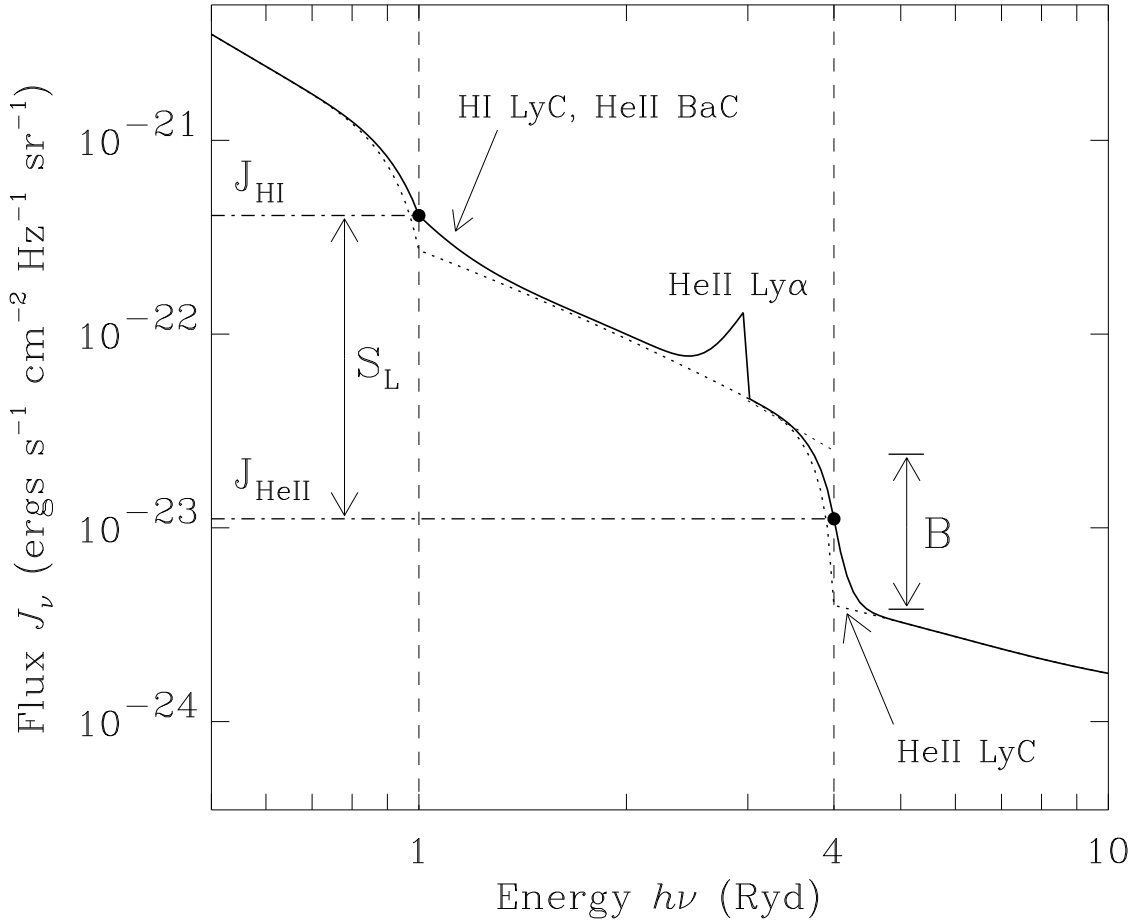


Fig. 5.— Schematic picture of the ionizing background. The dotted line shows the spectrum with the cloud re-emission omitted. The parameter  $S_L$  is the ratio of intensities at 1 Ryd and 4 Ryd (see eq. [7]), while  $B$  is the 4 Ryd break.

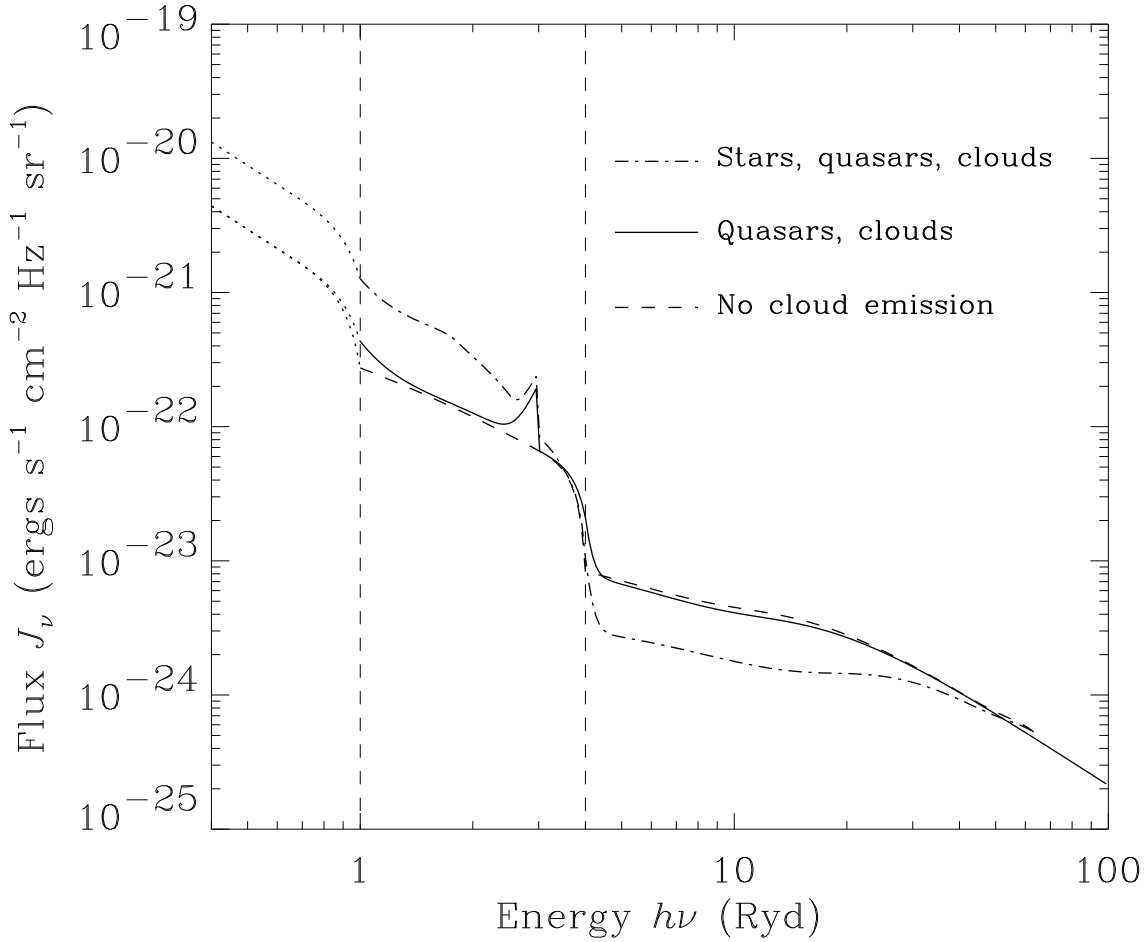


Fig. 6.— Typical spectra produced by the radiative transfer simulations, for  $z = 3$ . These curves assume quasar model Q1, opacity model A2, and an ionizing slope of  $\alpha_s = 1.8$ . The upper curve includes a stellar contribution, fixed at 1 Ryd to have an emissivity twice that of the quasars. The effect of re-emission from the clouds can be seen in the bump at 3 Ryd and the enhanced radiation just above the H I and He II thresholds. The region below 1 Ryd affects neither the H I nor He II ionization rates, and so we have not bothered to include processes that affect it, such as H I Ly $\alpha$  emission; hence it is unrealistic and shown with dotted lines.

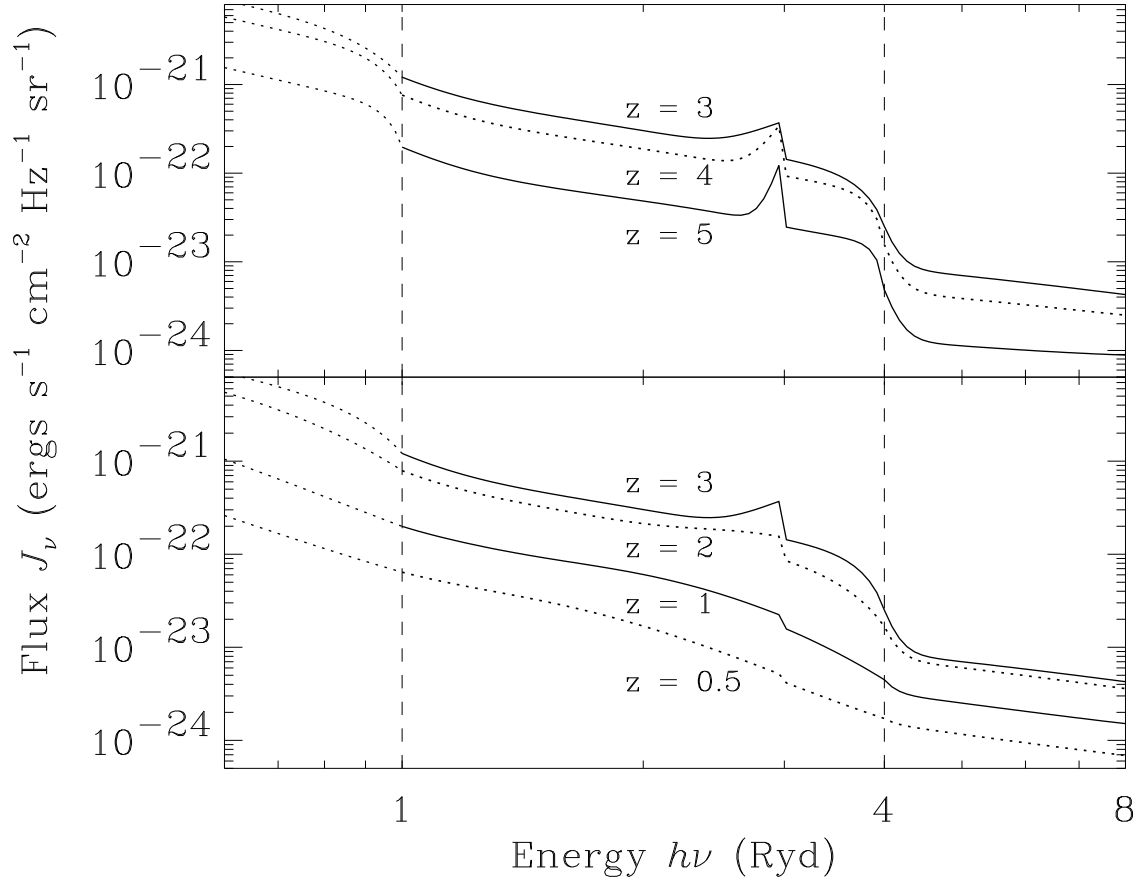


Fig. 7.— Evolution of the ionizing background with redshift, assuming quasar model Q2 with spectral index  $\alpha_s = 2.1$  and absorption model A2. Top panel:  $3 \leq z \leq 5$ . Bottom panel:  $0.5 \leq z \leq 3$ . See discussion in § 3.

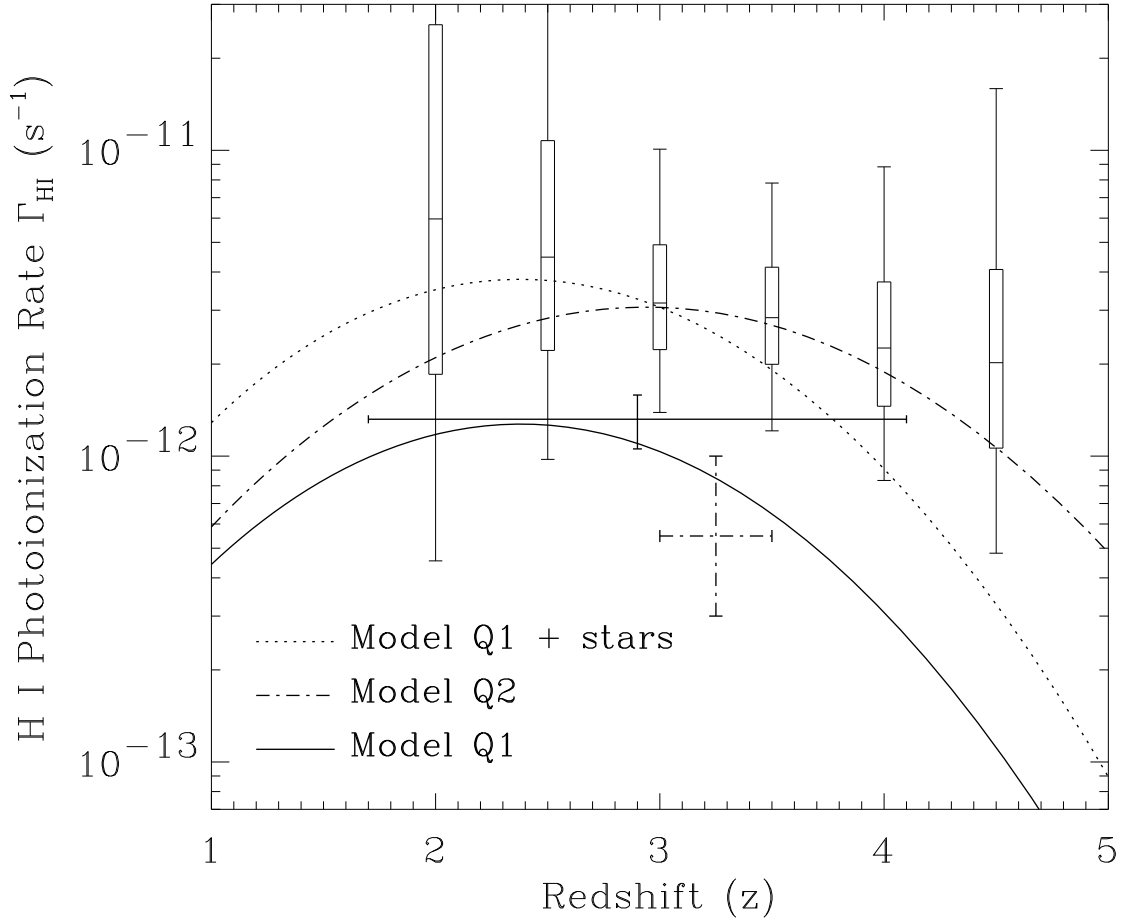


Fig. 8.— Photoionization rate of H I atoms from our models, assuming absorption model A2 and quasar spectral index  $\alpha_s = 1.8$ . Analytic fits to  $\Gamma_{\text{HI}}(z)$  are provided in text (see eq. [16]). Data points, based on the proximity effect, are converted from  $J_\nu$  as discussed in § 3. Box plots from Cooke, Espey, & Carswell (1997) show the median, quartiles, and 95% limits. The single point with solid lines is from Giallongo et al. (1996). The dot-dashed point is the preferred range from hydrodynamical simulations by Zhang et al. (1997). The “Model Q1 + stars” curve includes a stellar contribution with emissivity twice that of the quasars at the H I Lyman edge. Models assume quasar spectral index  $\alpha_s = 1.8$ .

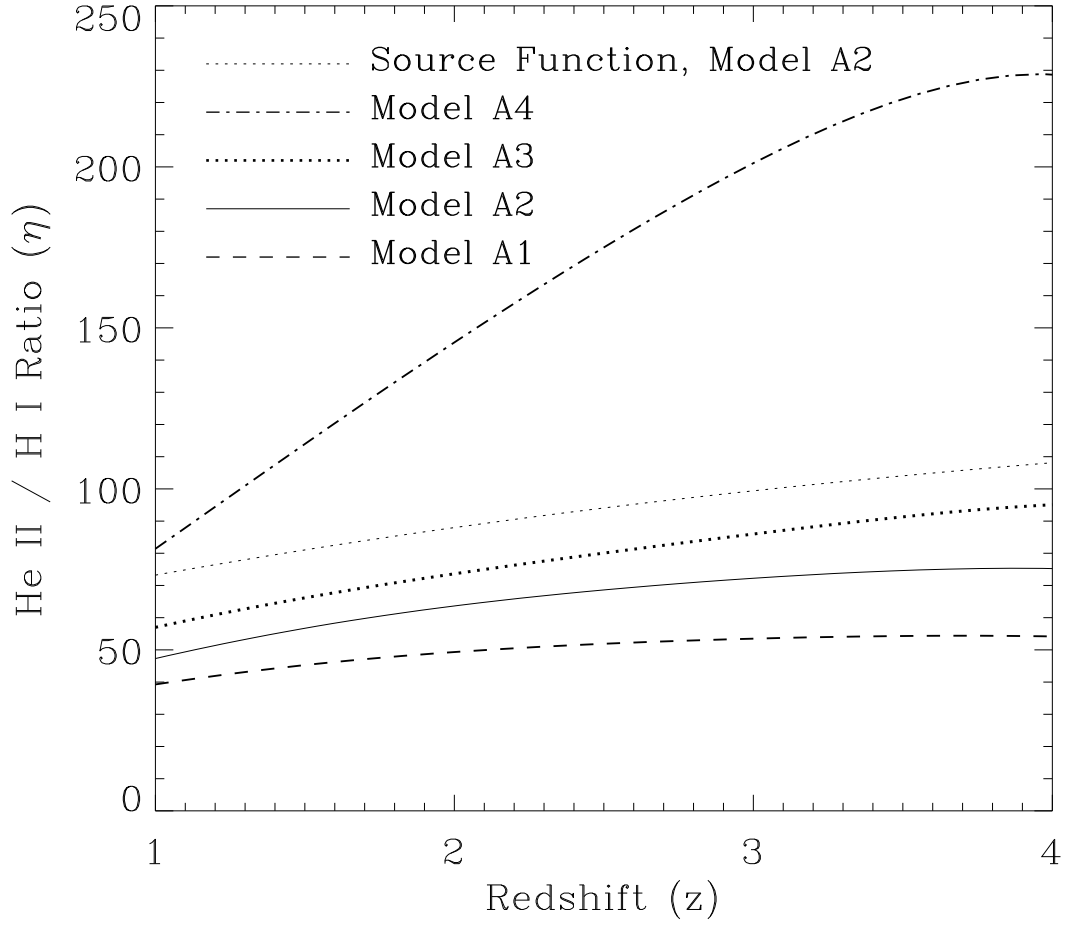


Fig. 9.— The ratio  $\eta \equiv N_{\text{HeII}}/N_{\text{HI}}$  as a function of redshift. (a) Effect of the absorption-line model, assuming quasar model Q2 with spectral index  $\alpha_s = 1.8$  and including cloud re-emission. The results of the source-function approximation are shown as well.

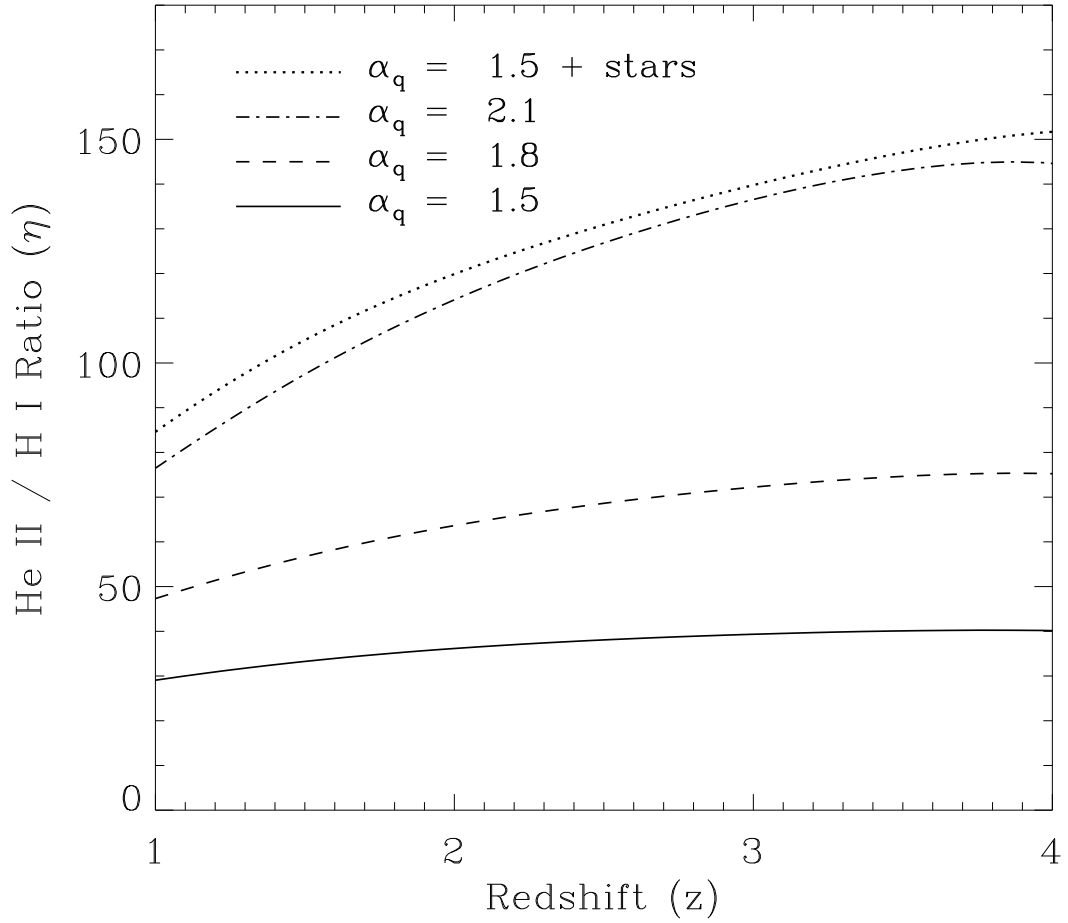


Fig. 9.— (b) Effect of the ionizing spectrum. Uses absorption model A2 and quasar model Q2. Three curves spanning the uncertainty in the mean quasar spectrum are shown. In addition, we include a model that includes a stellar component, of magnitude 1.3 in relation to the quasar contribution at 1 Ryd. As argued in the text, this should produce results comparable to making the quasar spectral index larger (softer) by  $\ln(1 + 1.3)/\ln(4) = 0.6$ , and this is indeed seen in the plot. The agreement is not exact because the stellar and quasar spectral shapes are different near 1 Ryd.

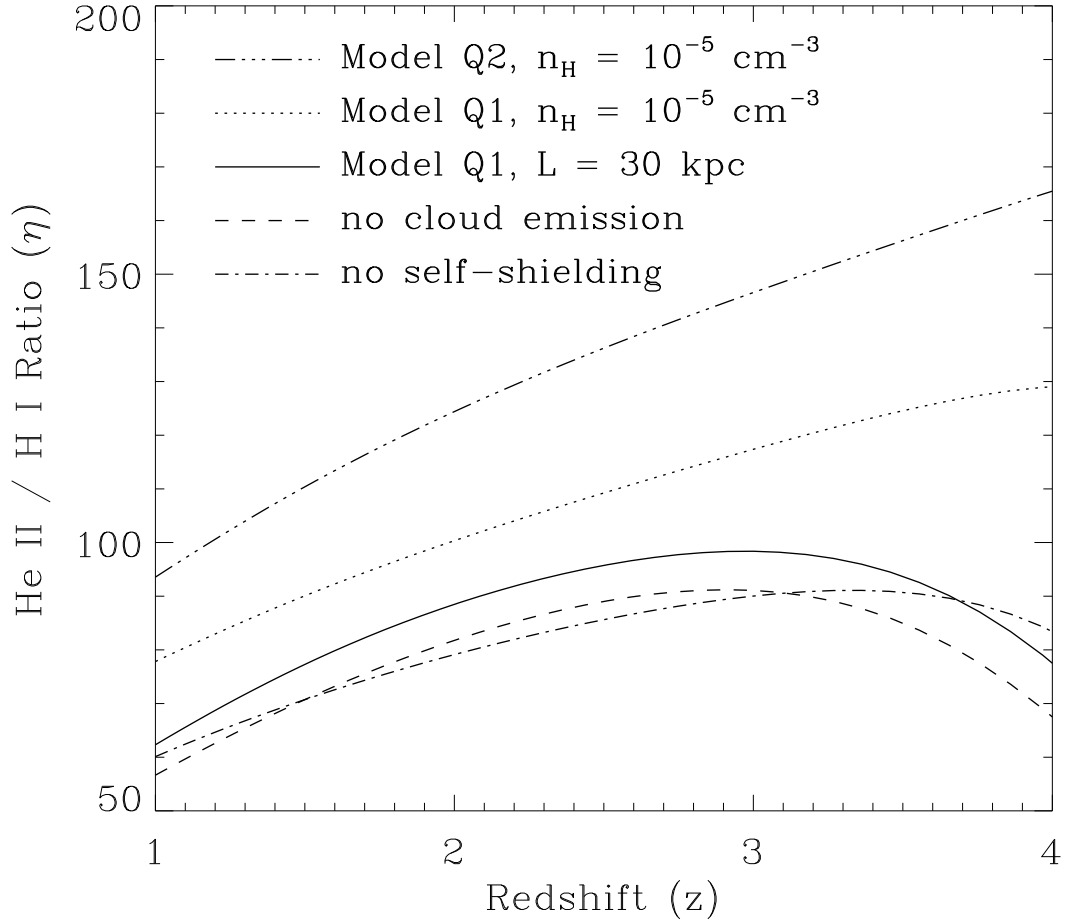


Fig. 9.— (c) Influence of the density within the absorbing clouds, the quasar luminosity function, and the emission and self-shielding processes. All curves use opacity model A2 with a quasar spectral index  $\alpha_s = 2.1$ . The bottom three curves all use a density of  $n_H = 10^{-4} \text{ cm}^{-3}$  within the clouds and the Q1 luminosity function, but we have omitted the cloud re-emission in the dashed curve and the self-shielding in the dot-dashed.

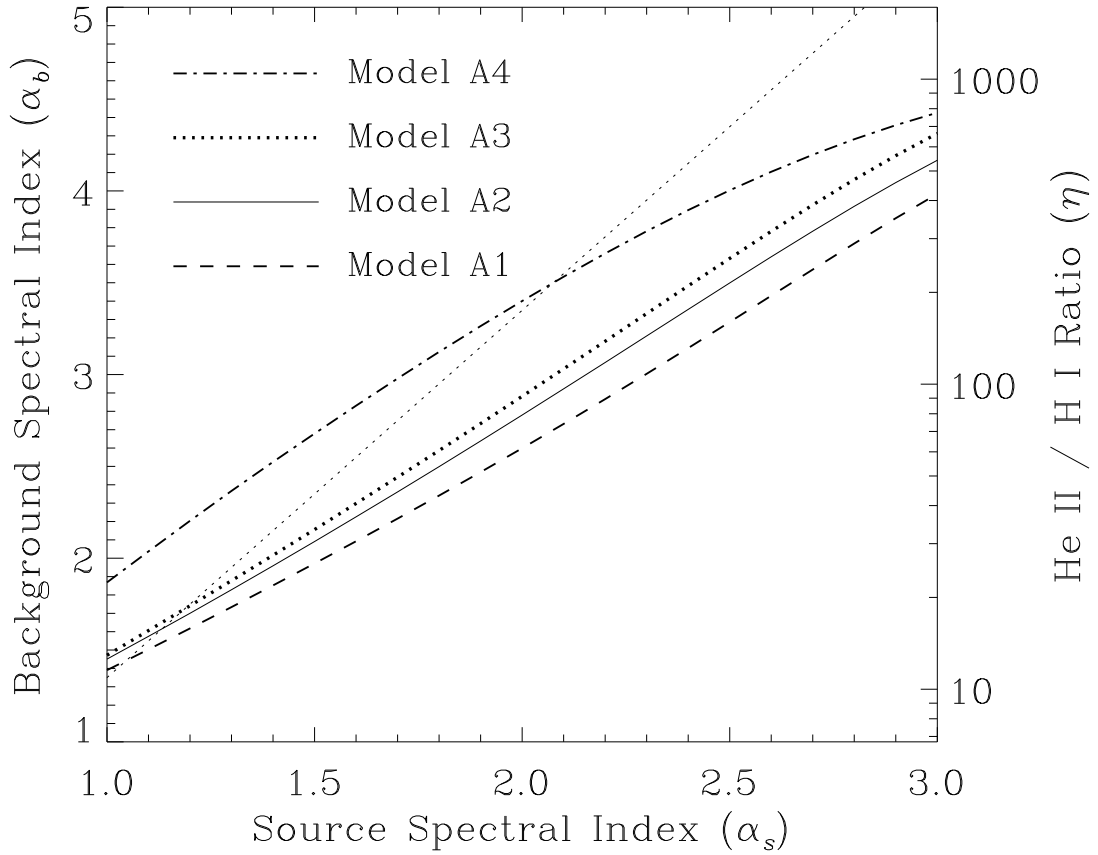


Fig. 10.— Dependence of the background spectral index  $\alpha_b$  upon the intrinsic spectral index  $\alpha_s$  of ionizing sources, for the four opacity models in the text, for quasar model Q1 and  $z = 3$ . The light dotted line shows the analytic model,  $\alpha_b = 2.0\alpha_s - 0.64$ , of § 2.2. It is somewhat steeper than the numerical models, partly because it ignores the finite-density effects that affect models with soft spectra.

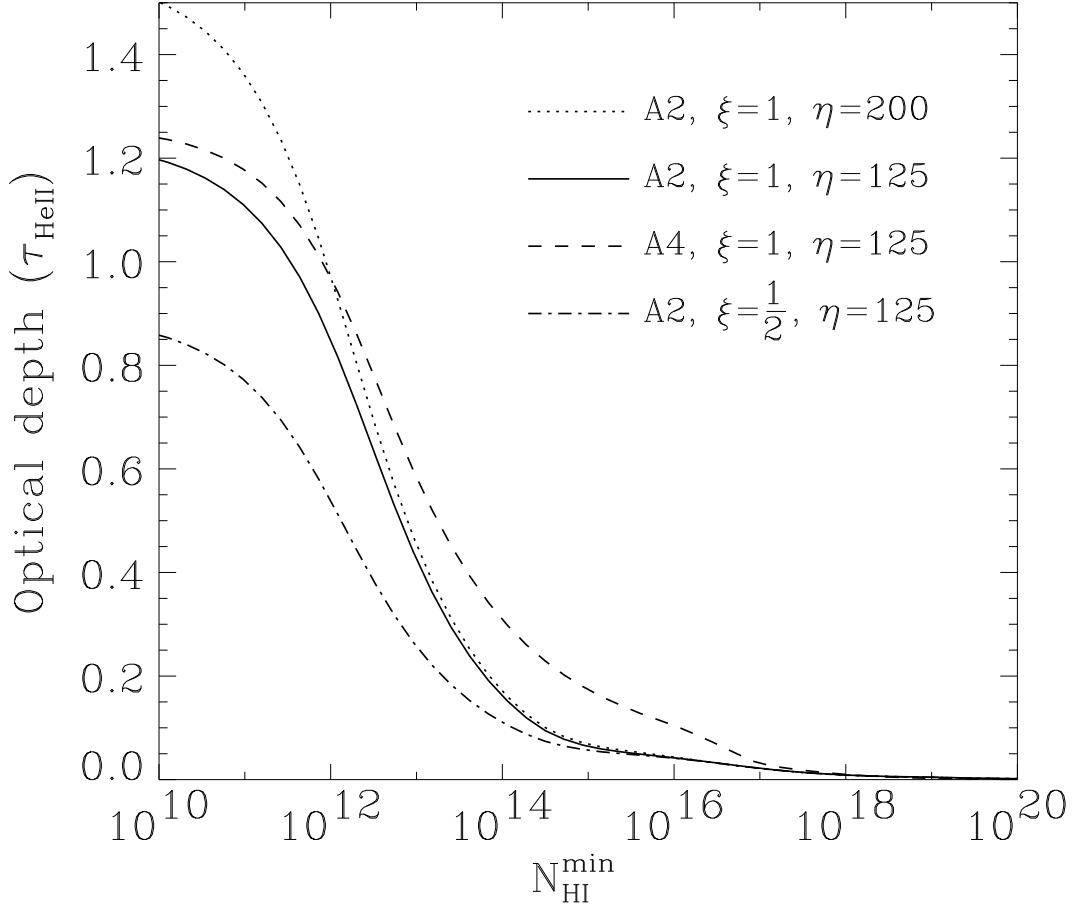


Fig. 11.— Cumulative value of  $\tau_{\text{HeII}}$  with decreasing  $N_{\text{HI}}^{\text{min}}$  in distribution of column densities, for several opacity models at  $z = 2.4$ . The solid line shows the results of our “standard” model without diffuse IGM. This uses opacity model A2, bulk He II Doppler widths, quasar model Q2, source spectrum  $\alpha_s = 2.1$ , resulting in  $\eta = 125$ . Three variants are also shown: with a softer source spectrum of  $\alpha_s = 2.3$  giving  $\eta = 200$ ; with thermal He II Doppler widths; and with the opacity model A4 (with  $\alpha_s = 1.6$  to give  $\eta = 125$  as in our standard model).

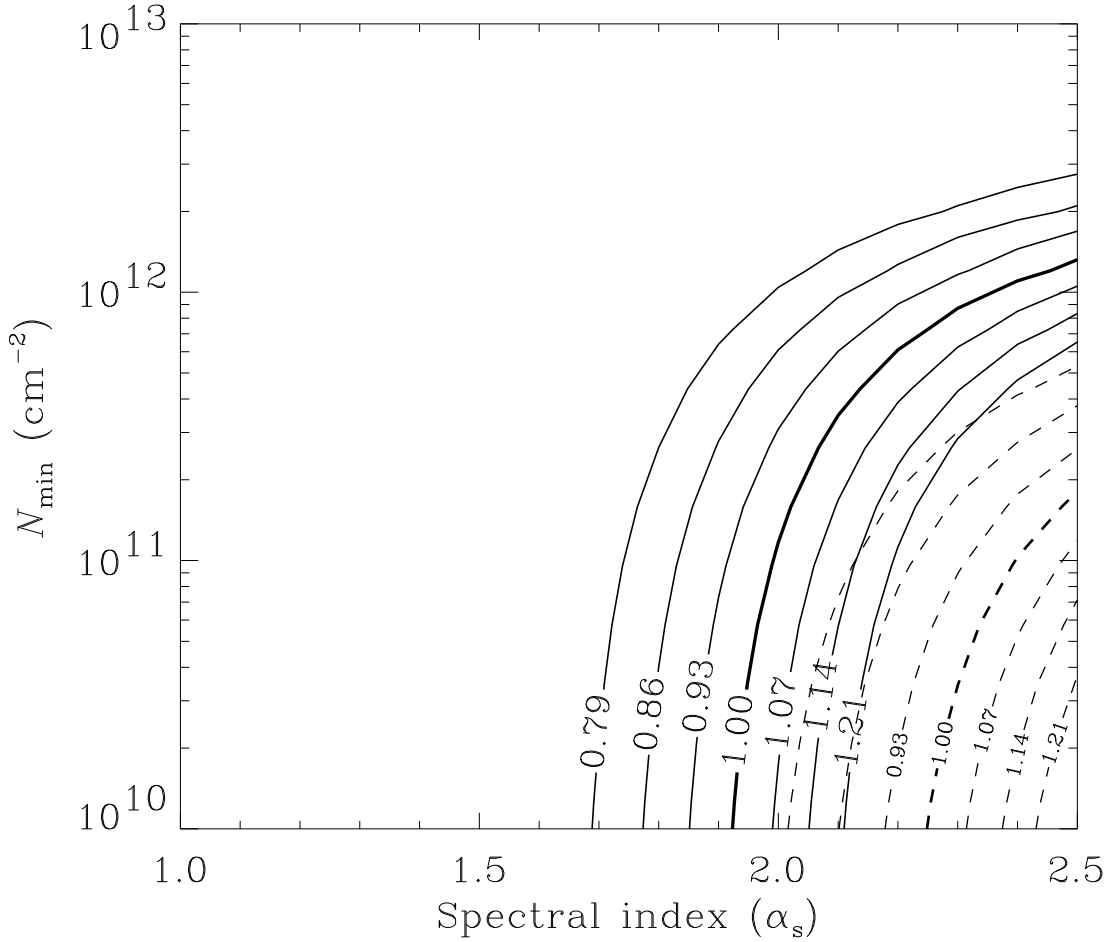


Fig. 12.— Contours of the cumulative optical depth,  $\tau_{HeII}(N_{HI} > N_{min})$ , as a function of the quasar spectral index  $\alpha_s$ , at  $\langle z_{abs} \rangle = 2.4$  to match D96’s observations of HS1700+6416. Contours are in  $1\sigma$  intervals of 0.07 around their best value of  $\tau_{HeII} = 1.00$ . Curves are shown for bulk Doppler widths ( $\xi_{HeII} = 1$ , solid lines), and thermal widths ( $\xi_{HeII} = 0.5$ , dotted lines). We assume negligible ionizing radiation from galaxies and adopt opacity model A2 and quasar model Q2.

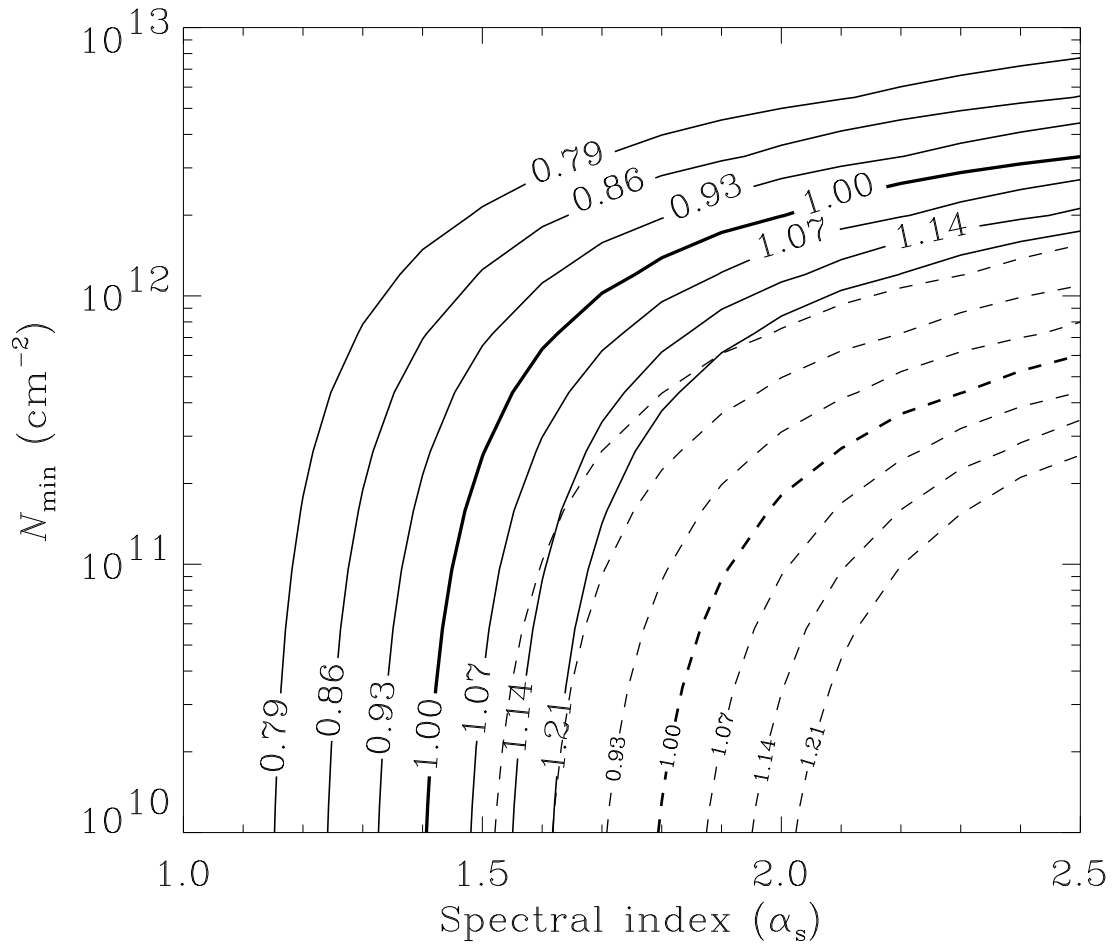


Fig. 12.— (b) Same, but for absorption model A4.

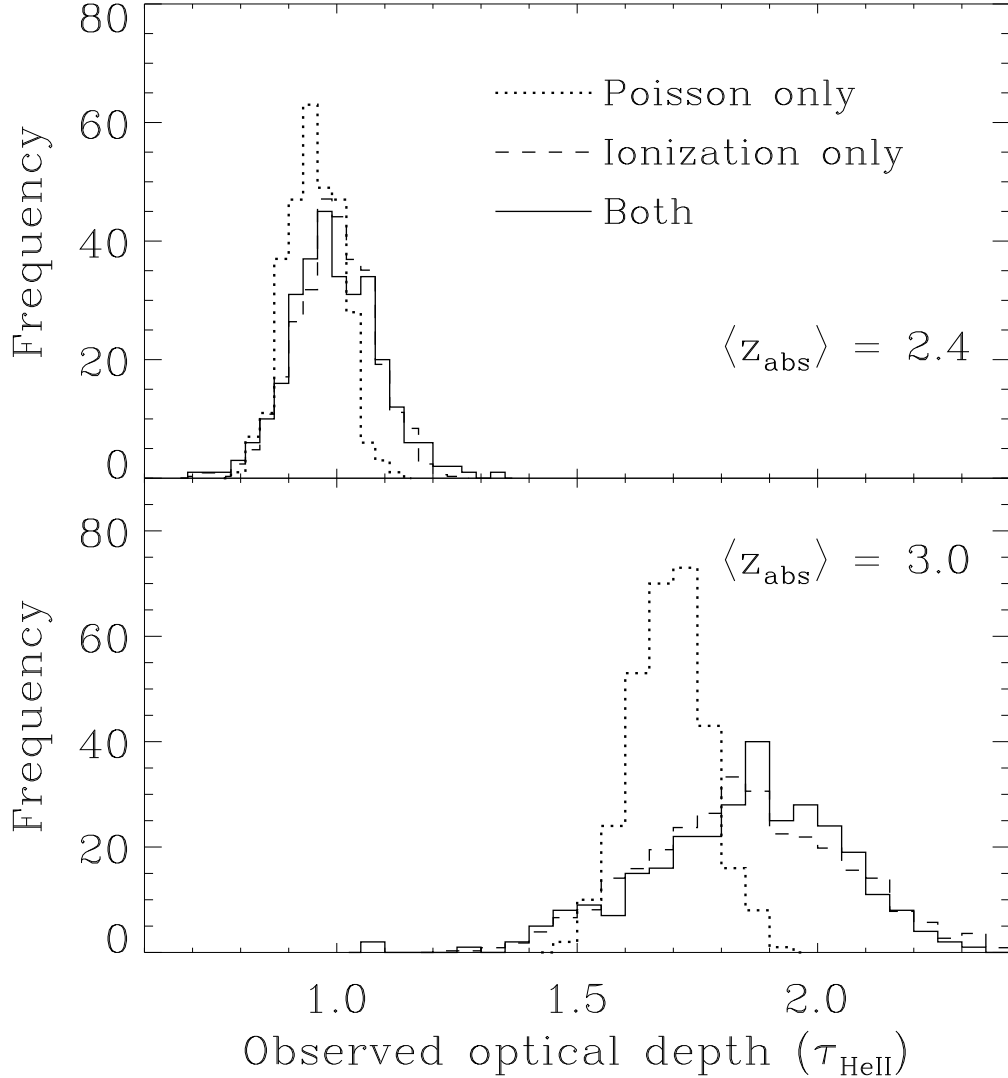


Fig. 13.— Histogram from Monte Carlo simulations of the observed effective optical depth  $\tau_{\text{HeII}} = -\ln(\bar{T})$  in the He II “ $D_A$  window”, from 262–294 Å in the rest frame of a quasar. Top panel: towards a quasar with  $z_{em} = 2.7$  like HS1700+6416. Bottom panel: towards a quasar with  $z_{em} = 3.37$ , giving a mean absorption redshift of  $z_{abs} = 3.0$ . The dotted line incorporates effects of Poisson fluctuations only, the dashed line the effects of ionization fluctuations only (averaging over the absorbers), while the solid line includes both types of fluctuations. Uses absorption model A2 and bulk Doppler widths ( $\xi_{\text{HeII}} = 1$ ), and quasar model Q1 with spectral index  $\alpha_s = 2.1$  giving  $\eta = 95$ . The strength of the ionization fluctuations increases rapidly with redshift, in contrast to the intrinsic fluctuations.

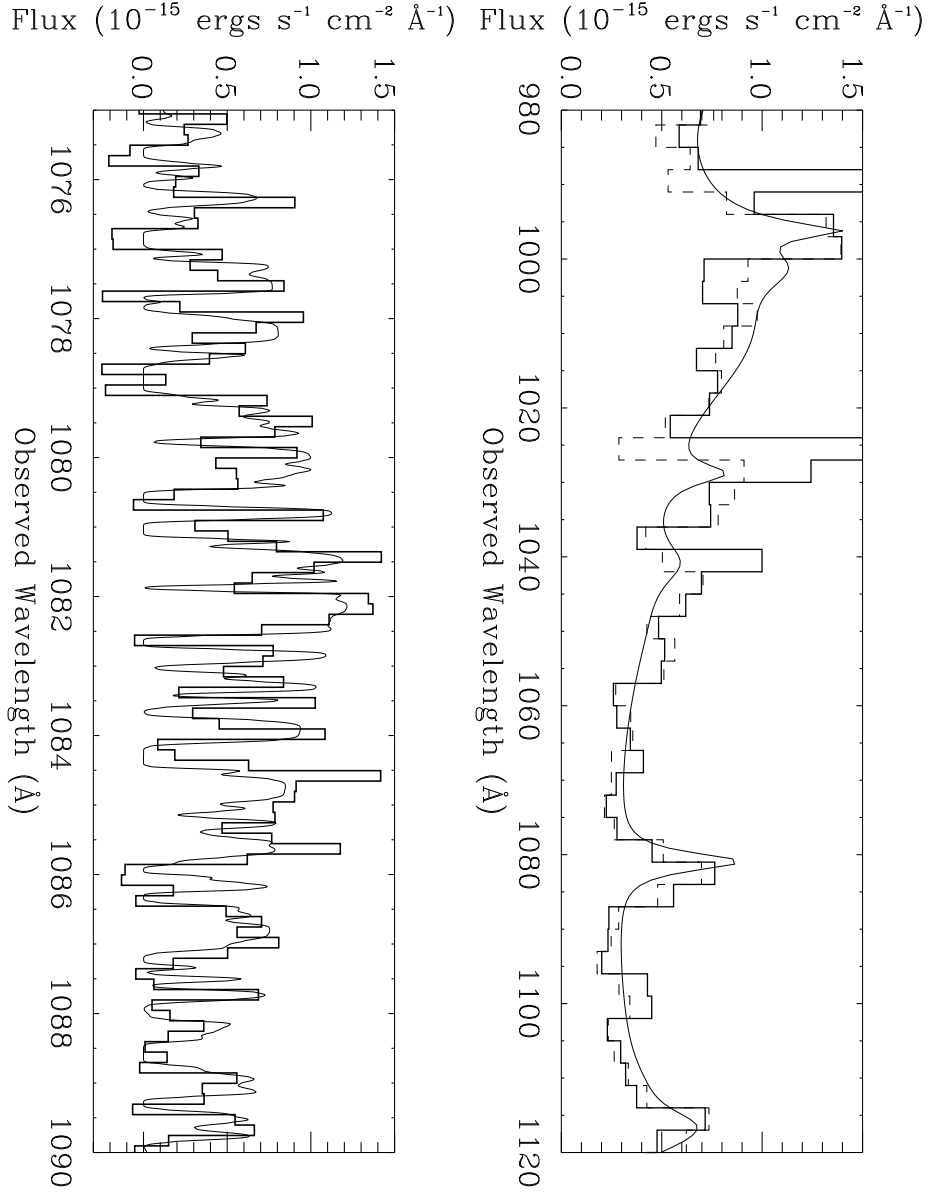


Fig. 14.— Simulation of an observation of He II Ly $\alpha$  absorption with the FUSE satellite, showing the spectrum of a QSO like HS1700+6416 with  $z_{em} = 2.7$  and flux at the He II Lyman limit  $1.25 \times 10^{-15} \text{ erg s}^{-1} \text{ cm}^{-2} \text{ Hz}^{-1} \text{ \AA}^{-1}$ . Assumes absorption model A2 with thermal linewidths ( $\xi_{HeII} = 1$ ), model Q1,  $\alpha_s = 1.8$ , and a substantial IGM with  $\Omega_{IGM} = 0.026$ ; in this model  $\eta = 53$ . The exposure time is  $3 \times 10^5 \text{ s}$ . The upper panel shows the large-scale view, with a solid curve indicating the mean absorption as a function of wavelength. The dashed histogram is the binned intrinsic spectrum, while the solid histogram incorporates the effects of finite resolution, photon statistics, and sky and detector backgrounds (including an H I  $\lambda 1025.72 \text{ Ly}\beta$  line). In this particular realization, several quasars near the line of sight induce peaks in the ionizing background and thus in the transmission. The lower panel shows a smaller view with  $0.15 \text{ \AA}$  pixels, centered on the peak at  $1082 \text{ \AA}$ . In this panel the light solid line is the intrinsic spectrum and the heavy histogram is the observed spectrum. Even with thermal widths, the structure in the spectrum is resolved by the FUSE detector.

